The Upsilon spectrum and the determination of the lattice spacing from lattice QCD including charm quarks in the sea

R. J. Dowdall, B. Colquhoun, J. O. Daldrop, C. T. H. Davies, I. D. Kendall, E. Follana, T. C. Hammant, R. R. Horgan, G. P. Lepage, C. J. Monahan, and E. H. Müller (HPQCD Collaboration)

Phys. Rev. D **85**, 054509 — Published 21 March 2012

DOI: 10.1103/PhysRevD.85.054509

The Upsilon spectrum and the determination of the lattice spacing from lattice QCD including charm quarks in the sea

R. J. Dowdall,[1,*] B. Colquhoun,[1] J. O. Daldrop,[1,†] C. T. H. Davies,[1,‡] I. D. Kendall,[1] E. Follana,[2] T. C. Hammant,[3] R. R. Horgan,[3] G. P. Lepage,[4] C. J. Monahan,[3,§] and E. H. Müller[5] (HPQCD collaboration),[¶]

[1]*SUPA, School of Physics and Astronomy, University of Glasgow, Glasgow, G12 8QQ, UK*
[2]*Departamento de Física Teórica, Universidad de Zaragoza, Cl. Pedro Cerbuna 12, E-50009 Zaragoza, Spain*
[3]*DAMTP, University of Cambridge, Wilberforce Road, Cambridge CB3 0WA, UK*
[4]*Laboratory of Elementary-Particle Physics, Cornell University, Ithaca, New York 14853, USA*
[5]*SUPA, School of Physics, University of Edinburgh, King's Buildings, Edinburgh, EH9 3JZ, UK*

We give results for the Upsilon spectrum from lattice QCD using an improved version of the NRQCD action for b quarks which includes radiative corrections to kinetic terms at $\mathcal{O}(v^4)$ in the velocity expansion. We also include for the first time the effect of up, down, strange and charm quarks in the sea using 'second generation' gluon field configurations from the MILC collaboration. Using the Υ $2S-1S$ splitting to determine the lattice spacing, we are able to obtain the $1P-1\overline{S}$ splitting to 1.4% and the $3S-1S$ splitting to 2.4%. Our improved result for $M(\Upsilon)-M(\eta_b)$ is 70(9) MeV and we predict $M(\Upsilon')-M(\eta_b')=35(3)$ MeV. We also calculate π, K and η_s correlators using the Highly Improved Staggered Quark action and perform a chiral and continuum extrapolation to give values for M_{η_s} (0.6893(12) GeV) and f_{η_s} (0.1819(5) GeV) that allow us to tune the strange quark mass as well as providing an independent and consistent determination of the lattice spacing. Combining the NRQCD and HISQ analyses gives $m_b/m_s = 54.7(2.5)$ and a value for the heavy quark potential parameter of $r_1 = 0.3209(26)$ fm.

I. INTRODUCTION

Lattice QCD calculations have developed rapidly both in accuracy and in scope in the last few years. This growth has built on the first demonstration that numerical simulations including u, d and s quarks in the sea with light enough u/d quarks give results in agreement with experiment for simple 'gold-plated' quantities across the full range of hadron physics [1]. Errors at the level of a few % make this highly non-trivial. A key element of those calculations was the determination of the Υ spectrum because there are many gold-plated states below threshold for strong Zweig-allowed decay. In addition radial and orbital excitation energies are very insensitive to quark masses (including that of the b itself) making them useful for determining the lattice spacing, a, without a complicated tuning process. A further incentive for lattice Υ studies is the importance of testing b quark physics from lattice QCD so that the same action can be used for results in B physics required, in conjunction with experiment, for the determination of elements of the Cabibbo-Kobayashi-Maskawa matrix. Here we give new results for the Υ spectrum improving on those earlier results in several ways to keep pace with improvements in other areas of lattice QCD. We have improved statistical errors, improved the NRQCD action and we are also now using 'second generation' gluon field configurations that include charm quarks in the sea.

The b quarks in these first calculations that included the full effect of sea quarks [2, 3] were implemented using lattice Nonrelativistic QCD (NRQCD) with an action accurate through v^4 in the velocity expansion for the b quark [4]. The coefficients of the v^4 terms were matched to full QCD at tree level, having removed the most significant source of radiative corrections, that of tadpole diagrams generated in lattice QCD from the form of the lattice gluon field, by the use of 'tadpole-improvement' [5]. The gluon field configurations used were generated by the MILC collaboration [6] using a Symanzik-improved gluon action in which radiative corrections at $\mathcal{O}(\alpha_s a^2)$ were included except for radiative corrections from quark loops [7] ($\mathcal{O}(n_f \alpha_s a^2)$ where n_f is the number of sea quark flavors), which were omitted. Configurations at three different values of the lattice spacing were available: 'super-coarse' ($a \approx 0.18$fm); 'coarse' ($a \approx 0.12$fm) and 'fine' ($a \approx 0.09$fm). u/d and s sea quarks were included using the improved staggered (asqtad) action [8–10] which is numerically relatively fast. A range of u/d masses (taken to be the same) were used ranging down to a ratio with the s sea quark mass of around 0.2. The key mass splittings in the bottomonium spectrum studied were those between the ground S-wave states and the first radially excited S-wave states, the $2S-1S$ splitting, and that between the first P-wave states and the ground S-wave states, the $1P-1S$ splitting. The statistical errors from

*Rachel.Dowdall@glasgow.ac.uk
†Current address: Helmholtz Institut für Strahlen und Kernphysik and Bethe Centre for Theoretical Physics, Universität Bonn, 53115 Bonn, Germany
‡c.davies@physics.gla.ac.uk
§Current address: Department of Physics, College of William and Mary, Williamsburg, VA 23187, USA
¶URL: http://www.physics.gla.ac.uk/HPQCD

the lattice calculation for these splittings were 1–2% (i.e. 5-10 MeV) and systematic errors were estimated to be similar to this or smaller, depending on the lattice spacing. Within these errors, agreement with experiment was confirmed.

More recently the Υ spectrum has been calculated using the same NRQCD action on gluon configurations at a 'coarse' ($a \approx 0.11$ fm) and a 'fine' ($a \approx 0.09$ fm) lattice spacing generated by the RBC/UKQCD collaboration using the Iwasaki gluon action and 2+1 flavors of sea quarks implemented with the domain wall formalism [11, 12]. Results in close agreement and with similar errors to those found on the MILC configurations are obtained, confirming the independence of the results from the sea quark formalism.

The systematic errors in the calculation of the Υ $2S-1S$ and $1P-1S$ splittings were studied in some detail in [2]. Sources of error there were missing radiative corrections to the v^4 terms in the lattice NRQCD action (beyond tadpole-improvement), as well as radiative corrections to discretisation correction terms and from higher order (v^6) missing relativistic corrections. In addition systematic errors from the missing radiative corrections to the improvement terms in the gluon action were estimated. These errors were typically each of order 1% in the $1P-1S$ splitting on the fine lattices and about half that for the $2S-1S$ splitting because of some cancellation between $1S$ and $2S$ states. Errors were similar for the radiative and relativistic errors on coarser lattices but of course the discretisation errors were larger.

Subsequent to this, we have made estimates of the effect of missing c quarks in the sea [13, 14]. These have negligible effect on mesons apart from bottomonium, where internal momenta can be large enough to generate c quarks from the vacuum. We found the shift in the ground-state S wave masses might be of $\mathcal{O}$(5MeV) [14] (it is spin-independent) with approximately half the shift for $2S$ states because of a smaller 'wave-function at the origin' and no shift for $1P$ states. This would give rise to systematic errors of 0.5% for the $2S-1S$ splitting and 1% for the $1P-1S$ splitting, similar to the systematic errors from other effects quoted above.

The conclusion from these results is that the errors in bottomonium masses and radial and orbital mass splittings have been pinned down and tested from this NRQCD action at the level of 5-10 MeV. There is also a contribution to systematic errors at the same level coming from the gluon field configurations. The NRQCD systematic errors also feed in to the calculation of B, B_s and B_c meson masses using NRQCD b quarks. The state-of-the-art calculation for the masses of these mesons has $\mathcal{O}$(10 MeV) errors dominated by systematic errors from this NRQCD action [14, 15].

In the last five years, however, other lattice QCD calculations have become increasingly accurate. For example the mass of the D_s meson was recently calculated by HPQCD with combined statistical and systematic errors of 3 MeV and its decay constant calculated to 1% [13]. These errors are at the level where we must allow for missing electromagnetism from lattice QCD.

There have been several contributions to this progress. Advances in computational speed have meant better statistical errors from calculating many more meson correlators on larger samples of configurations. It has also been possible to generate lattices with smaller lattice spacing, so that the D_s calculation includes 'superfine' ($a \approx 0.06$ fm) and 'ultrafine' ($a \approx 0.045$ fm) lattices [6]. Significant improvements have been made to relativistic quark actions too. For example, the D_s meson mass calculation used the Highly Improved Staggered Quark (HISQ) action for both valence quarks. The HISQ action [16] has smaller discretisation errors than the asqtad action by about a factor of 3 and can be used for quarks as heavy as charm on lattices with a lattice spacing of 0.1fm or smaller. This has revolutionised charm physics calculations [17] in lattice QCD and is having an impact also on calculations for mesons containing a b quark through a combination of an extrapolations in the mass of the heavy HISQ quark acting as the 'b' to the physical point for the real b quark, combined with extrapolations to the continuum ($a \to 0$) limit from results at many values of a [18]. The heavy HISQ calculations are computationally much more expensive than those using NRQCD and this currently limits their utility. The results for B_s and B_c meson masses have comparable errors to the existing NRQCD results, but are dominated by statistical and $a \to 0$ extrapolation uncertainities. They then provide a complementary way of testing b physics to that of NRQCD and it is clear that combining the strengths of both methods will be optimal in future.

Meanwhile the MILC collaboration have moved on to the production of 'second generation' gluon field configurations which have a number of improvements over the earlier ensembles [19]. They include a more highly improved gluon action [20], HISQ quarks in the sea with the addition of c quarks as well as u, d and s and with lighter u and d masses than before.

The availability of these configurations along with the incentives discussed above to improve errors in Υ and B physics using NRQCD b quarks has meant that we have begun a new programme of improved NRQCD calculations. Here we present the first results, giving the radial and orbital splittings in the Υ spectrum, tuning the lattice b quark mass and determining the lattice spacing from the $(2S-1S)$ splitting. As well as using the second generation gluon field configurations we have improved the NRQCD action by adding radiative corrections to the v^4 kinetic terms including discretisation errors. We also have improved statistics and improved methods for tuning the b quark mass. This has meant that we can test the effect of radiative corrections to the v^4 kinetic terms on the meson dispersion relation. Using both perturbative and nonperturbative methods for determining the radiative corrections to spin-dependent terms we are able to improve the determination of the Υ hyperfine splitting.

A useful complementary method for determining the lattice spacing was developed in [21]. It uses the fictitious $s\overline{s}$ pseudoscalar particle known as the η_s. This particle does not exist in the real world because of mixing with light quarks to form the η and η' but on the lattice this can be prevented. The mass and decay constant of the η_s can be determined accurately in a lattice QCD calculation using the Highly Improved Staggered Quark (HISQ) action and their physical values fixed from M_π, M_K, f_π and f_K from a simultaneous chiral and continuum extrapolation. Here we update the results of [21] for these 2+1+1 configurations and use these also to give a determination of the lattice spacing.

The two different methods for determining the lattice spacing can be combined through the use of a third quantity, r_1 [22], which can be derived accurately from determination of the heavy quark potential [23]. r_1/a values are provided for these configurations by the MILC collaboration [24]. r_1/a provides a good determinant of the relative lattice spacing between different sets of gluon configurations but its physical value must be determined from other quantities. From the separate determination of the lattice spacing from the two methods above we have two sets of results for r_1 in fm as a function of lattice spacing. From this we are able to test that the two methods give the same result in the continuum and chiral limits (which they do) and provide a physical value of r_1 that could be used, in the absence of either of the other methods, to determine the lattice spacing on other ensembles with 2+1+1 flavors of sea quarks.

We also combine results for tuned b quark masses in NRQCD and tuned s quark masses from HISQ along with one-loop renormalisation constants to give a value for m_b/m_s for comparison to other results obtained purely from the HISQ action.

The layout of the paper is as follows. Section II discusses the second-generation gluon field ensembles giving more details of the improvements present there. Section III describes the improvements to the NRQCD calculations and results for the Υ spectrum. Section IV discusses the π, K, η_s analysis on these same configurations and the additional information that provides to determine the lattice spacing. This is tied together via the determination of the heavy quark potential parameter, r_1, in section V and m_b/m_s in section VI. Section VII provides our conclusions.

II. SECOND GENERATION 2+1+1 GLUON FIELD ENSEMBLES

The gauge configurations used in this calculation are listed in Table I [19]. These were generated by the MILC collaboration using a tadpole-improved Lüscher-Weisz gauge action with coefficients corrected perturbatively through $\mathcal{O}(\alpha_s)$ including pieces proportional to n_f, the number of quark flavors in the sea [20] (see Appendix A). The gauge action is then improved completely through $\mathcal{O}(\alpha_s a^2)$, unlike the earlier asqtad configurations. Sea quarks are included with the HISQ action [16] which also has smaller discretisation errors compared to the asqtad action (see the discussion in section IV). The configurations include a sea charm quark in addition to up, down and strange. These configurations are then said to have 2+1+1 flavors in the sea, since the u and d quarks are taken to have the same mass, which is heavier than average u/d mass in the real world, and the s and c masses are tuned as closely as possible to their correct values at that lattice spacing. The tuning of the sea s quark mass is much more accurately done – to better than 5% – than on the previous asqtad configurations. This means that the u/d quark mass (denoted m_l here) can be more accurately calibrated in terms of the s quark mass for chiral extrapolations. Here we use a ratio of m_l/m_s as low as one tenth (see Table I) whereas in our previous work on the asqtad configurations our most chiral ensemble had a ratio of the $m_{l,sea}/m_{s,physical}$ of one quarter. This means that we have a much smaller chiral extrapolation to do to reach the physical u/d mass (where $m_l = m_s/27$ [6]) than before.

TABLE I: Details of the MILC gluon field ensembles used in this paper. $\beta = 10/g^2$ is the $SU(3)$ gauge coupling and L/a and T/a are the number of lattice spacings in the space and time directions for each lattice. am_l, am_s and am_c are the light (up and down taken to have the same mass), strange and charm sea quark masses in lattice units. r_1/a is the static-quark potential parameter in lattice units determined by the MILC collaboration [19, 24]. Note that this has not been 'smoothed'. The ensembles 1 and 2 will be referred to in the text as "very coarse", 3 and 4 as "coarse" and 5 as "fine."

Set	β	r_1/a	am_l	am_s	am_c	$L/a \times T/a$
1	5.80	2.041(10)	0.013	0.065	0.838	16×48
2	5.80	2.0621(45)	0.0064	0.064	0.828	24×48
3	6.00	2.574(5)	0.0102	0.0509	0.635	24×64
4	6.00	2.623(11)	0.00507	0.0507	0.628	32×64
5	6.30	3.549(13)	0.0074	0.037	0.440	32×96

The sea quarks are included with the standard method of incorporating the determinant of the quark matrix raised to the one quarter power for each flavor, in order to implement the correct counting for sea staggered quarks. The algorithm used for including the sea quarks has now been improved by MILC to the exact RHMC algorithm [19] i.e. all errors in the time step for the updating algorithm have been removed.

The configurations are separated by 5 trajectories in the time units of the updating algorithm for the very coarse and coarse ensembles and by 6 trajectories for the fine ensemble. In subsections III B and IV A we will study the autocorrelations in our meson correlators to show how independent the configurations are for different observables.

The r_1/a values given in Table I are determined by the MILC collaboration after extraction of the potential between two infinitely heavy (static) quarks at separation

r/a in lattice units. r_1/a is defined [22] as the point where the force $F(r)$ derived from the derivative of the potential satisfies

$$r^2F(r) = 1. \quad (1)$$

The values of r_1/a for these ensembles have been chosen to match approximately those of the previous results including 2+1 flavors of asqtad quarks and can be used to determine the lattice spacing if the physical value for r_1 is known. Using the r_1 value determined previously on configurations with 2+1 flavors of sea quarks, this means that the lattice spacing values will be approximately 0.15 fm, 0.12fm and 0.09fm. The physical spatial size of the lattices then exceeds 2.5 fm and is as high as 3.8 fm on the ensembles that correspond to $m_l/m_s = 0.1$. In section V we will derive a physical value for r_1 based on the results from sections III and IV to calibrate more accurately the lattice spacing values for these configurations.

III. THE UPSILON SPECTRUM

A. The NRQCD action

The spectrum of bottomonium mesons is extracted by computing appropriate correlators constructed from b-quark propagators on the gluon field ensembles listed in Table I. We make use of NRQCD, an effective field theory that gives an expansion of the Dirac action in powers of the heavy quark velocity, v. This is discretised onto a space-time lattice as lattice NRQCD [4, 25] and is a good formalism to use for b quarks since they are known to be very nonrelativistic inside their bound states ($v^2 \approx 0.1$). As used on the lattice NRQCD has the advantage that propagators can be generated using a simple time evolution equation rather than having to invert the Dirac matrix. The quark and antiquark fields are separated in this formalism as 2-component spinors.

The NRQCD Hamiltonian we use is given by:

$$\begin{aligned} aH &= aH_0 + a\delta H; \\ aH_0 &= -\frac{\Delta^{(2)}}{2am_b}, \\ a\delta H &= -c_1\frac{(\Delta^{(2)})^2}{8(am_b)^3} + c_2\frac{i}{8(am_b)^2}\left(\nabla\cdot\tilde{\mathbf{E}} - \tilde{\mathbf{E}}\cdot\nabla\right) \\ &\quad -c_3\frac{1}{8(am_b)^2}\sigma\cdot\left(\tilde{\nabla}\times\tilde{\mathbf{E}} - \tilde{\mathbf{E}}\times\tilde{\nabla}\right) \\ &\quad -c_4\frac{1}{2am_b}\,\sigma\cdot\tilde{\mathbf{B}} + c_5\frac{\Delta^{(4)}}{24am_b} \\ &\quad -c_6\frac{(\Delta^{(2)})^2}{16n(am_b)^2}. \end{aligned} \quad (2)$$

Here ∇ is the symmetric lattice derivative and $\Delta^{(2)}$ and $\Delta^{(4)}$ the lattice discretization of the continuum $\sum_i D_i^2$ and $\sum_i D_i^4$ respectively. am_b is the bare b quark mass. $\tilde{\mathbf{E}}$ and $\tilde{\mathbf{B}}$ are the chromoelectric and chromomagnetic fields calculated from an improved clover term [2]. The $\tilde{\mathbf{B}}$ and $\tilde{\mathbf{E}}$ are made anti-hermitian but not explicitly traceless, to match the perturbative calculations done using this action.

In terms of the velocity expansion H_0 is $\mathcal{O}(v^2)$ and δH is $\mathcal{O}(v^4)$, including discretisation corrections. H_0 contains the bare quark mass parameter which is nonperturbatively tuned to the correct value for the b quark as discussed below in subsection III C. The terms in δH have coefficients c_i whose values are fixed from matching lattice NRQCD to full QCD. This matching takes account of high momentum modes that differ between NRQCD and full QCD and so it can be done perturbatively, giving the c_i the expansion $1 + c_i^{(1)}\alpha_s + \mathcal{O}(\alpha_s^2)$. In previous calculations [2] we used the tree level value of 1 for all the c_i, after tadpole-improving the gluon fields. This means dividing all the gluon fields, $U_\mu(x)$ by a tadpole-parameter, u_0, before constructing covariant derivatives or $\mathbf{E}$ and $\mathbf{B}$ fields for the Hamiltonian above. The u_0 parameter corrects for tadpole diagrams that arise in a universal way from the way in which the lattice gluon field is constructed. For u_0 we took the mean trace of the gluon field in Landau gauge, u_{0L}. With tadpole-improvement in place we expect the radiative corrections to the c_i coefficients to be of normal size i.e. $\mathcal{O}(1)$ [26]; without this they can be rather large.

Here, on top of tadpole-improvement with u_{0L}, we use $\mathcal{O}(\alpha_s)$ corrected coefficients for the kinetic terms, i.e. c_1, c_5 and c_6, so improving on the NRQCD action used previously, and significantly reducing the systematic errors in the tuning of the b quark mass and in the determination of the radial and orbital mass splittings. The calculation of the $c_i^{(1)}$ for $i = 1, 5, 6$ is discussed in Appendix B [27]. Table II gives the values for c_1, c_5 and c_6 that we use on the very coarse, coarse and fine lattices as a result. As expected, after tadpole-improvement, the coefficients $c_{1,5,6}^{(1)}$ are not large and they are well-behaved as a function of the b quark mass. In subsection III C we test these coefficients through a precision study of the dispersion relation for Υ and η_b mesons.

The other coefficients in the NRQCD action are c_2, c_3 and c_4. c_3 and c_4 multiply spin-dependent terms that give rise respectively to spin-orbit and spin-spin fine structure in the spectrum. Most of the splittings we will discuss here are 'spin-averaged' to remove the effect of these terms and so we will generally set c_3 and c_4 to their tree level values of 1. However, in section III E 3 we will discuss the hyperfine splitting $(M(\Upsilon) - M(\eta_b))$ and show results for both perturbatively improved and nonperturbatively determined c_4. The calculation of the appropriate $c_4^{(1)}$ [28] is discussed in Appendix B, and the nonperturbative determination of c_4 and c_3 in Appendix C. The nonperturbative studies indicate that the value of c_3 is very close to 1 for this NRQCD action. c_2 multiplies a spin-independent term, the Darwin term, which can affect spin-independent splittings such as ra-

TABLE II: The coefficients c_1, c_5 and c_6 used in the NRQCD Hamiltonian of equation 2 on the very coarse (sets 1 and 2), coarse (sets 3 and 4) and fine (set 5) ensembles. Other coefficients had values 1 except for calculations in which we specifically changed their values to test the effect, as described in the text.

Set	c_1	c_5	c_6
very coarse	1.36	1.21	1.36
coarse	1.31	1.16	1.31
fine	1.21	1.12	1.21

dial and orbital excitation energies. Because the Darwin term is field-dependent we do not expect it to have such a large effect as kinetic terms, and therefore do not expect radiative corrections to c_2 to be as important as for c_1, c_5 and c_6. However, in subsection III C we will investigate the effect of changing c_2 so that we can estimate concretely the systematic error from not knowing its $\mathcal{O}(\alpha_s)$ correction.

Given the NRQCD action above, the time evolution of the heavy quark propagator is given by:

$$G(\mathbf{x},t+1) = \left(1-\frac{a\delta H}{2}\right)\left(1-\frac{aH_0}{2n}\right)^n U_t^\dagger(x) \times \left(1-\frac{aH_0}{2n}\right)^n \left(1-\frac{a\delta H}{2}\right) G(\vec{x},t) \quad (3)$$

with starting condition:

$$G(\mathbf{x},0) = \phi(\mathbf{x})\mathtt{1}. \quad (4)$$

The smearing function $\phi(\mathbf{x})$ is used to improve the projection onto a particular state in the spectrum. Including a variety of smearing functions is essential to obtain accurate results for the splittings between the low lying excited states. Full details of the smearing functions used will be given in subsection III B. The 1 in equation 4 is the unit matrix in color and (2-component) spin space. The parameter n has no physical significance, but is included for improved numerical stability of high momentum modes that do not contribute to bound states [4]. In [2] it was demonstrated that radial and orbital mass splittings were the same within the statistical errors available there for $n = 2$ and $n = 4$ on coarse lattices. The minimum value of n for stability increases as the b quark mass in lattice units falls on finer lattices. Rather than varying n as we change the quark mass, here we use $n = 4$ throughout which is the value appropriate to the fine lattices. At zero spatial momentum the anti-quark propagator is the complex conjugate of the quark propagator for a source of the kind given in equation 4.

Details of various parameters used in our calculation are listed in table III. Tuning of the bare b quark mass will be discussed in subsection III C. The tadpole parameters u_{0L} were calculated by fixing a subset of each ensemble to lattice Landau gauge using a Fourier-accelerated steepest descents algorithm [29] to maximise the average trace link ($\sum_{\mu=1,4;x} \mathrm{Tr}U_\mu(x)$), which value, normalised, then becomes u_{0L}. The whole ensemble was then fixed to Coulomb gauge by using the same algorithm to maximise the spatial trace link ($\sum_{i=1,3;x} \mathrm{Tr}U_i(x)$) to allow us to use 'wave-function' smearing operators, with parameter a_{sm} as described in subsection III B. Propagators were calculated from 16 time sources on each configuration to minimise statistical errors. Because in NRQCD we operate a simple time evolution we can choose the time length of each propagator. This we take to be greater than or equal to half the time extent of the lattice as detailed in Table III.

TABLE III: Parameters used in the NRQCD action for our calculations that included a full 5×5 matrix of correlators. Other parameters have been used in subsidiary test calculations as described in the text. am_b is the bare b quark mass and u_{0L} the Landau link tadpole-improvement factor used in the NRQCD action. The different number of digits given in the u_{0L} column reflect the precision with which it was determined. $n_{\rm cfg}$ gives the number of configurations used in each ensemble and n_t is the number of starting time sources per configuration. T_p is the time length of each propagator in lattice units. a_{sm} is the parameter for the smearing function described in subsection III B.

Set	am_b	u_{0L}	$n_{\rm cfg}$	n_t	T_p	a_{sm}
1	3.42	0.8195	1021	16	40	0.79
2	3.39	0.82015	1000	16	40	0.80
3	2.66	0.834	1053	16	40	1.0
4	2.62	0.8349	1000	16	40	1.0
5	1.91	0.8525	874	16	48	1.37

B. Smearing functions and multiexponential fits

Quark propagators are generated using three different smearing functions which we label as local, ground state and excited state. They are chosen to improve the projection onto different radially excited states and previous experience has shown that 'hydrogen-like' wavefunctions work well [2].

$$\begin{aligned} \phi_l(r) &= \delta_{r,0} \\ \phi_{gs}(r) &= \exp(-r/a_{sm}) \\ \phi_{es}(r) &= (2a_{sm}-r)\exp(-r/a_{sm}). \end{aligned} \quad (5)$$

a_{sm} is the smearing radius and is chosen to be approximately the same in physical units for each ensemble. Values are given in Table III. Since a different smearing function can be applied separately to the quark and anti-quark we can make five different combinations as detailed in Table IV.

A different smearing can also be applied at the source and the sink making correlator cominations labelled by e.g. lg,le,gG. The different smearing combinations allow the construction of up to a 5×5 matrix of correlators for the S-wave states that can be fit simultaneously. The

TABLE IV: Smearing combinations used for either the source or the sink in the construction of S-wave correlators.

Name	quark smearing	anti-quark smearing
l	ϕ_l	ϕ_l
g	ϕ_{gs}	ϕ_l
e	ϕ_{es}	ϕ_l
G	ϕ_{gs}	ϕ_{gs}
E	ϕ_{es}	ϕ_{es}

cross-correlators provide further useful information beyond that in the diagonal terms that can be used in the fitting to extract the excited states more precisely. The correlators with quantum numbers of $^3S_1$ or $^1S_0$ are distinguished by the insertion of either a σ or a $\mathbf{1}$ in spin space at source and sink [30].

To make P-wave states we use only the l and g smearings above and apply a symmetric difference operator, Δ to the smeared source to give a P-'wavefunction'. This propagator is combined with that from a δ function source and a derivative applied at the sink to make a P-wave meson correlator. The complete set of combinations of σ matrices with derivatives that are needed for the P-wave states is given in [30]. On the lattice the 5-dimensional spin 2 representation is split into E and T_2 representations of the lattice rotational group and we fit these representations separately since differences in mass between them can arise from discretisation errors on the lattice.

For the S-wave states, statistical errors were improved further by using random wall sources in combination with the smearings discussed above. The delta function quark source is replaced with a (pseudo-)random colour vector $\eta_a(\vec{x}) \in U(1)$ at each spatial point of the initial time slice. When the meson correlator is constructed, the white noise property $\langle \eta_a(\vec{x})\eta_b^\dagger(\vec{y})\rangle = \delta_{ab}\delta(\vec{x}-\vec{y})$ ensures that the random noise cancels at all points except those where the initial spatial sites are the same. This can be combined with the smearing functions by distributing the random number associated with the centre of each smearing function along with the smearing function. Then once again the white noise property will mean that the resultant correlator averages over the initial time source the effect of having a smeared source at every point [31]. Previous studies have found a significant improvement in the precision of the Upsilon ground state energy using random wall sources [21]. The improvement is less clear for excited states and therefore we did not use this technique for the P-wave states.

Propagators were calculated from 16 time sources on each configuration but to avoid correlations between time sources, the correlators were binned over all sources on the same configuration. Autocorrelations between results on successive configurations in an ensemble were studied by calculating the autocorrelation function $C_{\Delta T}$ [32]:

$$C_{\Delta T} = \frac{\langle x_i x_{i+\Delta T}\rangle - \langle x_i\rangle\langle x_{i+\Delta T}\rangle}{\langle x_i^2\rangle - \langle x_i\rangle^2}. \quad (6)$$

Here x_i represents a correlator on a given ensemble, i. $x_{i+\Delta T}$ is the correlator on an ensemble separated by ΔT from i in the ordered ensemble i.e. $\Delta T = 1$ corresponds to neighbouring configurations in the ensemble. The ensembles have been generated taking into account the fact that autocorrelations increase on finer lattices. Thus neighbouring configurations are 5 trajectories apart for very coarse and coarse ensembles but 6 trajectories apart for the fine ensemble [19]. $C_{\Delta T}$ is plotted against ΔT in Figure 1 for the case where x is an Υ correlator measured with a time separation on the lattice of approximately 0.6 fm. This value was chosen to correspond to a point where correlators were dominated by the ground-state. The picture is qualitatively the same for different time separations, however. $C_{\Delta T}$ drops to zero very rapidly, within the separation $\Delta T = 1$. We therefore do not have to worry about autocorrelations between configurations but can treat them all as statistically independent.

Bayesian fitting is used to extract the spectrum from the correlators [33]. The fit function

$$G_{\rm meson}(n_{sc}, n_{sk}; t) = \sum_{k=1}^{n_{\rm exp}} a(n_{sc}, k)a^*(n_{sk}, k)e^{-E_k t} \quad (7)$$

is used, where aE_k is the energy of the $(k-1)$th radial excitation in lattice units and $a(n_{sc/sk}, k)$ are the corresponding amplitudes labelled by the smearing used at the source and sink of the correlator, i.e. $sc, sk \in \{l, g, e, G, E\}$. We fit the full range of t values for the correlator from 1 to T_p, where T_p values are given for S-wave fits in Table III and $T_p = 20$ for P-waves. The number of terms, $n_{\rm exp}$, in the fit is varied, however, and Bayesian model selection criteria are applied to determine which fit is used. In practice, this means adding additional terms to the fit until the results and the errors stabilise. An example is given in Figure 2.

The Bayesian approach allows the inclusion of prior data into the fitting procedure. The χ^2 test function is amended to

$$\chi^2_{\rm aug} = \chi^2 + \chi^2_{\rm prior} \quad (8)$$

and the function $\chi^2_{\rm aug}$ is minimised. By Bayes' theorem this corresponds to maximising the posterior probability p(parameters|data) as opposed to a standard χ^2 test which maximises only the likelihood function p(data|parameters). $\chi^2_{\rm prior}$ is taken to be

$$\chi^2_{\rm prior} = \sum_k \frac{(p_k - \tilde{p}_k)^2}{\tilde{\sigma}^2_{p_k}} \quad (9)$$

for each fit parameter p_k. This assumes that the prior probablility density function for each parameter is a

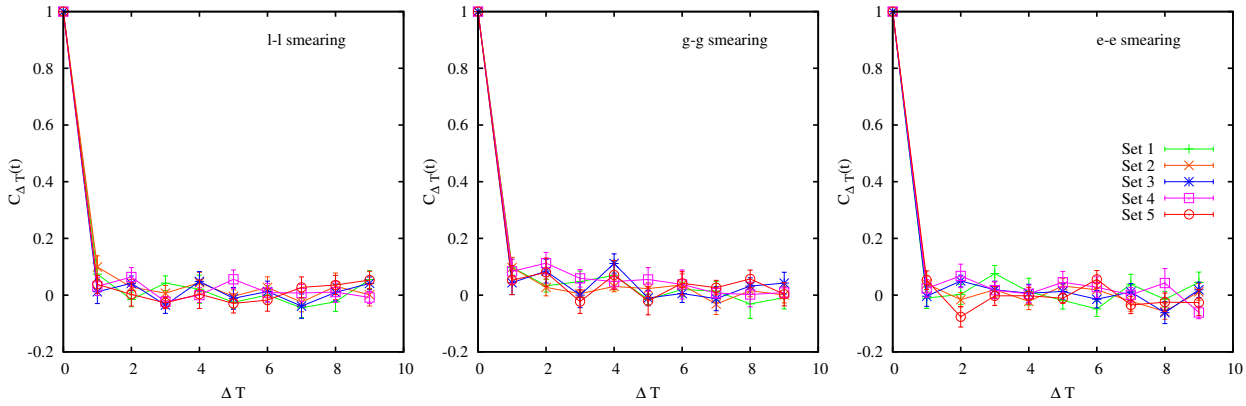

FIG. 1: Autocorrelation function $C_{\Delta T}$ for Υ correlators made from different smearing combinations, from left to right: ll, gg and ee. Different symbols are given to different ensembles according to the key on the right in the ee plot (color online). The correlators are evaluated at lattice time separation $t/a = 4$ on very coarse lattices (sets 1 and 2), $t/a = 5$ on coarse lattices (sets 3 and 4) and $t/a = 8$ on fine lattices (set 5). This corresponds to a t value where the gg correlators have reached the ground-state plateau and the ee correlators have a short plateau corresponding approximately to the first excited state mass. ΔT gives the separation at which the autocorrelation is measured in units of numbers in the ordered ensemble list.

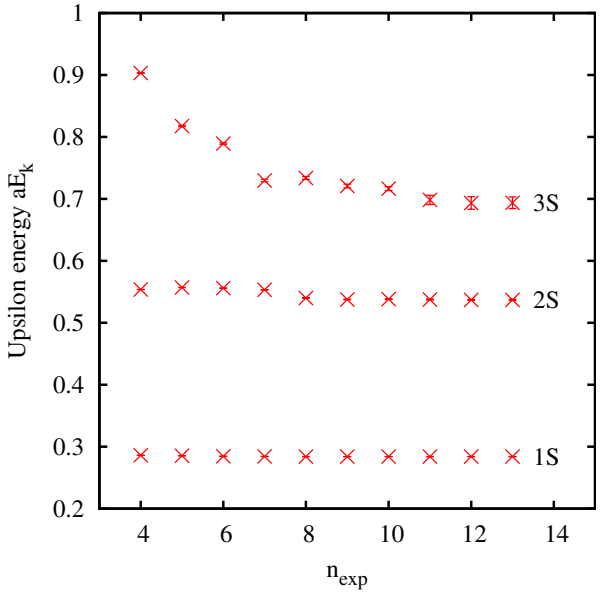

FIG. 2: Energies in lattice units of the low lying Υ states for the fine ensemble, set 5, from the full 5×5 lgeGE fit plotted against the number of exponentials, $n_{\rm exp}$, included in the fit.

Gaussian with central value p_k and width $\tilde{\sigma}_{p_k}$. The fit parameters are: the amplitudes, which are taken to have a prior of 0.1 ± 1.0; the ground state energies $\ln(E_0)$ which are estimated from an effective mass plot and given a suitably wide width; and the splittings $\ln(E_{n+1} - E_n)$ which prior information tells us should be of the order 500 MeV with a width of 250 MeV. Taking the fit parameters to be the logarithms of the energy splittings ensures that the ordering of the states is respected.

$\chi^2_{\rm aug}$ is minimised using the singular value decomposition (SVD) method. In the larger matrix fits, the correlation matrix can become ill-conditioned and it can be necessary to introduce a cutoff, $w_{\rm cut}$, on the lowest eigenvalues of the correlation matrix in order to fit the data. A variation of this method is used in which, instead of setting eigenvalues below $w_{\rm cut} w_{\rm max}$ to zero, they are set to $w_{\rm max}$ times $w_{\rm cut}$. This is a less severe truncation of the correlation matrix and it improves the fits in some cases. $w_{\rm cut}$ was typically taken to be 10^{-4} for the 5×5 matrix fits.

In order to determine whether the inclusion of five different smearing operators actually leads to improved results, the energies of the low lying Υ states are plotted in Figure 3 for a variety of different matrix fits from the fine ensemble. The effect on the precision of the ground state is negligible but the full 5×5 fit has significantly smaller errors for the first two excited states.

Because NRQCD is a nonrelativistic effective theory, there is an energy offset. Thus the energies obtained from correlators at zero momentum do not correspond to meson masses. Energy differences do correspond to mass differences, however and so, for example, the mass difference between the Υ' and the Υ (in lattice units) is given simply by $aE_2 - aE_1$ from equation 7. To obtain absolute mass values requires the study of correlators for mesons at nonzero spatial momentum as discussed in Sec. III C.

C. NRQCD systematics in tuning the b quark mass

In this calculation the parameters of QCD that need to be determined are the b quark mass and $\Lambda_{\rm QCD}$. In practice this translates into the fact that we need to tune the b quark mass parameter in the lattice NRQCD Hamiltonian until we obtain the correct value for one calibration hadron mass and we need to determine the lattice spacing from another calibration hadron mass. After that is done all other hadron masses are determined with no further tuning. The two calibration hadrons should be

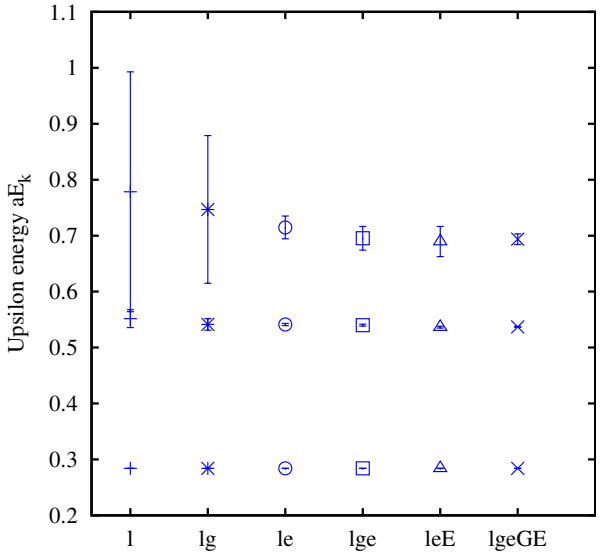

FIG. 3: Comparison of the effect of different smearing combinations for extraction of the energies of the ground and first two radially excited Υ states. The energy in lattice units from the fine ensemble is shown for a 1×1 l fit (plus), 2×2 fits lg (star) and le (circle), 3×3 fits lge (square) and leE (triangle), and the 5×5 fit containing all sources lgeGE (cross).

chosen with rather different properties. The mass chosen to fix the b quark mass should ideally be very sensitive to that value; the mass chosen to determine the lattice spacing should be as independent of the b quark mass as possible to avoid a complicated iterative tuning process. To determine the lattice spacing we choose the radial excitation energy of the Υ, i.e. $M(\Upsilon') - M(\Upsilon)$. This is known from experiment to be very insensitive to the heavy quark mass since it changes by only 4% between the b and the equivalent quantities for the c quark, which has a mass a factor of 4.5 smaller. The determination of the lattice spacing from this quantity will be discussed in section III E. Here we focus on the tuning of the b quark mass and in particular on the effect of the improvements to the NRQCD action which we have implemented here for the first time.

As discussed in section III B the fitted energy from a zero momentum hadron correlator made from NRQCD propagators is not the hadron's mass because there is an energy offset. Instead we must determine the 'kinetic mass' from the energy-momentum dispersion relation:

$$aM_{\rm Kin} = \frac{a^2P^2 - (a\Delta E)^2}{2a\Delta E}, \tag{10}$$

where $a\Delta E$ is the energy difference between the meson with momentum Pa in lattice units and the meson at rest. Equation 10 assumes a fully relativistic dispersion relation, i.e.

$$aE(P) = aE(0) + \sqrt{a^2P^2 + a^2M_{\rm Kin}^2}. \tag{11}$$

Systematic errors will then be present in the kinetic mass for lattice NRQCD both because the action is only accurate to a specific order in the expansion in v^2/c^2 and from lattice discretisation errors. Here we study both of these effects. First it is worth briefly recapitulating a discussion from the literature (see, for example, [34]) on how the kinetic mass is built up in a nonrelativistic approach as successive orders in v^2/c^2 are added to the nonrelativistic expansion, because it provides a useful handle on systematic errors.

By definition the mass of a meson is given by the sum of the masses of its constituent quarks plus the binding energy. The binding energy has contributions from the internal kinetic energy, i.e. the motion of the constituent quarks relative to the centre of mass, and from the interaction energy. If we write the meson dispersion relation in the standard nonrelativistic expansion as:

$$E(\mathbf{P}) = M_1 + \frac{\mathbf{P}^2}{2M_2} + \ldots \tag{12}$$

then M_1 is known as the static mass and M_2 is the kinetic mass, equal to $M_{\rm Kin}$ in equation 10 up to relativistic corrections. It should be possible to construct the correct meson mass from both M_1 and M_2 i.e. the binding energy contribution needs to feed correctly into both of them.

To see how this works in outline it is sufficient to study two free particles. The total energy of the two particle system is the sum of the masses, m_i, plus the kinetic energies, $\mathbf{q}_i^2/2m_i$ for each particle. In the center of mass frame ($\mathbf{P} = 0$) this is simply $m_1 + m_2$ plus the internal kinetic energy. As is well-known, the internal kinetic energy can be written to leading nonrelativistic order as $\mathbf{p}^2/2\mu$ where $\mathbf{p}$ is the momentum of either particle in this frame and μ is the reduced mass ($1/\mu = 1/m_1 + 1/m_2$). Thus M_1 takes the expected form for this two particle system. To study M_2 we must include the motion of the centre of mass and expand the sum of the two particle kinetic energies to $\mathcal{O}(\mathbf{P}^2)$. For M_2 to have the correct form including the leading piece of the internal kinetic energy we need $E(P)$ to take the form

$$\begin{aligned} E(P) &= m_{q1} + m_{q2} + \frac{\mathbf{p}^2}{2\mu} + \ldots \\ &+ \frac{\mathbf{P}^2}{2(m_{q1}+m_{q2})}\left(1 - \frac{\mathbf{p}^2}{2\mu(m_{q1}+m_{q2})} + \ldots\right) \end{aligned} \tag{13}$$

i.e. we need to locate a $\mathbf{P}^2\mathbf{p}^2$ term in the sum of the individual particle kinetic energies. This requires the individual kinetic energies to be expanded beyond leading order in the nonrelativistic expansion to include terms at fourth order in the momentum. Thus M_2 will have the correct form to leading order in the internal kinetic energy if the individual kinetic energy terms are correct through next-to-leading-order in momentum. In an interacting theory we also need the interaction terms to be correct through $\mathcal{O}(v^4)$ to have the binding energy correctly included in the kinetic mass.

These issues are discussed in some detail in [34] for heavy quarks using the clover action since there are

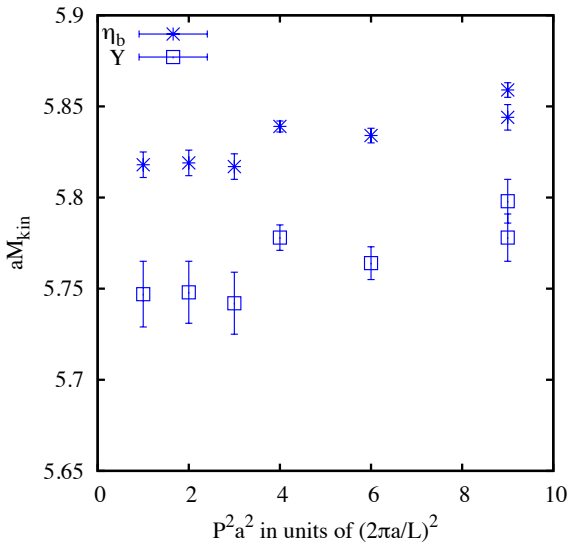

FIG. 4: Kinetic mass values in lattice units obtained on the coarse ensemble, set 3, for the am_b and c_i values given in Tables II and III. Kinetic mass values are given separately for the Υ and η_b and plotted against the square of the lattice momentum in units of $2\pi a/L$. The two results at x-axis value of 9 correspond to momenta with indices $(3,0,0)$ and $(2,1,1)$. The higher one is (3,0,0).

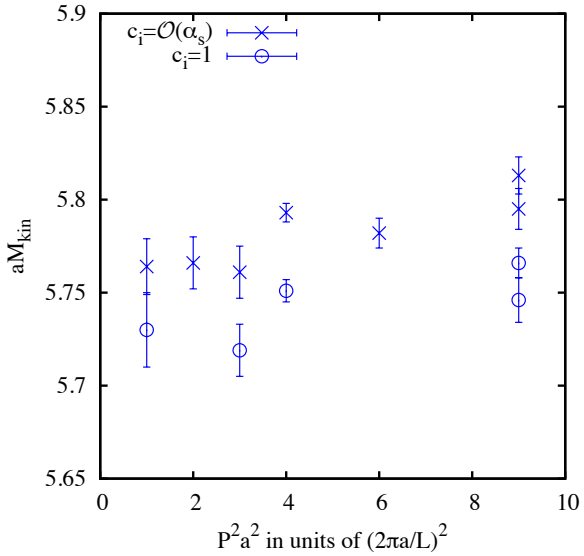

FIG. 5: Spin-averaged values for the kinetic mass in lattice units obtained on the coarse ensemble, set 3, for $am_b = 2.66$ (as in Table III). Results for the c_i values given in Table II are compared to the results for $c_i = 1$. The kinetic mass is plotted against the square of the lattice momentum in units of $2\pi a/L$.

important differences in discretisation errors there between choosing M_1 or M_2 as the appropriate meson mass against which to tune the quark mass. In NRQCD we must use M_2 ($M_{\rm Kin}$). The quark Hamiltonian given in equation 2 has no quark mass term, so to reconstruct the meson mass from M_1 would require adding back in the zero of energy. This is perturbatively calculable but we wish the tune the quark mass fully nonperturbatively. M_2 on the other hand acquires its quark mass pieces from the quark kinetic energy terms and so has no zero of energy problem. As discussed above, M_2 will also correctly include the internal kinetic energy if the v^4 relativistic corrections to the kinetic energy are included in the quark Hamiltonian, as they are in equation 2. Indeed we are now including the radiative corrections to the v^4 kinetic terms through adjustments to c_1, c_5 and c_6, and we will show below the effect that this has.

We can determine the kinetic mass very precisely by use of propagators made starting with a random wall source patterned by an $\exp(i\mathbf{p}\cdot\mathbf{x})$ factor to give the quark momentum [31]. We use only a $\delta(x)$ smearing function for these calculations so they are very fast, but we must evolve both a quark and an antiquark propagator because the complex conjugate of a quark propagator of momentum $\mathbf{p}$ is an antiquark of momentum $-\mathbf{p}$. Typically we take quark and antiquark momenta to be equal so that the meson momentum, when they are combined, is $\mathbf{P} = 2\mathbf{p}$.

We fit the meson correlator of momentum $\mathbf{P}$ simultaneously with the meson correlator at rest so that the energy difference $a\Delta E$ between the ground state energies can be

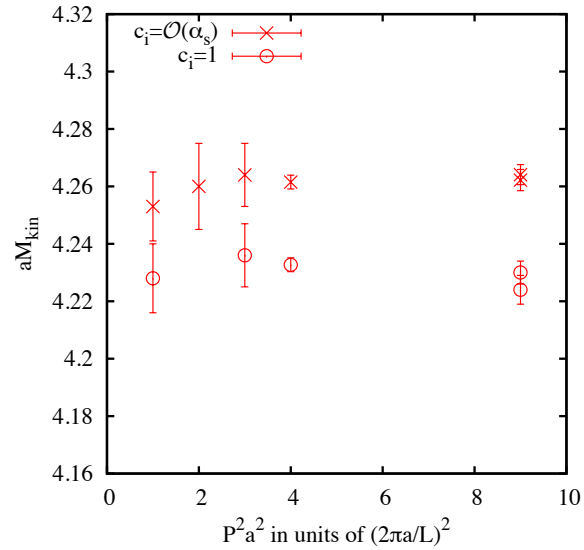

FIG. 6: Spin-averaged values for the kinetic mass in lattice units obtained on the fine ensemble, set 5, for the am_b and c_i values given in Tables II and III, compared to the results for $c_i = 1$. The kinetic mass is plotted against the square of the lattice momentum in units of $2\pi a/L$.

determined directly by the fit taking the correlations into account. In this way we obtain $a\Delta E$ values with errors typically in the 5th decimal place. To avoid cluttering the main body of the text, the detailed tables of values for Υ and η_b energies as a function of momentum and $aM_{\rm kin}$ are collected in Appendix D. Propagators were

calculated for the full number of configurations given for each ensemble in Table III, but in some cases we used fewer time sources per configuration than is given there.

We can then plot out the kinetic mass for a range of meson momenta to study systematic effects in equation 10 which would show up as a disagreement between kinetic masses obtained from different momentum values. Previous calculations saw no significant differences in kinetic mass values for momenta up to $P^2a^2 = 9$ with errors of around 1% [2]. This is equivalent to a test, as a function of momentum, of the constancy of the 'speed of light'. Here we are able to achieve errors down to 0.1%, depending on the momentum. Then systematic variations of $aM_{\rm Kin}$ with momentum can be seen at the 0.5% level.

$aM_{\rm Kin}$ values for Υ and η_b mesons on the coarse lattices, set 3, are plotted in Figure 4 and show several features. One is that there is a systematic difference between the values of $aM_{\rm Kin}$ for on-axis (those in one lattice direction only) and off-axis momenta. This was hinted at in [2] but the errors were too large for it to be clear. The on-axis kinetic masses are higher, and this reflects a breaking of rotational invariance on the lattice which is a discretisation error. It is particularly obvious for the momenta with components along the spatial directions labelled by integers (3,0,0) and (2,2,1), both of which have $P^2a^2 = 9(2\pi a/L)^2$. The difference is tiny but visible. We will return to this point below.

Another feature of Figure 4 is that the kinetic mass for the η_b is above that of the Υ which is the opposite way round to the energy difference at zero momentum and to experiment. A similar but somewhat smaller effect is seen on the fine lattices. The discussion above on the way in which the meson kinetic mass is built up order by order in the nonrelativistic expansion shows how this has happened. It results from the fact that the $\sigma \cdot B$ term that gives rise to the hyperfine splitting is only included at leading order in our NRQCD action, equation 2. Relativistic corrections to this term would be needed for it to feed correctly into the kinetic mass, M_2. The effect of the $\sigma \cdot B$ term splitting is correctly incorporated in the meson energy at zero momentum (M_1), however, and it is from differences in M_1 for Υ and η_b that we determine the hyperfine splitting (see subsection III E 3). This small but non-zero systematic error in M_2 is simply removed by working instead with the spin-averaged kinetic mass of the Υ and η_b:

$$\overline{M}_{\rm Kin}(1S) = \frac{(3M_{\rm Kin}(\Upsilon) + M_{\rm Kin}(\eta_b))}{4} \qquad (14)$$

and using this to fix the b quark mass.

The above arguments also allow insight into the effect of radiative corrections to the v^4 kinetic terms in the NRQCD Hamiltonian that we include here for the first time. Changing the coefficient of the $p^4/8m_b^3$ term, c_1, from 1 to $1 + \mathcal{O}(\alpha_s)$ will modify the amount of the internal kinetic energy that is incorporated into the meson kinetic mass, effectively correcting for an $\mathcal{O}(\alpha_s)$ mismatch between this contribution to M_1 and M_2 from binding energy effects. The effect of this radiative correction is seen clearly in Figure 5 where we compare the spin-averaged kinetic mass with all c_i set to 1 to that from having the radiatively improved coefficients given in Table II. The difference would be expected to be $\mathcal{O}(\alpha_s \times B)$ where B is the binding energy of $\mathcal{O}(500$ MeV). This could in principle be as large as 150–200 MeV. From Figure 5 we see that the effect is somewhat smaller than this on the coarse ensemble set 3 – a shift of kinetic mass of 0.05 in lattice units corresponds to around 80 MeV on these lattices. The shift is clearly visible, however. The radiative correction acts to increase the kinetic mass for a given bare b quark mass. This is because $c_1 > 1$ and the binding energy is positive. Thus the correctly tuned quark mass will be lower (by the same percentage shift as that for the kinetic mass) when radiative corrections are included. A similar shift is observed on the fine lattices as shown in Figure 6.

Remaining systematic errors from higher order radiative corrections to v^4 terms in the NRQCD action will be suppressed by a further power of α_s beyond the shift seen here. We therefore expect the remaining error in the kinetic mass from this source to be $\mathcal{O}(0.3\%)$. Systematic errors from missing higher order, v^6, terms at tree level in the NRQCD action are a factor of v^2, or 10%, smaller than the size of the effect of v^4 terms, and therefore of similar size to missing $\alpha_s^2 v^4$ terms. They will also have the effect of correcting for momentum-dependence in $M_{\rm Kin}$. From Figure 5 we can see that there is a sign of an upward drift of $M_{\rm Kin}$ with momentum but the effect is smaller than the shift of $M_{\rm Kin}$ with the radiative correction to the c_i coefficients.

We now return to the issue of discretisation errors in the kinetic mass. These arise from the replacement of time and space derivatives in the NRQCD action with finite differences on the lattice. The terms with coefficients c_5 and c_6 contain a^2v^4 and av^4 correction terms to remove these errors. With the inclusion of radiative corrections to c_5 and c_6, the remaining errors are at $\mathcal{O}(\alpha_s^2 a^2 v^4)$ in this calculation. The term with coefficient c_5, i.e. the term proportional to $\Delta^{(4)}$ is of interest because this is rotationally non-invariant. The signal for a lack of continuum rotational invariance in our results is a disagreement between the kinetic mass for on-axis momenta, that typically have a high value for P_i^4, and off-axis momenta. This was seen in Figure 4 for the coarse lattices. Less variation is evident on the fine lattices (Figure 6), as expected for a discretisation effect.

To make clearer the way in which the rotationally non-invariant discretisation errors depend on the lattice spacing Figure 7 plots the energy difference in physical units between mesons with momentum (3,0,0) and (2,2,1) as a function of a^2 using results from all three values of the lattice spacing. $P^2a^2 = 9(2\pi a/L)^2$ corresponds to approximately the same physical momentum at all three lattice spacing values, so the results should be a good test of how rotational invariance is restored as $a \to 0$. In

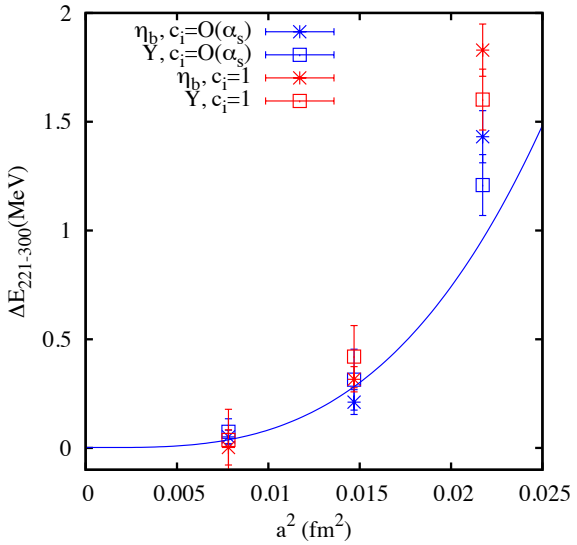

FIG. 7: The energy difference in MeV between mesons with momentum (3,0,0) and (2,2,1) in units of $2\pi a/L$ on the lattice plotted against the square of the lattice spacing in fm. Results are shown for the case $c_{1,5,6} = 1$ as well as for $c_{1,5,6}$ taking their α_s-improved values. An example fit curve with a^4 and a^6 dependence is shown through the Υ data for $c_{1,5,6}$ α_s-improved.

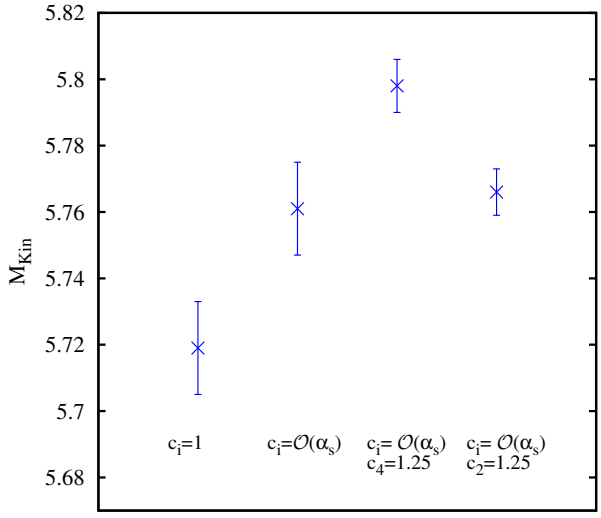

FIG. 8: Comparison of values obtained for the kinetic mass from a variety of different parameter values on coarse set 3.

fact the energy difference is tiny on all except the very coarse lattices, where it reaches 1 MeV. The case in which the $c_{1,5,6}$ coefficients are set to their tree level values of 1 is plotted as well as the case with the $c_{1,5,6}$ coefficients taking the radiatively improved values that we have used for the rest of our calculation here. The radiatively improved values give very slightly smaller energy splittings, since they have improved the a^2 contribution to this error by one order in α_s to $\alpha_s^2 a^2 v^4$. The energy difference between mesons with momentum (3,0,0) and (2,2,1) also has contributions at $\mathcal{O}(a^4 v^6)$, however, and both the effect of radiative improvement and the shape of the curve in Figure 7 tend to imply that these a^4 terms dominate over any remaining a^2 terms.

Rotationally invariant discretisation errors would give rise to a kinetic mass that varied with P^2. This is the same effect as that of relativistic errors, because the correcting operators are the same. Discretisation errors require an a-dependent coefficient to correct them. However, as discussed above under relativistic corrections, there is no sign in our results of such errors to better than 0.5%.

The conclusion from this subsection is that, to minimise systematic errors, we should tune the b quark mass by calculating the spin-averaged kinetic mass $\overline{M}_{\rm Kin}(1S)$ and matching that to experiment. We do this from the comparison of meson energies at zero momentum and the 'maximally off-axis' momentum (1,1,1) to minimise discretisation errors. Table V gives results for this kinetic mass on all ensembles for the given values of the b quark mass and coefficients, c_i. To convert these results to physical units we need a value for the lattice spacing to be determined in subsection III E. Table V gives statistical/fitting errors on the values. As discussed above, remaining systematic errors from missing radiative, relativistic and discretisation errors amount to a total of 0.5%. We are able to pin down the size of these systematic errors by using the improved methods described here to study the dispersion at this level of detail.

Figure 8 compares the results for the spin-averaged kinetic mass on the coarse ensemble, set 3 for a variety of different choices for the coefficients in the NRQCD action to show the size of variations in the kinetic mass. The figure shows that we can see the difference between taking tree-level values for $c_{1,5,6}$ and radiatively improved values. Changing c_2 (the coefficient of the Darwin term) has very little effect. The effect of changing c_4 (the coefficient of the $\sigma \cdot \mathbf{B}$ term which should be spin-averaged away at leading order in this kinetic mass) is also not large. Another check of this is given in Table V on set 1.

The experimental result for the Υ mass is 9.4603(3) GeV and that of the η_b, 9.391(3) GeV, [35] giving a spin-average of 9.443(1) GeV. The real world includes effects that are missing from our lattice calculation, however, and so we must correct for this. Electromagnetism affects the Υ and η_b approximately equally and, from a potential model we estimate that it reduces their masses by 1.6 MeV [14]. In addition the η_b can annihilate to gluons and we estimate that this effect also reduces its mass by 2.4 MeV, taking the same value as that estimated for the η_c [16]. The 'experimental' mass that we should compare our results to is then increased from above to 9.445(2) GeV where we allow for a 100% error in our estimate of the shifts in the masses [60].

Set	am_b	$c_{1,5,6}$	c_2	c_4	$aM_{\rm Kin}(\Upsilon)$	$aM_{\rm Kin}(\eta_b)$	$a\overline{M}_{\rm Kin}(1S)$
1	3.42	α_s	1	1	7.269(18)	7.405(10)	7.303(15)
1	3.42	α_s	1	1.22	7.271(22)	7.472(10)	7.321(18)
2	3.39	α_s	1	1	7.228(10)	7.345(4)	7.257(8)
2	3.42	α_s	1	1	7.310(14)	7.423(7)	7.338(13)
3	2.66	1	1	1	5.703(17)	5.767(7)	5.719(14)
3	2.66	α_s	1	1	5.742(17)	5.817(7)	5.761(14)
3	2.66	α_s	1.25	1	5.748(8)	5.823(4)	5.766(7)
3	2.66	α_s	1	1.25	5.767(10)	5.889(4)	5.798(8)
4	2.62	α_s	1	1	5.706(9)	5.761(4)	5.719(7)
4	2.66	α_s	1	1	5.778(11)	5.833(5)	5.792(10)
5	1.91	1	1	1	4.230(13)	4.252(6)	4.236(11)
5	1.91	α_s	1	1	4.256(14)	4.287(6)	4.264(11)
5	2.0	α_s	1	1	4.431(11)	4.466(5)	4.439(10)

TABLE V: Summary of the kinetic masses obtained on different ensembles for a variety of parameter values. We use the energy difference between lattice momentum zero and momentum $a\mathbf{p} = (1,1,1)$ in units of $2\pi a/L$. The column $c_{1,5,6}$ denotes whether the $\mathcal{O}(\alpha_s)$ improved coefficients were used in the action and the columns c_2, c_4 indicate additional values of those coefficients that were run on coarse set 3 and very coarse set 1 to estimate systematic errors.

D. NRQCD systematics in radial and orbital splittings

Here we discuss the remaining sources of systematic error in our calculation of the radial and orbital excitation energies. These systematic errors will feed subsequently into the determination of the lattice spacing from the Υ $2S-1S$ splitting.

Radial and orbital excitation energies arise at leading order from the time derivative and H_0 in the NRQCD action (equation 2). The relativistic corrections at v^4 in δH thus provide relative $\mathcal{O}(v^2) \approx 10\%$ corrections to these splittings. Missing radiative corrections to the v^4 terms dominated the errors in earlier calculations [2, 11], since $\alpha_s v^2 \approx 2{-}{-}3\%$ is larger than $v^4 \approx 1\%$ from missing higher order relativistic corrections. We now include for the first time the radiative corrections to most of the v^4 terms in δH. The remaining errors are then largely at relative $\mathcal{O}(\alpha_s^2 v^2)$, i.e. less than 1%.

Table VI lists the remaining systematic errors from spin-independent terms in the $2S-1S$ and $1P-1S$ splittings in more detail following [2]. The errors were determined using a potential model to make estimates of the energy shifts in each of the $1S$, $2S$ and $1P$ states. For example, radiative corrections at $\mathcal{O}(\alpha_s^2)$ to the $p^4/(8m_b^3)$ term in the NRQCD action give shifts of size $\alpha_s^2 < p^4 > /4m_b^3$ where $< p^4 >$ is the expectation value of p^4 in that state.

The effects of the Darwin term term appear at $\mathcal{O}(\alpha_s v^4)$ since we have not included a radiative correction to c_2. However, since this term vanishes in the free theory it is already suppressed by an additional power of α_s. Its effects are proportional to the square of the wavefunction at the origin so it does not affect P-wave states. A very similar term arises from missing spin-independent 4-quark opertors. The spin-dependent 4-quark operators are discussed in Appendix B along with the coefficients they have in order to match NRQCD to QCD. The spin-independent ones arise from the same diagrams and the calculation of their coefficients is in progress. Here we take an error from missing these 4-quark operators which is of the same size as the error from radiative corrections to the Darwin term.

Note that errors cancel to a significant extent between the $2S$ and $1S$ states because of their similarities [2]. This is the reason for focussing on the $2S-1S$ splitting to determine the lattice spacing, because it has the smallest systematic error.

We see from Table VI that the largest remaining systematic error is now that from missing v^6 terms. The key kinetic term at v^6 that would appear in a higher order NRQCD action is $-(\Delta^{(2)})^3/(16(am_b)^5)$ at tree level. This term is proportional to $+(v^2)^3$ and so, if it dominates the v^6 errors, they will have the same sign at every value of the lattice spacing. Including this v^6 term would act in the direction of reducing both the $2S-1S$ and $1P-1S$ splitting but the $1P-1S$ splitting would be reduced the most.

Table VII similarly quantifies remaining systematic errors from missing α_s^2 radiative corrections to the discretisation correction terms with coefficients c_5 and c_6. These are significantly reduced over our earlier calculations [2] now that the α_s radiative corrections are included. In addition the gluon action is now improved completely through $\mathcal{O}(\alpha_s^2 a^2)$ [20] and this means that the discretisation errors coming from the gluon action are similarly reduced.

We can estimate the size of a^4 errors from the analysis in subsection III C where we study discretisation errors in the kinetic mass. The energy difference between mesons of momenta $(3,0,0)$ and $(2,2,1)$ in units of $2\pi a/L$ can be taken as a measure of at least the rotationally non-invariant a^4 errors, as discussed there. The energy difference (Figure 7) is barely visible except on the very coarse lattices where it amounts to 1 MeV, or 0.2% of the $2S-1S$ splitting. This is much less than the esti-

Correction	relativistic	radiative kinetic	radiative Darwin	4-quark spin-independent	**Total** relativistic + radiative
Form	$\delta p^6/(m_b)^5$	$\alpha_s^2\delta p^4/4(m_b)^3$	$4\pi\alpha_s^2\psi(0)^2/(3m_b^2)$	$\alpha_s^2\psi(0)^2/m_b^2$	
Est. %age in $2S-1S$					
very coarse	0.5	0.2	0.4	0.4	0.8
coarse	0.5	0.15	0.3	0.3	0.7
fine	0.5	0.1	0.2	0.2	0.6
Est. %age in $1P-1S$					
very coarse	1.0	0.7	0.9	0.9	1.8
coarse	1.0	0.5	0.7	0.7	1.5
fine	1.0	0.3	0.4	0.4	1.2

TABLE VI: An estimate of systematic errors in the $2S-1S$ and $1P-1S$ splittings in the Υ in our lattice QCD calculation arising from missing higher order relativistic and radiative corrections to the NRQCD action that we use (equation 2).

Correction	discretisation in NRQCD action (i)	discretisation in NRQCD action (ii)	discretisation in gluon action	**Total** discretisation
Form	$\alpha_s^2 a\delta p^4/8n(m_b)^2$	$\alpha_s^2 a^2\delta p_i^4/12m_b$	$4\pi\alpha_s^2 a^2\psi(0)^2/15$	
Est. %age in $2S-1S$				
very coarse	0.2	0.4	0.3	0.5
coarse	0.1	0.2	0.15	0.3
fine	0.05	0.06	0.05	0.1
Est. %age in $1P-1S$				
very coarse	0.7	2.0	1.0	2.3
coarse	0.4	1.0	0.5	1.2
fine	0.2	0.3	0.1	0.4

TABLE VII: An estimate of systematic errors in the $2S-1S$ and $1P-1S$ splittings in the Υ in our lattice QCD calculation arising from discretisation errors in the NRQCD and gluon actions.

mate of remaining a^2 errors in that case so we do not include it in Table VII.

E. Results

1. *Radial and orbital excitation energies*

Our main results for the fitted energies for the ground-state and first two radial excitations of the Υ and η_b are given in Table VIII. The values come from multi-exponential fits to a 5×5 matrix of correlators for each meson as described in section III B. We take 9 exponentials on sets 1, 2 and 3; 11 exponentials on set 4 and 12 on set 5. We also give the fitted ground-state energy for the $h_b(1P)$ state on sets 3 and 5 from a 5 exponential fit to 2×2 matrix of correlators. The b quark masses and coefficients, c_i, used in the NRQCD action are those of Tables II and III. Errors are very small on the ground-state S-wave masses but increase rapidly with the radial excitation number. The table also includes energy splittings in lattice units for radial and orbital excitations.

As explained earlier we can use the radial excitation energy, $M(\Upsilon')-M(\Upsilon)$, to fix the lattice spacing, by setting

$$a^{-1}(\mathrm{GeV}) = \frac{0.5630(9)}{aE(2^3S_1)-aE(1^3S_1)}. \qquad (15)$$

0.5630(4) GeV is the experimental mass difference and we have increased the error to allow for a possible relative shift in the two masses as a result of the electromagnetic attraction between quark and antiquark missing in our calculation. As discussed earlier, a potential model estimate would give a shift of 1.6 MeV to the Υ from the electrostatic attraction between quark and antiquark, and somewhat less for the Υ' since typical separations between quark and antiquark are larger. We do not shift the result but allow for an error of 0.8 MeV.

As long as we deal with spin-averaged splittings we do not have to consider errors in spin-dependent terms. However, for the $2S-1S$ splitting the match to experiment cannot be spin-averaged since no experimental information is available for the $\eta_b(2S)$. In that case we have to consider sources of systematic error in the hyperfine splitting that will induce errors in the Υ and Υ' energies. This will discussed further in subsection III E 3.

The main source of error is from missing radiative corrections when we take the coefficient of the $\sigma\cdot B$ term, c_4, to be 1. In section III E 3 we compare results for $c_4=1$ to those from c_4 corrected perturbatively through $\mathcal{O}(\alpha_s)$ and nonperturbatively, to give the correct 1^3P fine structure. Both methods for correcting c_4 give values above 1 and increase the lattice result for the hyperfine splitting (which is proportional to c_4^2 at leading order). Thus with $c_4=1$ the Υ energy is too low. Since $M(\Upsilon)=M(1\overline{S})+(M(\Upsilon)-M(\eta_b))/4$, the shift from c_4 in

	1	2	3	4	5
$aE(1^1S_0)$	0.25080(5)	0.25361(3)	0.26096(3)	0.26524(2)	0.25851(2)
$aE(2^1S_0)$	0.6898(16)	0.6909(8)	0.6235(8)	0.6246(6)	0.5248(7)
$aE(3^1S_0)$	0.975(14)	0.940(22)	0.849(9)	0.854(4)	0.677(11)
$aE(1^3S_1)$	0.28532(6)	0.28809(3)	0.29245(3)	0.29681(2)	0.28405(2)
$aE(2^3S_1)$	0.7078(14)	0.7074(8)	0.6416(7)	0.6393(9)	0.5370(9)
$aE(3^3S_1)$	0.988(16)	0.975(8)	0.855(11)	0.867(10)	0.693(10)
$aE(2\overline{S}-1\overline{S})$	0.4266(11)	0.4238(7)	0.3525(6)	0.3467(7)	0.2563(7)
$aE(3\overline{S}-1\overline{S})$	0.708(12)	0.687(8)	0.569(9)	0.575(8)	0.411(8)
$aE(2^1S_0-1^1S_0)$	0.4390(16)	0.4373(8)	0.3626(8)	0.3594(6)	0.2663(7)
$aE(3^1S_0-1^1S_0)$	0.724(14)	0.687(22)	0.588(9)	0.588(4)	0.418(11)
$aE(2^3S_1-1^3S_1)$	0.4225(14)	0.4193(8)	0.3492(7)	0.3425(9)	0.2530(9)
$aE(3^3S_1-1^3S_1)$	0.703(16)	0.687(8)	0.563(11)	0.570(10)	0.409(10)
R_S	1.664(38)	1.638(19)	1.611(32)	1.665(31)	1.617(40)
$a\Delta$	0.00190(1)	0.00190(1)	0.00151(1)	0.00151(1)	0.00091(1)
$aE(1^1P_1)$	-	-	0.5654(23)	-	0.4833(10)
$aE(1^1P_1-1\overline{S})$	-	-	0.2809(22)	-	0.2056(10)
R_P	-	-	0.808(7)	-	0.816(5)
$aE(1^3S_1-1^1S_0)$	0.03452(8)	0.03448(4)	0.03149(4)	0.03157(3)	0.02554(3)
$aE(2^3S_1-2^1S_0)$	0.0180(21)	0.0165(11)	0.0181(11)	0.0147(10)	0.0122(11)
R_H	0.521(62)	0.479(33)	0.575(35)	0.465(34)	0.478(45)

TABLE VIII: Radial, orbital and S-wave fine structure splittings in lattice units for sets 1 to 5 for the NRQCD parameters and coefficients given in Tables II and III. $c_3 = c_4 = 1.0$. Errors are statistical/fitting only. R_S, R_P and R_H are defined in the text.

	3	4	5
c_3	1.0	1.0	1.0
c_4	1.25	1.25	1.10
$aE(1^1S_0)$	0.20943(3)	0.21289(2)	0.23204(2)
$aE(2^1S_0)$	0.5796(6)	0.5777(7)	0.5021(12)
$aE(3^1S_0)$	0.788(12)	0.802(6)	0.660(12)
$aE(1^3S_1)$	0.25628(4)	0.25978(2)	0.26206(3)
$aE(2^3S_1)$	0.6022(7)	0.5999(7)	0.5170(18)
$aE(3^3S_1)$	0.827(7)	0.821(5)	0.663(24)
$aE(2\overline{S}-1\overline{S})$	0.3520(6)	0.3463(6)	0.2584(13)
$aE(3\overline{S}-1\overline{S})$	0.573(6)	0.568(4)	0.405(18)
$aE(2^1S_0-1^1S_0)$	0.3702(6)	0.3648(7)	0.2701(12)
$aE(3^1S_0-1^1S_0)$	0.579(12)	0.589(6)	0.428(12)
$aE(2^3S_1-1^3S_1)$	0.3460(7)	0.3401(7)	0.2549(18)
$aE(3^3S_1-1^3S_1)$	0.571(7)	0.561(5)	0.401(24)
R_S	1.651(20)	1.650(15)	1.573(95)
$aE(1^1P_1)$	0.5247(22)	0.5253(20)	-
$aE(1^1P_1-1\overline{S})$	0.2801(22)	0.2773(20)	-
R_P	0.810(7)	0.815(6)	-
$aE(1^3S_1-1^1S_0)$	0.04684(5)	0.04689(3)	0.03003(4)
$aE(2^3S_1-2^1S_0)$	0.0226(9)	0.0222(10)	0.0149(22)
R_H	0.482(19)	0.473(21)	0.496(73)

TABLE IX: Radial, orbital and S-wave fine structure splittings in lattice units for sets 3, 4 and 5 with NRQCD coefficients and parameters as in Tables II and III. In addition c_4 is nonperturbatively tuned taking values from Table XIII. $c_3 = 1$ for all results. Errors are statistical/fitting only. Reduced statistics of 400 configurations were used for the S-wave states from set 5. R_S, R_P and R_H are defined in the text.

the Υ mass is one quarter of the change in the hyperfine splitting. In section III E 3 we also determine the ratio of the $2S$ hyperfine splitting to that of the $1S$ hyperfine splitting and find a result close to 0.5, independent of c_4. Thus the shift from a change in c_4 to the $2S-1S$ splitting is one eighth of change in the 1S hyperfine splitting. An increase in c_4 above 1 reduces the $2S-1S$ splitting. From Table XIV we can compare results for the 1S hyperfine splitting for $c_4 = 1$ to the value obtained for c_4 improved through $\mathcal{O}(\alpha_s)$ for sets 1, 3 and 5. Dividing by 8 then gives shifts in lattice units that can be applied to correct the $2S-1S$ splitting on very coarse, coarse

Set	a_Υ (fm)	a_{η_s} (fm)	$a_{r_1/a}$ (fm)
1	0.1474(5)(14)(2)	0.1546(10)(5)	0.1569(8)(13)
2	0.1463(3)(14)(2)	0.1526(6)(5)	0.1553(3)(13)
3	0.1219(2)(9)(2)	0.1234(7)(4)	0.1244(2)(10)
4	0.1195(3)(9)(2)	0.1218(5)(4)	0.1221(5)(10)
5	0.0884(3)(5)(1)	0.0899(6)(3)	0.0902(3)(7)

TABLE X: Lattice spacing values in fm determined from several methods. The first column gives results from the Υ $2S-1S$ splitting. The first error is from statistics/fitting, the second from remaining systematic errors from the NRQCD action (from Tables VI and VII) and the third is a correlated 0.2% error from experiment and electromagnetic corrections. The second column gives lattice spacing values from the decay constant of the η_s meson as described in section IV. The first error is from statistics/fitting and the second is a correlated 0.3% error from the uncertainty in the physical value of f_{η_s} as discussed in section IV. The third column gives lattice spacing values determined from r_1/a values in Table I. The first error is from statistics/fitting and the second is a correlated 0.8% error from the uncertainty in the physical value of r_1 as discussed in section V.

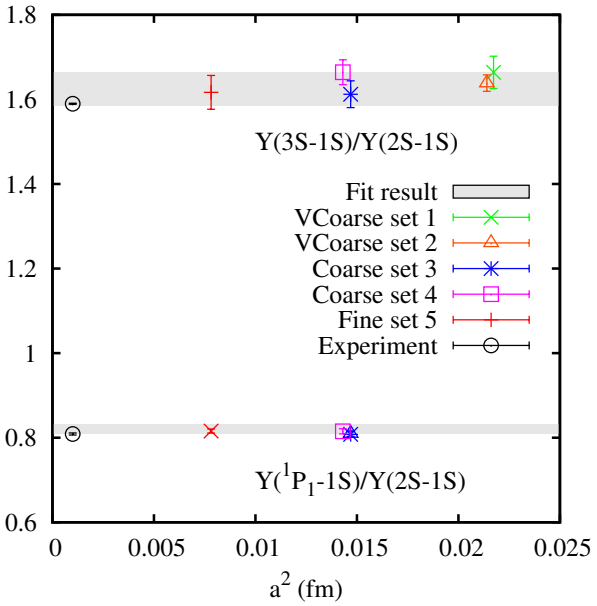

FIG. 9: Results for the ratio of the $3S-1S$ and $1P-1S$ splittings to the $2S-1S$ in the Υ system plotted against the square of the lattice spacing determined from the $2S-1S$ splitting. The grey shaded bands give the physical result obtained from a fit to the data as described in the text. The black open circles slightly offset from $a=0$ are from experiment [35].

and fine lattices. These shifts are denoted by $a\Delta$ in Table VIII, and are to be subtracted from the $2S-1S$ splitting to give the corrected lattice result. It can be seen that $a\Delta$ is not much larger than the statistical errors on the $2S-1S$ splitting. The statistical error in $a\Delta$ is negligible, but there is a systematic error which is taken as $0.5\times a\Delta$. This accounts for the errors in the hyperfine splitting from 4-quark operators, higher order radiative corrections to c_4 and relativistic corrections to the $\sigma\cdot\mathbf{B}$ term. This error is then included in the systematic error for the corrected $2S-1S$ splitting.

Note that we do not expect the spin-orbit term with coefficient c_3 to have significant effect on the S-wave states. In any case our nonperturbative determination of c_3 discussed in Appendix C gives a result consistent with the value of 1.0 that we are using. Possible errors from radiative corrections to c_2 are included in our systematic error budget for NRQCD (Table VI).

Table X gives the values of the lattice spacing in fm obtained from the $2S-1S$ splitting on each ensemble, along with their associated statistical/fitting error and systematic error. The systematic errors are combined in quadrature from Tables VI and VII and from $a\Delta$ in Table VIII. The systematic errors are dominated by those from missing higher order relativistic corrections to the NRQCD action and these will be correlated to some extent between ensembles. There is an additional overall systematic error of 0.2% coming from the experimental value for the splitting and electromagnetic effects missing from our calculation.

In Table IX we give results for cases where c_4 is set to its nonperturbatively tuned value on sets 3, 4 and a test value of 1.10 on set 5 (the nonperturbatively tuned value is in fact 1.18, see Appendix C). Changing c_4 shifts the fitted energies of all the states but this is simply because the zero of energy has changed. As expected, changing c_4 has very little effect on splittings between spin-averaged S wave states or between the $^1P_1$ mass and the spin-averaged $1S$ state.

An important test of the results is whether, using these values for the lattice spacing, we get results in agreement with experiment for other mass differences i.e. whether ratios of splittings are correct. In our previous work on 2+1 flavor gluon configurations [2] agreement with experiment was found within 3% statistical/systematic errors. Here we have substantially improved errors, including improved statistical errors, so we can improve on our earlier analysis.

Table VIII gives values for the ratios of the Υ $3S-1S$ and $1^1P_1-1\overline{S}$ splittings to the Υ $2S-1S$ splitting from our results for $c_4=1$. Table IX gives the same ratios for the case where c_4 takes its nonperturbatively tuned value. In forming the ratio $R_P=(1^1P_1-1\overline{S})/(2^3S_1-1^3S_1)$ for the case $c_4=1$ we correct the denominator for c_4 errors using the $a\Delta$ values in Table VIII. The numerator should not be sensitive to c_4 because the S-state energies have been spin-averaged and the $^1P_1$ state is unaffected by c_4, as discussed in Appendix C. Both the Υ $3S-1S$ and $2S-1S$ splittings will have some sensitivity to c_4. However, any shifts will cancel between the two splittings up to an amount equal to one quarter of the difference in the $3S$ and $2S$ hyperfine splittings. This is negligible compared to statistical errors in this ratio. The ratio $R_S=(3^3S_1-1^3S_1)/(2^3S_1-1^3S_1)$ in Table VIII is therefore not corrected for c_4.

The ratio R_S from Table VIII, where we have results

for all five sets, is plotted against the square of the lattice spacing in Figure 9. We see very little dependence on lattice spacing and on the u/d sea quark mass (the s and c sea quark masses are already well-tuned to their physical values, see section IV). Figure 9 also shows results for R_P, combining results from Tables VIII and IX since we have results for only 2 ensembles in each table. The results change very little between the ensembles, however, as Figure 9 shows.

To derive a physical value for each ratio we can use the results to fit for the dependence on these two quantities and then determine the result at physical sea quark mass and at $a = 0$ to compare to experiment. For the sea u/d quark mass dependence a simple polynomial in m_l/m_s (values in Table I) suffices because the m_l values are already very close to the physical point with $m_l/m_s = 0.1$ and 0.2. The dependence on the lattice spacing is more complicated because in NRQCD we must allow for unphysical a-dependence coming from am_b-dependent radiative corrections to discretisation errors. This am_b-dependence is mild when am_b is sufficiently large, as here, and this is seen explicitly in the radiative corrections that are included in our calculation for c_5 and c_6 (Table II).

We therefore fit each ratio, R, to the following functional form:

$$\begin{aligned} R &= R_{\rm phys}\,[1 \\ &+ \sum_{j=1,2} c_j (a\Lambda)^{2j}(1 + c_{jb}\delta x_m + c_{jbb}(\delta x_m)^2) \\ &+ 2b_l \delta x_l (1 + c_l (a\Lambda)^2)\big]\,. \end{aligned} \tag{16}$$

Here δx_l is $(am_l/am_s) - (m_l/m_s)_{\rm phys}$ for each ensemble. $(m_l/m_s)_{\rm phys}$ is taken from lattice QCD as 27.2(3) [6]. The strange sea quark mass is tuned to better than 3% with the lattice spacing taken from the Υ $2S-1S$ splitting so we can ignore any effects from this mistuning since sea quark mass effects are so small. δx_m allows for variation in the value of am_b over the range we are using and therefore a change in the NRQCD radiative corrections to discretisation errors. We choose δx_m to vary from -0.5 to +0.5 over our full range of masses by setting $\delta x_m = (am_b - 2.65)/1.5$. Λ sets the scale for physical a-dependence. We take it to be 500 MeV.

The fit prior on $R_{\rm phys}$ is taken to be 0.8 ± 0.1 for R_P and 1.6 ± 0.2 for R_S. Since tree-level a^2 errors have been removed in this calculation we take the prior on a^2 terms to be 0.0 ± 0.3; we take 0.0 ± 1.0 for higher order terms in a. c_l allows for $\mathcal{O}(\alpha_s a^2)$ staggered quark taste-changing discretisation errors. For b_l we take 0.0 ± 0.015 allowing for a 3% shift if the u/d quarks were as heavy as strange. Previous results [2] saw a 10% shift in results in the quenched approximation.

Good fits using the form in equation 17 are easily obtained for both R_P and R_S. For $\chi^2/{\rm dof}\{{\rm dof}\}$ we obtain $0.2\{4\}$ and $0.4\{5\}$ for R_P and R_S respectively. The physical results we obtain are:

$$\begin{aligned} \frac{1^1P_1 - 1\overline{S}}{(2S-1S)_\Upsilon} &= 0.820(12) \\ \frac{(3S-1S)_\Upsilon}{(2S-1S)_\Upsilon} &= 1.625(39) \end{aligned} \tag{17}$$

These values are plotted along with the lattice results in Figure 9.

The complete error budget for the two ratios is given in Table XI. Most of the errors are obtained directly from our fit. The NRQCD systematic error in R_P is taken from combining results in Tables VI and VII. Since these errors are correlated between the numerator and denominator of R_P we take the systematic error in R_P to be the difference between them. The total NRQCD systematic error at each lattice spacing is then included in our fit as a correlated error on the data. In fact we find no significant difference whether we include it as a correlated or uncorrelated error. We obtain the error in our final result from this systematic error by observing the change in the final answer from including it or not including it. Variation in the NRQCD systematic errors as a function of am_b is included in our fit form and the error from this estimated from the variation of χ^2 in the fit. We use the same approach for R_S and take the NRQCD systematic error to be the same as for R_P. We might expect some further cancellation of errors within R_S because of the similarity between the S-wave states. However, this is less true when comparing $3S$ to $1S$ than for $2S$ and $1S$ so we ignore that possibility to be conservative.

We believe that errors from any mistuning of m_b are completely negligible. R_P and R_S change experimentally very little between b and c and we have very well-tuned b masses except on the very coarse lattices where our mistuning amounts to 4%.

We also believe that finite volume errors are negligible. A study using the heavy quark potential derived from a quenched lattice QCD calculation in [36] calculated wavefunctions for radially excited Υ states. None of the wavefunctions for the states being considered here extended beyond a radius of 1.5 fm and the $2S$ and $1P$ extended little beyond 1.0 fm. When sea quarks are included, as here, the size of the states will be smaller because the Coulomb coefficient in the heavy quark potential is larger. Thus 1.5 fm is an overestimate for the size of the states. The physical extent of our lattices range from 2.3 fm for set 1 to 3.8 fm for set 4, so should be large enough to contain the Υ states without any finite-volume errors from their being squeezed.

In Table XI we include a 0.2% error from electromagnetic effects and the possibility of η_b annihilation, neither of which is included in our calculation. Electromagnetic effects we estimated earlier at 1.6 MeV in the $1S$ mass and 0.8 MeV (correlated) in the $2S$ mass. If we take the effects on the $1P$ and $3S$ masses to be much smaller then we arrive at a possible error in R_S and R_P of the order of 0.1% to 0.2%. η_b annihilation affects the spin-averaged $1S$ mass, shfting it by approximately 0.5 MeV.

TABLE XI: Complete error budget for the ratios of mass splittings, $R_P = (1^1P_1 - 1\overline{S})/(2S - 1S)_\Upsilon$ and $R_S = (3S - 1S)_\Upsilon/(2S - 1S)_\Upsilon$. Errors are given as a percentage of the ratio. Errors which are negligible compared to the others are indicated by '0'.

	R_P	R_S
stats/fitting	1.0	1.8
a-dependence	0.6	1.2
m_l-dependence	0.6	0.5
NRQCD am_b-dependence	0.1	0.2
NRQCD systematics	0.5	1.0
finite volume	0	0
m_b tuning	0	0
electromagnetism/ η_b annihilation	0.2	0.2
Total	1.4	2.4

This amounts to a possible 0.1% effect in R_P, whereas R_S is unaffected.

Our result for the ratio R_P of 0.820(12) is to be compared with the experimental result 0.8088(23). Agreement is good within our 1.4% errors. Similarly we obtain 1.625(39) for R_S to be compared with the experimental result 1.5896(12). Again agreement is good, but now with 2.4% errors, dominated by our statistical/fitting error because the $3S$ state is a doubly excited state. The fact that our central value is slightly higher than experiment for both R_S and R_P is consistent with the expected effect of missing v^6 terms, included in our errors, as discussed in section III D.

Our result for R_P can be converted to a result for $M(h_b) - M(1\overline{S}) = 0.461(7)$ GeV. This can be compared to the result $0.440 \pm 17^{+10}_{-0}$ GeV with over double the error obtained on configurations including 2+1 flavors of sea quarks using the Fermilab heavy quark action [37]. The experimental result for $M(h_b) - M(1\overline{S})$ is 0.4553(17) GeV [35, 38].

Our result for R_S gives $M(\Upsilon'') - M(\Upsilon) = 0.914(23)$ GeV compared to an experimental result of 0.8949(6) GeV [35]. We have not included in our error budget any effect from coupling of the Υ'' to virtual decay channels. The Υ'' is 200 MeV below threshold for real decay to a pair of B mesons. This is considered large enough for the Υ'' to be 'gold-plated' and for the decay channel to have no impact on the mass.

2. Tuned b quark masses

We now return to the tuning of the b quark mass. Although not an issue for the mass splittings just discussed, it is an important source of systematic error for spin-dependent mass splittings. We use our determination of the lattice spacing from the Υ $(2S - 1S)$ splitting, given in Table X to convert the kinetic mass values given in section III C to physical units. As described in section III C the appropriate experimental value for comparison is 9.445(2) GeV.

Set	$am_b(a\Upsilon)$	$am_s(a\Upsilon)$	$am_s(a_{\eta_s})$
1	3.297(11)(35)(7)(16)	0.0641(4)(12)(2)	0.0705(9)(4)
2	3.263(7)(35)(4)(16)	0.0636(3)(12)(2)	0.0692(5)(4)
3	2.696(4)(22)(7)(13)	0.0528(2)(8)(2)	0.0541(6)(3)
4	2.623(7)(22)(7)(13)	0.0512(3)(8)(2)	0.0531(4)(3)
5	1.893(6)(12)(5)(9)	0.0364(2)(4)(1)	0.0376(5)(2)

TABLE XII: Tuned b and s quark masses in lattice units on each set of configurations. The second column gives am_b and the third am_s using the Υ $2S - 1S$ splitting to determine the lattice spacing. The first two errors in these two columns come from statistical errors and systematic errors respectively in the lattice spacing determination. The third and fourth errors in the am_b case are the statistical and systematic errors in determining the kinetic mass. Statistical errors in the determination of am_s mass are negligible. The third error in the am_s case is a correlated 0.3% error from the square of the physical value of the η_s mass. The fourth column gives am_s using the η_s decay constant to determine the lattice spacing. The first error is from statistics/fitting and the second is a correlated 0.6% error from the square of the physical value of the η_s decay constant.

When this is done we see that the masses are very well-tuned except on the very coarse lattices where they are 4% high. For small changes in the b quark mass the change in kinetic mass is approximately twice the change in quark mass, as can be seen from Table V. For the slight changes that we need to make this is a sufficiently good approximation. We simply adjust the quark mass by one half the error in the kinetic mass to obtain the tuned quark mass values in lattice units given in Table XII.

Three errors are given in Table XII. The first is from the statistical error in the kinetic mass determined on each ensemble. The second error comes from the total error in the determination of the lattice spacing in Table X. This includes both statistical and systematic errors in determining the $2S-1S$ splitting. The third error is a 0.5% systematic error from NRQCD in the kinetic mass obtained from analysis of the dispersion relation in section III C.

3. The hyperfine splitting

The mass difference between the $^3S_1$ and $^1S_0$ states is an important test of our calculations because it is statistically very precise for the ground-state mesons. Controlling systematic errors is the key issue, and the main one is that of radiative corrections to c_4, the coefficient of the $\sigma \cdot \mathbf{B}$ term in the NRQCD action. At leading order the hyperfine splitting is proportional to c_4^2. Our previous calculation [2], with $c_4 = 1$, gave a prediction for $M(\Upsilon) - M(\eta_b)$ of 61(14) MeV with the error dominated by the then-unknown radiative corrections to c_4.

For this calculation we have results for c_4 including $\mathcal{O}(\alpha_s)$ corrections as well as c_4 tuned nonperturbatively. These determinations of c_4 are described in Appendix B and Appendix C respectively. The values obtained by the

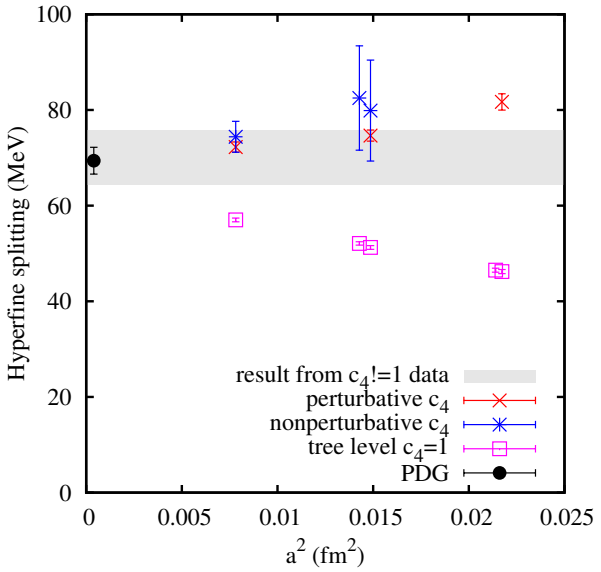

FIG. 10: Results for the hyperfine splitting, $M(\Upsilon) - M(\eta_b)$ plotted against the square of the lattice spacing. We show results for $c_4 = 1$ (cyan squares) as well as results for c_4 set equal to its perturbatively improved (red crosses) and nonperturbatively improved values (blue stars). The $c_4 = 1$ results include statistical errors only and are shown purely for comparison purposes – they are not included in the fit. The results for perturbative and nonperturbative c_4 include a correction for missing 4-quark operators and m_b-mistuning. The errors on these points are from statistics, the lattice spacing and the tuning of m_b. The results for nonperturbative c_4 also include statistical errors in the determination of c_4. Our final physical result including our full error budget is given by the grey shaded band. The full error budget includes errors from systematic uncertainties in setting c_4 and from missing v^6 terms in the NRQCD action.

TABLE XIII: Values for the coefficient of the $\sigma \cdot \mathbf{B}$ term, c_4, for different lattice spacing values. The error on the perturbative values is $1 \times \alpha_s^2$. The errors on the nonperturbative values are statistics, experiment and NRQCD systematics respectively. We did not extract a nonperturbative value on the very coarse lattices.

Sets	$c_4^{\rm pert}$	$c_4^{\rm nonpert}$
fine	1.16(5)	1.18(2)(1)(5)
coarse	1.20(7)	1.28(7)(1)(5)
very coarse	1.22(8)	-

two methods for c_4 are given in Table XIII. The nonperturbative values are slightly larger than the perturbative ones, but the differences are well within the expectations from additional α_s^2 corrections to the perturbative values and/or systematic errors in the nonperturbative values. Both sets of values get closer to 1 on the finer lattices, as expected, because they are functions of the strong coupling constant at a scale related to the inverse of the lattice spacing.

Table XIV gives results for the energies of the Υ and η_b for various combinations of values of coefficients in the NRQCD action. We also give the mass difference between the Υ and η_b which is the hyperfine splitting. This can be more precise than either mass separately because we fit both meson correlators together and extract the difference directly from the fit taking into account the correlations. Where we have fits to a 5×5 matrix of correlators, as in Tables VIII and IX, we give those results. In other cases we calculated only a single local correlator for each of the Υ and η_b which is quite sufficient to extract a splitting between the ground state masses. Results are not as precise for splittings between radially excited states in those cases, however, and we do not give them.

We see from Table XIV that changing c_4 does have a large effect on the hyperfine splitting, approximately in line with the expectation of variation as c_4^2. We also see that, on sets 3 and 5 where we have data for comparison, changing $c_{1,5,6}$ to their $\mathcal{O}(\alpha_s)$ improved values does increase the hyperfine splitting slightly. It is a small effect, however, of order 2%. Changing the coefficient of the Darwin term, c_2 also has a small effect of order 1(1)%.

We conclude from this that we have controlled all of the coefficients of v^4 terms in our NRQCD action at a level required to give few percent errors in the hyperfine splitting from these sources. We have not, however, included 4-quark operators in our NRQCD Hamiltonian and they can have an impact on the hyperfine splitting at an order equivalent to that of α_s corrections to c_4 [28].

In Appendix C we give coefficients for the 4-quark operators and a formula in equation B14 for the correction that they would induce in the hyperfine splitting. Table XV gives values for this correction, to be added to the results from Table XIV, on the very coarse, coarse and fine ensembles based on using a spin-averaged value of the 'wavefunction-at-the-origin', $\psi(0)$, for the Υ and η_b from our fits. This varies only very little with c_4, falling by at most 2% from $c_4 = 1$ to our nonperturbative c_4 values, so we ignore this variation. Our correlators are normalised by dividing by 6 after summing over 2 spins and 3 colors. Then $\psi(0)$ is given by the amplitude of our correlator fits; $a(l,1)$ for the $1S$ and $a(l,2)$ for the $2S$ from equation 7.

We see from Table XV that the correction is substantial on the very coarse lattices and very small on the fine lattices, because of the variation of the coefficients d_1 and d_2 with am_b. The corrected results are shown in Figure 10 along with the uncorrected results for $c_4 = 1$. We see that there is a substantial difference between the results coming from the change in c_4 and, to a lesser extent, from the correction for the 4-quark operator. The strong dependence on the lattice spacing seen in the $c_4 = 1$ results is reduced, in line with the expectation that improving an effective theory should reduce the cutoff dependence.

An additional small factor in Figure 10 is that we have corrected results for slight mistuning of the b quark mass

Set	am_b	$c_{1,5,6}$	c_2	c_4	aE_{η_b}	aE_Υ	$aE_\Upsilon - aE_{\eta_b}$
1	3.42	α_s	1	1	0.25080(5)	0.28532(6)	0.03452(8)
1	3.42	α_s	1	1.22	0.21432(5)	0.26400(6)	0.04968(7)
1	3.5	α_s	1	1	0.25015(6)	0.28392(9)	0.03377(10)
2	3.39	α_s	1	1	0.25361(3)	0.28809(3)	0.03448(4)
2	3.42	α_s	1	1	0.25344(5)	0.28759(5)	0.03416(6)
3	2.66	1	1	1	0.25529(4)	0.28626(6)	0.03097(7)
3	2.66	α_s	1	1	0.26096(3)	0.29245(3)	0.03149(4)
3	2.66	α_s	1.25	1	0.25627(24)	0.28728(33)	0.03101(41)
3	2.66	α_s	1	1.25	0.20943(3)	0.25628(3)	0.04684(5)
3	2.66	α_s	1	1.20	0.22040(5)	0.26394(7)	0.04354(4)
3	2.68	α_s	1	1	0.26108(7)	0.29249(9)	0.03141(11)
3	2.7	1	1	1	0.24375(8)	0.27483(11)	0.03108(13)
4	2.62	α_s	1	1	0.26524(2)	0.29681(2)	0.03157(3)
4	2.62	α_s	1	1.25	0.21289(2)	0.25978(2)	0.04689(2)
4	2.66	α_s	1	1	0.26546(3)	0.29662(4)	0.03116(5)
5	1.91	1	1	1	0.24652(3)	0.27153(5)	0.02501(6)
5	1.91	α_s	1	1	0.25851(2)	0.28405(2)	0.02554(3)
5	1.91	α_s	1	1.10	0.23204(2)	0.26206(3)	0.03003(4)
5	1.91	α_s	1	1.15^*	0.21772(22)	0.24984(40)	0.03213(30)
5	1.91	α_s	1	1.16	0.21519(2)	0.24802(4)	0.03283(2)
5	2.0	α_s	1	1	0.25935(3)	0.28397(4)	0.02462(5)

TABLE XIV: Fitted energies for ground state Υ and η_b mesons on all configuration sets. The column $c_{1,5,6}$ denotes whether the $\mathcal{O}(\alpha_s)$ improved coefficients were used in the action. Various values of c_2 and c_4 have also been used as indicated. $c_3 = 1$ except for the case indicated by $*$ in which $c_3 = 0.96$. Where possible the result from the full 5×5 matrix fit was taken. Otherwise, the values from the kinetic mass fits were used. In those cases a smaller number of configurations and/or time sources was sometimes used and this is reflected in the statistical errors.

TABLE XV: Corrections to the $1S$ and $2S$ hyperfine splittings from spin-dependent 4-quark operators missing from our NRQCD action. We use equation B14 inserting values for $\psi(0)$ from our fitted results and values for $\alpha_V(\pi/a)$ from Table XXII. We convert to physical units using lattice spacing values from Table X.

Sets	Correction to $1S$ hyperfine (MeV)	Correction to $2S$ hyperfine (MeV)
fine	-1.7	-1.0
coarse	5.2	3.4
very coarse	12.9	8.3

and we have included the error from the quark mass tuning in the hyperfine splitting error. The hyperfine splitting is expected to be approximately inversely proportional to the quark mass and this is seen in Table XIV. We assume this relationship to make small adjustments based on the tuned b masses from Table XII. The largest effect is a 4% one on the very coarse lattices. The lattice spacing error from the quark mass tuning is correlated with the lattice spacing error on the hyperfine splitting because of this inverse relationship. The lattice spacing error therefore appears with a factor of 2 in the hyperfine splitting.

To obtain a physical result for the hyperfine splitting we then combine results with perturbative and nonperturbative values of c_4 allowing for systematic differences between them from uncertainties in the determination of c_4. We must also allow for uncertainties from higher-order 4-quark operator effects and for lattice spacing and sea quark mass dependence. The nonperturbative c_4 results are given a correlated systematic error corresponding to the second and third errors in Table XIII and remembering that the hyperfine splitting is related to c_4^2. Similarly the results for perturbative c_4 are given a separate correlated systematic error corresponding to the α_s^2 errors given in Table XIII. We allow for higher order 4-quark operator effects with a correlated systematic error of size $6\alpha_s^3|\psi(0)|^2/m_b^2$ with a coefficient of possible size $\pm 1 \pm \ln(am_b)$. This does not assume that the small coefficient seen at $\mathcal{O}(\alpha_s^2)$ on the fine lattices is repeated at higher order.

We allow for lattice spacing and sea quark mass effects as in the fit function of equation 17. The prior on sea quark mass effects is now taken to allow 15% effects for $m_l \approx m_s$. This reflects the fact that a 40% difference was seen between quenched and dynamical results in [2]. In fact sea quark mass effects in our data are small. Figure 11 shows a comparison of the hyperfine splitting as a function of the light sea quark mass for the case $c_4 = 1$ where we have a complete set of data. Although these results are *not* used to determine our final answer for the hyperfine splitting they do provide a useful comparison between ensembles at the same lattice spacing and different light quark mass since the effects of c_4 are independent of sea quark mass. The results are adjusted for b quark mass mistuning and include errors from the b

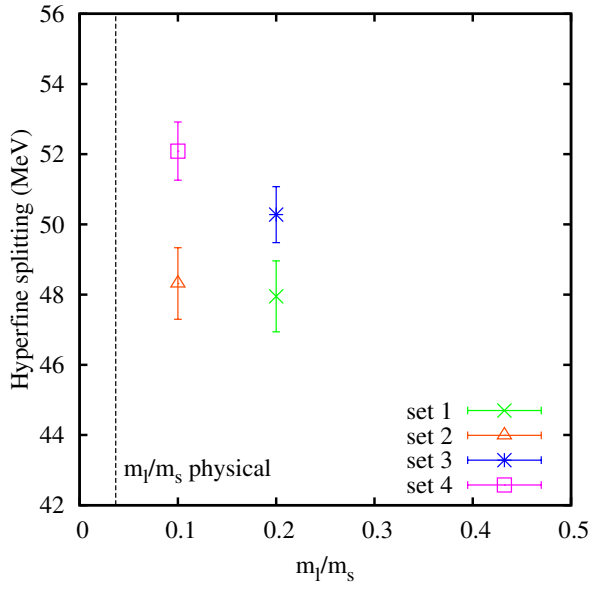

FIG. 11: Results for the hyperfine splitting obtained for $c_4 = 1$ (not used in our fit for the physical hyperfine splitting) compared as a function of sea light quark mass in units of the strange quark mass. Results are given for two values of m_l/m_s on very coarse (sets 1 and 2) and coarse (sets 3 and 4) lattices. The errors on the points include statistical/fitting errors, lattice spacing errors and m_b tuning errors.

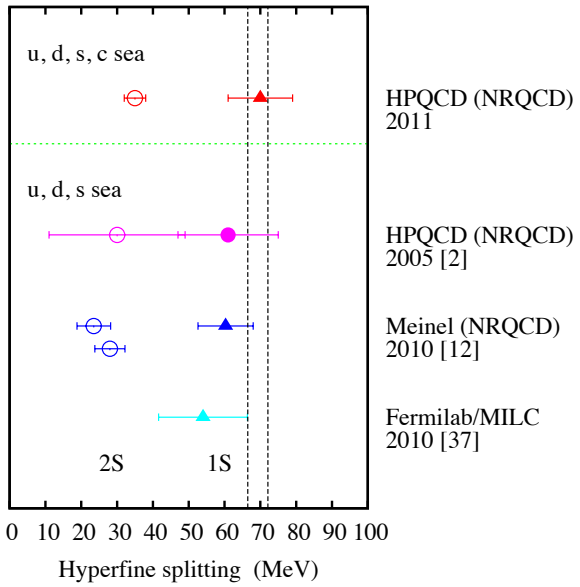

FIG. 12: Comparison of results for the hyperfine splittings, $M(\Upsilon) - M(\eta_b)$ and $M(\Upsilon') - M(\eta_b')$, from different full lattice QCD calculations. Filled symbols indicate the $1S$ hyperfine and open symbols, the $2S$ hyperfine. Circles indicate predictions and triangles postdictions. The top (red) points are the new results from this paper, and the points below that (pink) are from [2], when the $1S$ hyperfine was a prediction. The third line gives results from [12]. Two results are given for the $2S$ hyperfine; that from a ratio to the $1S$ hyperfine, as here, and that from a ratio to the combination of P-wave spin splittings sensitive to c_4 (see Appendix C). The top three results use the NRQCD formalism for b quarks; the bottom (cyan) result uses the Fermilab heavy quark action [37]. The black dashed lines mark the current experimental average [35].

TABLE XVI: Complete error budget for the $1S$ hyperfine splitting and the ratio of the $2S$ to the $1S$ hyperfine splittings. Errors are given as a percentage of the final result. * Note that the m_b tuning uncertainty does not include the lattice spacing uncertainty in m_b. Since that is correlated with the a uncertainty on converting the hyperfine splitting from lattice to physical units, they must be handled together and both are included in the a-uncertainty.

	$M(\Upsilon) - M(\eta_b)$	R_H
stats/fitting	0.1	4
a-dependence	1.5	5
a-uncertainty	0.5	0
m_l-dependence	3	3.5
NRQCD am_b-dependence	2	0.5
NRQCD v^6	10	5
NRQCD c_4 uncertainty	7	0
NRQCD 4-quark uncertainty	2	1
m_b tuning*	0.1	0
η_b annihilation	1	0.5
Total	13	9

quark mass and the lattice spacing. Variation with light quark mass is at most 2 MeV. Note that we are using much lighter sea quark masses than in previous calculations [2, 12]; indeed m_l is within a factor of 3 of its physical value.

We obtain a physical value for the hyperfine splitting from the above fit of 70(6) MeV. Fitting the results for perturbative c_4 on their own gives a consistent 67(7) MeV and the results for nonperturbative c_4 alone gives 75(9) MeV. Our best result therefore comes from combining the two. An additional 10% error must be allowed for higher order (v^6) spin-dependent terms in the NRQCD action, giving a final result of:

$$M(\Upsilon) - M(\eta_b) = 70(9)\text{MeV}. \quad (18)$$

Our complete error budget is given in Table XVI. The shift for the effect of η_b annihilation is included in our 4-quark operator correction (as discussed in Appendix C) but we separate out an error for that from the rest of the 4-quark operator error.

In Figure 12 we compare our new result for the hyperfine splitting to earlier full lattice QCD results and to experiment [35]. Earlier results using NRQCD are: 61(14) MeV from [2] with a treelevel v^4 NRQCD action and 60.3(7.7) MeV from [12] using an NRQCD with v^6 spin-dependent terms and c_4 determined from P-wave splittings but with no 4-quark operator corrections, which are potentially more significant than v^6 terms, or errors from them. The result obtained from the Fermilab heavy quark action [37] is 54.0(12.4) MeV. For this action the hyperfine splitting is sensitive to the coefficient of the $\mathcal{O}(a)$ improvement term known as the clover term.

In principle this coefficient does not have to be tuned but the approach to the continuum limit is slow. Here it was taken to have its tree-level value after tadpole-improvement and the quark mass was tuned using the spin-averaged kinetic mass of the B_s and B_s^* mesons.

All four lattice QCD results agree well with the current experimental average of 69.3(2.8) MeV [35] obtained from averaging results from experiments on radiative transitions to η_b from Υ' and Υ'' [39–41]. Preliminary experimental results using radiative transitions from the h_b indicate a somewhat lower value [42].

Our new result above contains the most complete analysis at $\mathcal{O}(v^4)$ in the NRQCD action. To improve it would require the inclusion of spin-dependent operators at $\mathcal{O}(v^6)$. The effect of spin-dependent v^6 operators was studied in [12], taking ratios of the hyperfine splitting to P-wave spin splittings to cancel the effect of c_4. Those results indicate that spin-dependent v^6 terms tend to reduce the hyperfine splitting by about 10%. We have included a (symmetric) 10% error in our results to account for missing v^6 terms.

The hyperfine splitting has also been calculated using continuum QCD perturbation theory [43]. A considerably smaller result is obtained of 41(14) MeV. This is not in disagreement with the nonperturbative lattice QCD results given the size of the errors. It has been suggested, however, that the inclusion of radiative corrections to c_4 in the lattice NRQCD calculation would reduce the value of the hyperfine splitting obtained [44]. That expectation was based on an incorrect analysis of the form of c_4 in the lattice NRQCD calculation and we see indeed from the results given here that the inclusion of radiative corrections to c_4 has had the opposite effect and increased our value for the hyperfine splitting.

The best way to study the $2S$ hyperfine splitting, $M(\Upsilon') - M(\eta_b')$ is through the ratio to the $1S$ hyperfine splitting. We define:

$$R_H = \frac{M(\Upsilon') - M(\eta_b')}{M(\Upsilon) - M(\eta_b)}. \qquad (19)$$

Then c_4 effects cancel as can be seen in the numbers in Tables VIII and IX and plotted in Figure 13. In the Figure we have corrected the results for missing 4-quark operator effects which are slightly different in the $1S$ and $2S$ states and so have an effect on the ratio. This is at most 4%, on the very coarse lattices. We have made no correction for the slight mistunings of m_b since they should largely cancel in this ratio.

Again we extract a physical result for R_H by allowing for m_l and a dependence as in equation 17. Here we relaxed the priors on the a-dependence so that they all had the form 0.0 ± 1.0. The prior on m_l-dependence (in units of m_s) was taken as 0.0 ± 0.15 as for the $1S$ hyperfine, allowing a 15% change from $m_l = m_s$ down to the physical point.

Our final physical value is:

$$R_H = 0.499(42). \qquad (20)$$

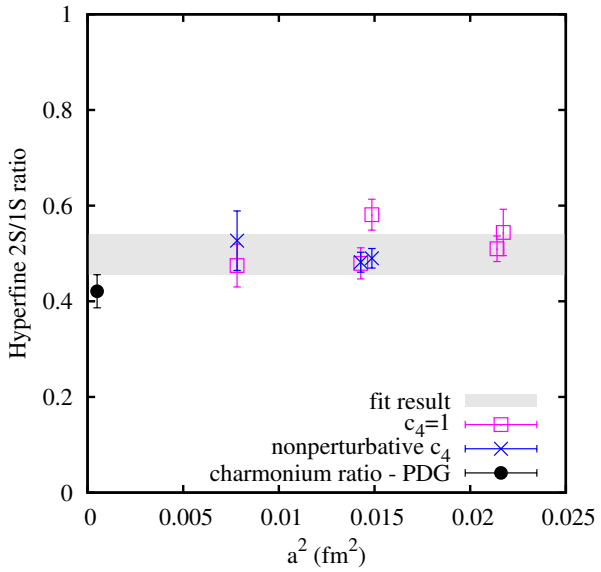

FIG. 13: The ratio of hyperfine splittings for $2S$ and $1S$ states, $(M(\Upsilon')-M(\eta_b'))/(M(\Upsilon)-M(\eta_b))$, plotted against the square of the lattice spacing. Points have been corrected for missing 4-quark operator effects. The shaded band shows our final physical result including our full error budget.

The full error budget is given in Table XVI where we allow a 5% error for missing spin-dependent v^6 terms, allowing for some cancellation of v^6 effects between the $1S$ and $2S$ hyperfine splittings.

Combining our result for R_H with the current experimental average for the $1S$ hyperfine splitting gives a result for the $2S$ hyperfine splitting of 35(3)(1) MeV, where the second error comes from the experimental $1S$ splitting. We predict the mass for the η_b' to be 9988(3) GeV.

Figure 12 compares our result for the $2S$ hyperfine splitting to earlier predictions. Meinel [12] gives 23.5(4.7) MeV from a ratio to P-wave spin splittings and 28.0(4.7) from a ratio to the $1S$ hyperfine splitting, as used here. He includes the effect of spin-dependent v^6 operators but without such a complete analysis as we have done here of v^4 operators. The conclusion from Figure 12 is that lattice QCD results give a fairly clear prediction of the $2S$ hyperfine splitting around 30 MeV, half the result for the $1S$ hyperfine splitting.

Figure 13 compares our result for the bottomonium ratio of $2S$ to $1S$ hyperfine splittings to the experimental charmonium ratio of 0.421(35). Our bottomonium result is somewhat higher, but not in disagreement with this value. This indicates that the heavy quark mass dependence in the $1S$ and $2S$ hyperfine splittings is very similar over the wide range of quark masses from c to b so that the ratio remains the same.

The S-wave hyperfine splittings can be compared to the much smaller result for the P-wave states. In Appendix C we determine the P-wave hyperfine splitting to be 2(2) MeV, consistent with zero.

IV. THE η_s MASS AND DECAY CONSTANT

To complement the computation in the previous section, the lattice spacing was also determined using the decay constant of the fictitious η_s meson, f_{η_s}. This is a pseudoscalar particle consisting of an $s\bar{s}$ pair whose properties can easily be computed in lattice QCD. It is particularly suitable for fixing the lattice spacing since there are no u/d valence quarks meaning that the error coming from the chiral extrapolation to physical u/d masses is small. The "physical" values of the M_{η_s} and f_{η_s} have to be fixed by comparison to M_π, M_K, f_π and f_K as in [21]. This requires a simultaneous chiral and continuum extrapolation for the masses and decay constants of the π, K and η_s. Previously we found, on ensembles including 2+1 flavors of sea quarks, that properties of the η_s were very close to those expected from leading order chiral perturbation theory, i.e. $M^2_{\eta_s} \approx 2M^2_K - M^2_\pi$ and $f_{\eta_s} \approx 2f_K - f_\pi$. We re-examine that issue here on these ensembles containing 2+1+1 sea quarks.

A. Simulation details and Fitting

s and u/d valence quark propagators were calculated on the ensembles given in Table I using the same HISQ action as used for the sea quarks. The HISQ action [16] is a further improved version of the improved staggered (asqtad) action that reduces discretisation errors coming from staggered taste effects for that action by about a factor of 3. The improved staggered action smears the gluon fields that appear in the quark action in a very specific way to reduce high-momentum taste-exchange interactions but without increasing discretisation errors [10]. The HISQ action takes this one step further by performing two smearing steps. The original version of the HISQ action used an SU(3) projection of the smeared links between the two smearing steps. However, this caused difficulties for the updating algorithm when these quarks were included as sea quarks [19]. Instead the sea quarks here use the HISQ action but with only a U(3) projection between the smearing steps. Whether U(3) or SU(3) projection it makes very little difference to the spectrum of mesons from HISQ quarks and so all the good features of the HISQ action demonstrated in [16] remain essentially unaltered. Note that the HISQ action does not use tadpole-improvement – the U(3) (or SU(3)) projection effectively takes care of large tadpole contributions in the same way that the use of the u_0 parameter does in the NRQCD and gluon actions.

The parameters of the valence quark propagators are listed in Table XVII. We took the light quark mass to be the same as that in the sea (except for a small difference on set 3), but we retuned the valence strange quark masses slightly to allow for mistuning of the strange sea quark mass (of course the final well-tuned s quark mass values cannot be decided until a value for the lattice spacing is determined so we will revisit this issue at the end of this section). We used delta function random wall sources as for the l-smeared b quark propagators discussed in section III. We also used 16 evenly-spaced time sources per configuration to increase statistics. The starting position of these time sources was shifted from configuration to configuration in the ensemble.

TABLE XVII: Valence light and strange quark mass parameters on each ensemble. The valence light quark masses are the same as in the sea (given in Table I), except for a slight difference on set 3. The valence strange quark masses have been retuned slightly to be closer to the physical values. Columns 4 and 5 give the number of configurations used from each ensemble and the number of time sources for propagators per configuration.

Set	$am_l^{\rm val}$	$am_s^{\rm val}$	n_{cfg}	n_t
1	0.013	0.0688	1021	16
2	0.0064	0.0679	1000	16
3	0.01044	0.0522	1053	16
4	0.00507	0.0505	1000	16
5	0.0074	0.0364	1008	16

The light meson pseudoscalar correlators are calculated by combining the light and strange quark propagators. Here we use the goldstone mesons, made with the local γ_5 operator. Then the correlators are simply given by the squared modulus of the propagators summed over a time-slice to project onto zero momentum. The correlators were binned over all time sources on a configuration.

To study the autocorrelations between configurations we proceed as in subsection III B to calculate the autocorrelation function $C_{\Delta T}$. Figure 14 shows $C_{\Delta T}$ against ΔT for both the π and η_s correlators at a source-sink lattice time separation appropriate to our fits. This time separation is increased as the lattice spacing decreases to remain approximately physical. We see from the Figure that the η_s shows little autocorrelation, although more than was visible for the Υ in Figure 1. We expect longer autocorrelation times for lighter mesons because they have a larger spatial extent and therefore decorrelation of the gluon field configuration on relevant spatial scales takes longer in Monte Carlo time. The π correlators on the coarse and very coarse lattices show a similar autocorrelation function to the η_s. However, on the fine lattices where autocorrelations might be expected to be worst, there are clear signs that neighbouring configurations in time are correlated. Note the difference between our result and that of [19]. There very little autocorrelation was seen in the π meson correlator, but fewer time sources were used per configuration (typically 4). Both here and in [19] the time sources are moved randomly from one configuration to the next. However, with 16 time sources there is not much scope for a large shift in time between configurations. To reduce autocorrelations we bin all of our fine light meson correlators by a factor of 8 in configuration number before fitting. From Figure 14 this can be seen to reduce the autocorrelation function well below e^{-1}.

The fitting method used for the correlators was the

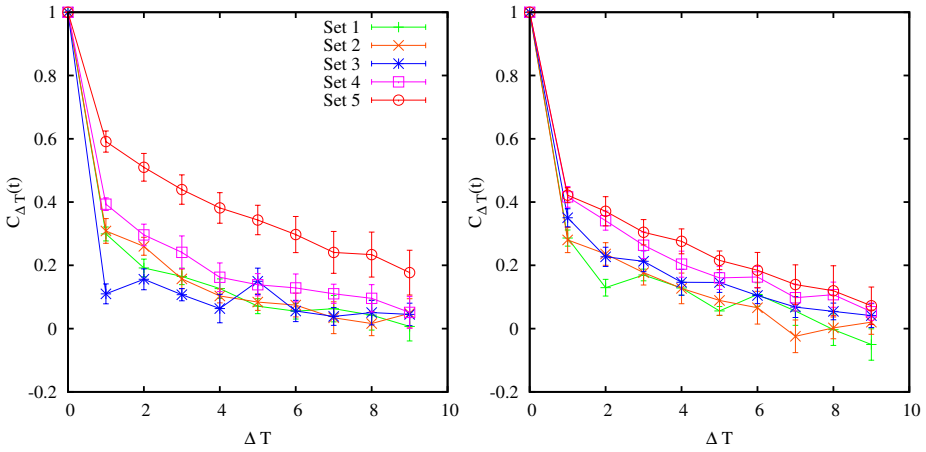

FIG. 14: Autocorrelation function $C_{\Delta T}$ for π (left) and η_s (right) correlators. These are made with a δ function random wall as described in the text. The key to results from different ensembles is (color online): set 1, green plus; set 2, orange cross; set 3 blue star; set 4 pink open square; set 5, red open circle. The correlators are evaluated at lattice time separation $t/a = 6$ on very coarse lattices (sets 1 and 2), $t/a = 8$ on coarse lattices (sets 3 and 4) and $t/a = 10$ on fine lattices (set 5). This corresponds to a t value, approximately constant in physical units across the lattice spacing values, where the π and η_s correlators have reached the ground-state plateau. ΔT is given in units of configuration number in the ordered list for each ensemble.

same as for the Upsilon correlators but with only a single source and sink smearing. For meson correlators made from relativistic quarks the fit function takes a 'cosh' form rather than simple exponentials because of propagation in both time directions. For staggered quarks in general we have to include an additional oscillating term from opposite parity mesons that couple through the time-doubler quark. The fit function then becomes:

$$G_{\rm meson}(t) = \sum_{k=0}^{n_{\rm exp}} a_k(e^{-E_k t} + e^{-E_k(T-t)}) - (-1)^{t/a} \sum_{ko=0}^{n_{exp}} a_{ko}(e^{-E_{ko} t} + e^{-E_{ko}(T-t)}). \quad (21)$$

The oscillating piece is absent for the π and η_s because the valence quark and antiquark have equal mass and the oscillation cancels. It is necessary to include it for the K meson. For each ensemble a simultaneous fit to all three correlators was performed using the appropriate form for each. This allowed us to take into account the correlations between the fit results for each meson in our subsequent chiral extrapolations. We use the full range of t values in the fit apart from the first 3–5 time-slices. Priors for energies and amplitudes are chosen as for the Υ fits described in section III B. We take results from 4 exponential fits, where ground-state masses and their errors have clearly stabilised.

The results that we use are the ground-state meson masses and amplitudes, i.e. $k = 0$ in equation 21. The meson masses are given by the parameter E_0 from each fit, since there is no energy offset for staggered quarks as there is for NRQCD. The decay constants are extracted from the fit using

$$f_{ab} = (m_a + m_b)\sqrt{\frac{2a_0}{E_0^3}} \quad (22)$$

for a meson containing quarks a and b with masses m_a, m_b, ground state mass E_0 and ground state amplitude, a_0, from the fit form above. Equation 22 uses the PCAC relation, valid for staggered quarks, to relate the matrix element of the pseudoscalar density to that of the temporal axial current and therefore the decay constant. The existence of the PCAC relation means that the temporal axial current is absolutely normalised and there is no uncertainty from lattice to continuum current matching factors as there can be in some other quark formalisms.

B. Results and chiral extrapolations

Our results for the π, K, and η_s meson masses and decay constants are listed in tables XVIII and XIX. We also give various ratios that are useful indicators of the sensitivity of the η_s parameters to the chiral extrapolation in the u/d sea quark mass, and to the lattice spacing.

We fit the three decay constants and meson masses simultaneously using SU(3) chiral perturbation theory, adapted to include discretisation effects. The usual approach is to use values for the decay constant and meson mass in GeV, having chosen a value of the lattice spacing on each ensemble. Extrapolation to the point where M_π and M_K take their physical values then allows comparison to experiment of the resulting values for f_π and f_K. Here instead we use values for r_1/a to fix the relative lattice spacing between ensembles and keep the

Set	1	2	3	4	5
aM_π	0.23637(15)	0.16615(7)	0.19153(9)	0.13413(5)	0.14070(9)
aM_K	0.41195(17)	0.39082(9)	0.32781(10)	0.30757(7)	0.23933(11)
aM_{η_s}	0.53361(14)	0.52797(8)	0.42351(9)	0.41476(6)	0.30884(11)
$M_{\eta_s}^2/(2M_K^2 - M_\pi^2)$	1.00426(43)	1.00317(28)	1.00636(34)	1.00474(26)	1.00660(27)

TABLE XVIII: Values for the ground state masses in lattice units (E_0 from eq. 21) for π, K and η_s mesons. The fourth row gives the ratio of the square of the η_s mass to a combination of π and K masses that would be 1 in leading order chiral perturbation theory.

Set	1	2	3	4	5
af_π	0.11183(9)	0.10511(5)	0.09075(5)	0.08451(4)	0.06621(5)
af_K	0.12689(8)	0.12268(4)	0.10185(5)	0.09788(3)	0.07427(4)
af_{η_s}	0.14199(6)	0.14026(3)	0.11312(4)	0.11119(2)	0.08238(4)
f_K/f_π	1.13467(58)	1.16717(38)	1.12231(38)	1.15819(35)	1.12170(39)
f_{η_s}/f_π	1.26974(80)	1.33442(59)	1.24653(68)	1.31568(53)	1.24416(69)
$f_{\eta_s}/(2f_K - f_\pi)$	1.00031(62)	1.00007(27)	1.00154(45)	0.99948(26)	1.00061(32)
f_{η_s}/M_{η_s}	0.26609(11)	0.26566(6)	0.26711(10)	0.26809(6)	0.26674(12)

TABLE XIX: Values for the ground state decay constants in lattice units (derived from a_0 in eq. 21 as described in the text) for π, K and η_s mesons. We also give various ratios of decay constants obtained from the simultaneous fit. The sixth row gives the ratio of the η_s decay constant to a combination of π and K decay constants that would be 1 in leading order chiral perturbation theory.

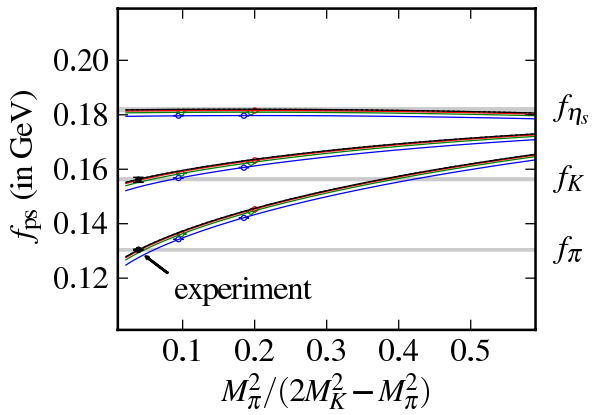

FIG. 15: The pseudoscalar decay constants plotted against the ratio of squared pseudoscalar masses that is approximately equal to m_l/m_s. The points have been adjusted for finite volume effects and for mistuning of the strange quark mass. The lines are from the tuned fit function at each lattice spacing, with results increasing in value from very coarse (blue) to fine (red) (color online). The top (black) line is the $a = 0$ curve and the black leftmost data points give the experimental value for f_π and f_K given values for V_{ud} and V_{us} [35].

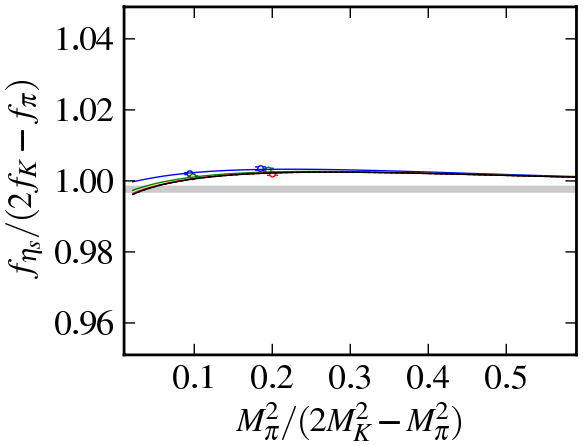

FIG. 16: The ratio of f_{η_s} to $2f_K - f_\pi$, which would be 1 in leading order chiral perturbation theory. The ratio of squared meson masses on the x-axis corresponds approximately to m_l/m_s. The blue, green and red points and fit curves correspond to very coarse, coarse and fine lattices respectively (color online). The black line is the continuum, $a = 0$, fit curve.

physical value of r_1 as a parameter to be obtained from the fit. The value for r_1 is determined by the requirement to match f_π and f_K from experiment in the chiral limit where the experimental values are included as extra pieces of 'data' for the fit. The experimental values for f_π and f_K come from experimental measurement of the leptonic decay rate and values of V_{ud} and V_{us} taken from elsewhere. We use [35]

$$\begin{aligned} f_\pi &= 0.1304(2)\text{GeV} \\ f_K &= 0.1561(9)\text{GeV}. \end{aligned} \tag{23}$$

The meson mass values that go with these decay constants in a world appropriate to lattice QCD without electromagnetism and in which $m_u = m_d$ are [45]:

$$\begin{aligned} M_\pi^2 &= M_{\pi^0}^2 \\ M_K^2 &= \frac{1}{2}\left(M_{K^0}^2 + M_{K^+}^2 - (1+\Delta_E)(M_{\pi^+}^2 - M_{\pi^0}^2)\right). \end{aligned} \tag{24}$$

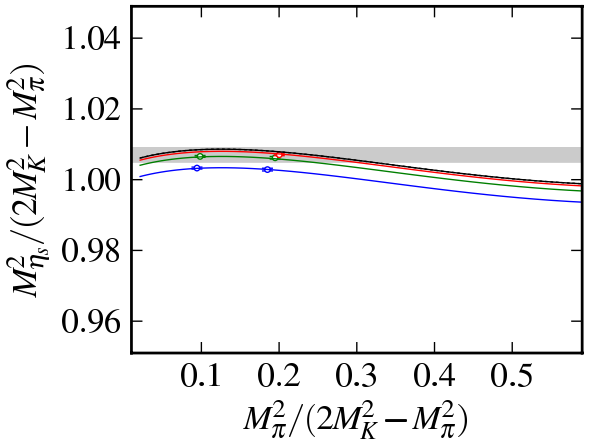

FIG. 17: The ratio of $M_{\eta_s}^2$ to $2M_K^2 - M_\pi^2$, which would be 1 in leading order chiral perturbation theory. The ratio of squared meson masses on the x-axis corresponds approximately to m_l/m_s. The blue, green and red points and fit curves correspond to very coarse, coarse and fine lattices respectively (color online). The black line is the continuum, $a = 0$, fit curve.

We take Δ_E, which parameterizes the violations of Dashen's theorem, to have the value 1 ± 1. The decay constants are already defined to be results in pure QCD, provided electromagnetic effects have been removed from the experimental leptonic decay rates [35]. The residual error in f_K from the fact that it is the decay constant of the K^+ whereas the K mass in equation 25 is the isospin average is less than 0.1% [45], so we ignore it here.

Our fit also returns a physical value for f_{η_s} and M_{η_s}. This can be used in subsequent analyses to tune the s quark mass and to fix the lattice spacing. It is a good meson to use for this purpose because its parameters are very insensitive to the sea quark masses, as we see in Tables XVIII and XIX.

The analysis is the same as that used in [21] except for two improvements. The first is that the fit is simplified because HISQ quarks are used in both the valence and sea sectors. The second is that we include correlations between all of the decay constants and meson masses on each ensemble by feeding into the fit the covariance matrix that resulted from the simultaneous fit to all three meson correlation functions. Below we provide a brief description of the chiral/continuum extrapolations following [21].

On each ensemble the decay constants and meson masses are a function of the masses of the valence quarks for that meson and of the masses of the sea quarks for that ensemble, with the coefficients of the mass dependence constrained to be the same for the π, K and η_s mesons. Because the quark masses run with energy scale it simplifies the fits to use a dependent variable related to the square of appropriate goldstone meson masses instead the quark mass. Thus we write

$$x_l = \frac{M_\pi^2/2}{\Lambda_\chi^2}, \tag{25}$$

where Λ_χ provides the cut-off scale of the chiral expansion,

$$\Lambda_\chi = 4\pi f_\pi/\sqrt{2}. \tag{26}$$

Similarly

$$x_s = \frac{M_K^2 - M_\pi^2/2}{\Lambda_\chi^2}. \tag{27}$$

In the cases where the sea and valence quark masses differ, the x parameters for the sea quark masses are obtained from those of the valence masses by rescaling in proportion to the quark mass. Then the decay constant made from valence quarks a and b takes the functional form

$$f(x_a, x_b, x_l^{\rm sea}, x_s^{\rm sea}, a) = f^{\rm NLO} + \delta f_\chi + \delta f_{\rm lat}, \tag{28}$$

where $f^{\rm NLO}$ is the full partially quenched chiral perturbation theory formula at next-to-leading order [46] and δf_χ and $\delta f_{\rm lat}$ include possible correction terms coming from higher order terms in the quark mass and finite lattice spacing corrections. Each of the terms contains a set of unknown coefficients which are given prior constraints in our fit allowing us to test their effect on our final result.

$f^{\rm NLO}$ [46] includes terms proportional to the squares of the appropriate meson masses as well as logarithmic terms that appear in combinations such as, for example, $(x_a + x_l^{\rm sea})\log(x_a + x_l^{\rm sea})$. The logarithmic terms are corrected for finite volume effects through the use of finite volume chiral perturbation theory. The finite volume correction is significant for f_π, particularly on set 1 where $M_\pi L = 3.8$ and the finite volume correction is 1.8%. For the other sets, with $M_\pi L > 4$, the correction ranges from 0.4% to 0.7%. For f_K and f_{η_s} the correction is much smaller. It is at its largest on set 1 with 0.7% for f_K and 0.2% for f_{η_s}.

δf_χ includes polynomial dependence on various combinations of the x_i up to and including x_i^4 terms [21]. Most of these terms only matter for the s quark and they allow for differences between the s and l sectors within SU(3) chiral perturbation theory. Since $x_s = 0.17$ including x_i^4 terms means that missing terms at x_s^5 are $\mathcal{O}(10^{-4})$, smaller than our statistical errors. It is sufficient to include polynomials because we cannot distinguish high-order logarithms from polynomials over this range in x_i.

$\delta f_{\rm lat}$ allows for dependence on powers of the square of the lattice spacing, since this is the form that discretisation errors take for staggered quarks. We include terms up to $(a\Lambda_{\rm QCD})^8$ where $\Lambda_{\rm QCD}$ is taken to be $\mathcal{O}(0.6{\rm GeV})$. The coefficients of the a-dependence are also allowed to have dependence on valence and sea mass dependence. This includes dependence on $\log(x_l)$ to model discretisation errors coming from staggered taste-changing effects [21].

TABLE XX: Complete error budget for r_1, f_{η_s}, M_{η_s} and f_{η_s}/M_{η_s}. Errors are given as a percentage of the physical value. Errors which are negligible compared to the others are indicated by '0'.

	r_1	f_{η_s}	M_{η_s}	f_{η_s}/M_{η_s}
stats/fitting	0.24	0.16	0.07	0.18
a-extrapolation	0.46	0.14	0.03	0.16
m_l-extrapolation	0.09	0.12	0.04	0.11
finite volume	0.04	0	0	0
r_1/a	0.73	0.12	0.02	0.12
initial r_1 uncertainty	0.26	0.02	0	0.02
M_π,M_K	0	0.05	0.14	0.09
Total	0.90	0.28	0.17	0.30

The terms in the chiral expansion are generally written so that the coefficients are expected to be $\mathcal{O}(1)$. For these coefficients we take the prior in our fit to be 0 ± 1. This is true for the higher order terms in the chiral expansion that relate to a-dependence and mass-dependence, except where the masses involved are sea-quark masses and then the prior is taken as 0 ± 0.3, simply because sea-quark effects are typically suppressed over valence quark effects by this amount. The prior on the bare decay constant parameter in chiral perturbation theory, f_0, is taken as 0.11 ± 0.02. In fact the parameter that is tuned by the fit is $\log(f_0)$ in order to keep f_0 positive. The prior on $\log(f_0)$ is then taken as -2.2 ± 0.18. The priors for the coefficients $L_{4,5,6,8}$ that multiply analytic terms at NLO in chiral perturbation theory are taken as 0 ± 0.01.

The meson masses are fitted simultaneously with the decay constants feeding in the 6×6 covariance matrix on each ensemble. The leading behaviour in chiral perturbation theory for the meson masses is now trivial. However the chiral fit, which shares some of the same coefficients as that of the decay constants [46], allows us to fix the higher order behaviour as a function of sea and valence masses. In particular it allows us to fix the behaviour of the η_s mass as the π and K masses vary, so that we can obtain its value at the physical point. The priors in the chiral fit for the meson masses take the same form as described above for the decay constant.

The fitting forms above were extensively tested for robustness against both real and fake data in [17] and [21].

The results of our fit are shown in Figure 15. The data points, adjusted for finite volume effects and for the slight mistuning of the valence and sea strange quark masses, are plotted as a function of x_l/x_s. The fit lines at each value of the lattice spacing are shown along with the $a = 0$ line. At the physical value for x_l/x_s we give the experimental values for f_π and f_K. This plot should be compared with Figure 4 in [21]. It is evident that these 'second generation' configurations have significantly smaller discretisation errors [19].

The fit has a χ^2/dof value of 0.3 for 36 degrees of freedom. The fitted value of f_0 is $\exp(-2.174 \pm 0.028)$, in agreement with SU(3) chiral fits using asqtad improved staggered quarks [47]. The resulting physical values for f_{η_s} and M_{η_s} are

$$\begin{aligned} f_{\eta_s} &= 0.1819(5)\text{GeV} \\ M_{\eta_s} &= 0.6893(12)\text{GeV} \\ f_{\eta_s}/M_{\eta_s} &= 0.2638(8). \end{aligned} \tag{29}$$

These are in agreement with the results obtained on $n_f = 2+1$ dynamical asqtad configurations [21] but considerably more accurate because our statistical precision is improved, and we have smaller continuum and chiral extrapolation errors. These last two are reduced because of the improvements in the gluon field configurations and because we are working closer to the chiral limit. Complete error budgets for f_{η_s}, M_{η_s} and their ratio are given in Table XX.

The results in equation 29 are very close, but in fact differ significantly from the expected result from leading order chiral perturbation theory. This is illustrated in Figures 16 and 17 in which the ratios $f_{\eta_s}/(2f_K - f_\pi)$ and $M^2_{\eta_s}/(2M^2_K - M^2_\pi)$ are plotted against x_l/x_s. Both ratios are very flat in x_l/x_s, never differing by as much as 1% from 1. We determine the physical values for the ratios to differ significantly from 1, however, with results:

$$\begin{aligned} f_{\eta_s}/(2f_K - f_\pi) &= 0.9977(6) \\ M^2_{\eta_s}/(2M^2_K - M^2_\pi) &= 1.0070(18). \end{aligned} \tag{30}$$

Since our fit uses r_1/a to set the relative lattice spacing we can determine a value for r_1 from the final match with experiment for f_π and f_K. We obtain

$$r_1(f_{\eta_s}) = 0.3209(29)\text{fm}. \tag{31}$$

The error budget for r_1 is given in Table XX. This physical result for r_1 agrees with the value obtained from the same analysis on $n_f = 2 + 1$ dynamical asqtad lattices [21], but is almost twice as accurate.

We can use f_{η_s} and M_{η_s} to determine the s quark mass and lattice spacing on each ensemble. This is done by tuning the s quark mass so that f_{η_s}/M_{η_s} takes the value in equation 29 and then the lattice spacing is read from the value of f_{η_s}. We do this here retrospectively by using our chiral fits to tune the s quark mass and work out the corresponding changes in f_{η_s} and M_{η_s}. For simplicity the sea light quark masses were also retuned to the physical value. The values of a obtained are given in Table X.

In Table XII we give tuned values of am_s on each ensemble as a result of tuning the η_s to the physical value given in equation 29. Over the short range needed for the retuning the relationship $m_s \propto M^2_{\eta_s}$ works very well. We give results for both the case of using the η_s decay constant to fix the lattice spacing and of using the Υ $2S-1S$ splitting. The values of am_s obtained from the two methods differ substantially on the very coarse lattices but come into agreement on the fine lattices as expected.

The errors in the tuned values of am_s are dominated by the errors in the lattice spacing. The relative error in a is doubled in am_s because the quark mass is proportional to the square of the meson mass. When the quark mass is converted to physical units one factor of the lattice spacing error disappears.

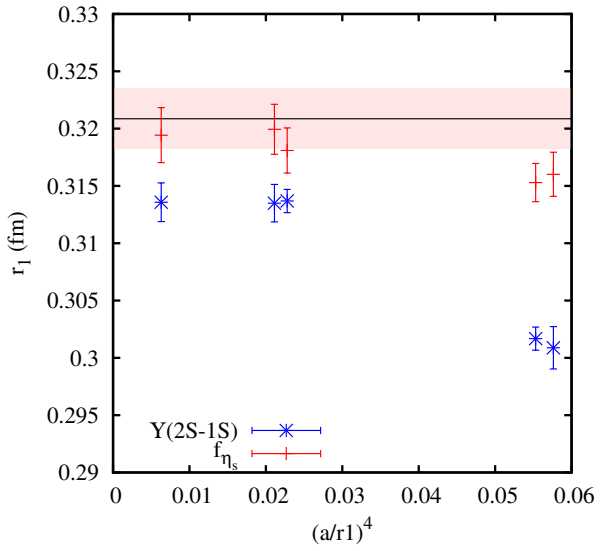

FIG. 18: Values for the heavy quark potential parameter r_1 obtained by combining values for r_1/a from MILC with either of our two methods for determining the lattice spacing. The red plus symbols correspond to using the η_s and the blue stars to using the Υ $2S-1S$ splitting (these points do not include the NRQCD systematic error which is correlated between the points). The black line with light red error band corresponds to the final value for r_1 from the combined fit to the results from both methods and includes the total error.

V. r_1

The values of the heavy quark potential parameter, r_1, can be determined by combining the values for r_1/a from MILC given in Table I with the values for the lattice spacing given from our two different methods in Table X. We use 'unsmoothed' values of r_1/a which are the results of an independent fit to the heavy quark potential on each ensemble. Figure 18 shows the results for r_1 from each method as a function of the lattice spacing. Differences are evident on the very coarse lattices as a result of discretisation errors but there is clear convergence as $a \to 0$. The results are plotted against $(a/r_1)^4$ since the leading tree-level discretisation errors are at a^4. Note that the behaviour of this plot is rather different from that obtained previously on the 2+1 flavor configurations (Figure 3 of [21]). There is a little less variation with a, to be expected because of the various improvements to the discretisation of QCD. The main difference however is the direction of approach to $a = 0$. The results for r_1 from f_{η_s} are now very flat and the results from the Υ approach $a = 0$ from below. This reflects a change in the relative discretisation errors of the quantities involved.

As discussed above, the chiral fits involving the η_s give a result for r_1 of 0.3209(29) fm. We can fit the results from using the Υ method to test if they are consistent with this. Using the η_s result as a prior for the Υ fit then enables us to extract an improved result for r_1 which combines both methods.

To extract a physical value for r_1 using the Υ results we use the same functional form for the fit as was used earlier for R_S and R_P, equation 17. This includes an allowance for variations as a function of the sea light quark masses, although it is clear from the results that any such dependence is very small. Indeed the quantities being used were chosen for their insensitivity to such effects. We also include an allowance for discretisation errors, both of the standard type, varying as $(a\Lambda)^n$ and the from various am_b-dependent type coming from radiative corrections in NRQCD. We also allow for the NRQCD systematic error from Tables VI and VII as a correlated error for all 5 ensembles.

The fit to the Υ values using a large width prior for the physical value (0.32(10)fm) gives $\chi^2/\mathrm{dof} = 0.79$ for 5 degrees of freedom and $r_1(\Upsilon) = 0.310(6)$ fm. This shows the required consistency in the determination of the lattice spacing from the two methods as $a \to 0$. The fit including the prior value from the η_s analysis gives $\chi^2/\mathrm{dof} = 0.76$ and result:

$$r_1 = 0.3209(26)\mathrm{fm}. \tag{32}$$

This is slightly improved over the η_s value on its own.

This final value for r_1 can now be used to determine a on other ensembles if values of r_1/a are available. We include in Table X the lattice spacing values on sets 1 to 5 from using r_1.

Our result for r_1 can be compared to our previous result of 0.3133(23) fm on the MILC 2+1 flavor dynamical asqtad lattices [21]. This is 2% lower than our current result with a combined uncertainty of 1% and so is not significant. In principle the two results do not have to agree because we are now including c quarks in the sea. However we expect this to have a small effect and then only in short-distance quantities [14]. We can obtain estimates for the effect on the Υ $2S-1S$ splitting from the fact that it is proportional to the hyperfine splitting. Missing c quarks in the sea increases the Υ mass by approximately 5 MeV with a smaller amount for excited states. It therefore reduces the $2S-1S$ splitting by approximately 2.5 MeV or 0.4%. This could have led previously to a 0.4% underestimate of r_1 from the Υ $2S-1S$ splitting if r_1/a itself was not affected. This effect is no larger than other sources of systematic error in the earlier calculation [2] coming from radiative corrections to v^4 terms that are also now included. Thus we cannot claim to see any strong evidence of an effect from c quarks in the sea. Indeed if we compare the r_1 values coming from the Υ analysis alone there is a change of 2(2)%, in which a 0.4% effect from c in the sea would be invisible. Any allowance for an effect on r_1 itself, also a fairly short distance quantity, would reduce this expected variation further. The η_s analysis would be expected to be very insensitive to sea charm because of the low internal momenta inside these light hadrons. For that case we see only a 0.5% change in the value of r_1 obtained, again with a 2% error.

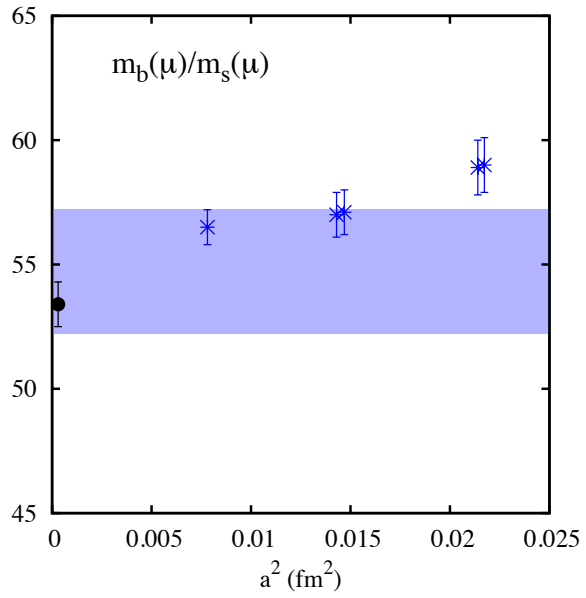

FIG. 19: Values for the ratio of the b quark mass to the s quark mass in the $\overline{MS}$ scheme at a given scale plotted against the square of the lattice spacing. Results are obtained from combining NRQCD b quark masses and HISQ s quark masses with an $\mathcal{O}(\alpha_s)$ perturbative renormalisation. The errors on the points include statistical/fitting errors, lattice spacing errors and NRQCD systematic errors. The final result, including the $\mathcal{O}(\alpha_s^2)$ perturbative error is plotted as the shaded blue band. The result from our previous fully nonperturbative calculation on ensembles including 2+1 flavors of sea quarks [48, 49] is given by the black filled circle at $a = 0$.

VI. m_b/m_s

From Table XII we can determine the ratio of the bare NRQCD b quark mass to the bare HISQ s quark mass on each ensemble. To do this we must use the same determination of the lattice spacing for the tuning of each mass, and so we use the lattice spacing determined from the Υ $2S-1S$ splitting (columns 2 and 3). The lattice spacing error appears doubled in m_s and once in m_b because of their different dependence on the meson masses used to fix them. These errors are correlated in the ratio m_b/m_s so one factor of the lattice spacing error cancels between numerator and denominator.

The ratio of masses in different schemes (NRQCD and HISQ) is not particularly useful. However, we can convert this using perturbation theory to a ratio of masses in the same mass-independent scheme, such as $\overline{MS}$, at the same scale, μ. The ratio then becomes scale-independent and the same in any scheme related to $\overline{MS}$ by a simple renormalisation. For both the NRQCD and the HISQ actions the mass renormalisation is known to $\mathcal{O}(\alpha_s)$.

The lattice to $\overline{MS}$ mass renormalisation constant is calculated by multiplying the lattice bare mass to pole mass renormalisation by the continuum pole mass to $\overline{MS}$ renormalisation. This latter renormalisation is given by:

$$m_q^{\overline{MS}}(\mu) = m_{\rm q,pole}\left(1+\alpha_s[-\frac{4}{3\pi}-\frac{2}{\pi}\ln\frac{\mu}{m_{\rm q,pole}}]+\ldots\right). \quad (33)$$

The lattice bare mass to pole mass renormalisation for HISQ quarks is given for small quark masses by [50, 51] [61]:

$$m_{\rm s,pole} = \frac{am_s}{a}\left(1+\alpha_s[-\frac{2}{\pi}\ln am_s + 0.5387]\ldots\right), \quad (34)$$

where we have written the equation explicity for the strange quark mass. When equations 33 and 34 are combined to obtain the conversion factor from the lattice bare mass to the $\overline{MS}$ mass at scale μ and $\mathcal{O}(\alpha_s)$ the logarithm multiplying α_s becomes $\ln(a\mu)$, and there is a constant given by 0.5387-4/(3π).

We can also write the NRQCD mass renormalisation in the form

$$m_{\rm b,pole} = \frac{am_b}{a}\left(1+\alpha_s[-\frac{2}{\pi}\ln am_b + A^{NRQCD}]\ldots\right). \quad (35)$$

although no $\ln(am)$ term is explicit in that calculation. On doing this we find that the remainder term, A^{NRQCD} given in Table XXIII, has very little am_b dependence.

Combining equations 33, 34 and 35 it is then clear that the ratio of $\overline{MS}$ masses for b and s is given to $\mathcal{O}(\alpha_s)$ by:

$$\frac{m_b^{\overline{MS}}(\mu)}{m_s^{\overline{MS}}(\mu)} = \frac{am_b}{am_s}\left[1+\alpha_s(A^{\rm NRQCD}-0.5387)+\ldots\right] \quad (36)$$

where the μ dependence cancels out. The ratio of bare lattice masses from columns 2 and 3 of Table XII varies very little with lattice spacing with values between 51 and 52. The renormalisation in equation 36 is a relatively mild one, with α_s coefficient varying between 0.31 and 0.39 with am_b value. We apply this one-loop renormalization with α_s values taken as $\alpha_V(1.8/a)$ from Table XXII. The energy scale for α_s is then in agreement with the Brodsky-Lepage-Mackenzie scale calculated for the light quark (asqtad) mass renormalisation in [50]. This gives the values for the $\overline{MS}$ m_b/m_s ratio plotted in Figure 19.

The results in Figure 19 show very little dependence on lattice spacing or sea quark mass within the 1% statistical and systematic errors from the lattice calculation. A much larger error is that from missing higher order powers of α_s in equation 36. We take account of this error by allowing a correlated error between the points of $1\times\alpha_V(1.8/a)^2$ along with a possible variation with am_b of the form $\alpha_V(1.8/a)^2\times\delta x_m/4$ (see equation 17 for a definition of δx_m). This allows the α_s^2 term to have both a coefficient and a mass dependence which is three times that of the known α_s term. We allow for possible dependence on sea quark masses and the lattice spacing by using a fit of the same form as that in equation 17.

The final fit result is then:

$$\frac{m_b^{\overline{MS}}(\mu)}{m_s^{\overline{MS}}(\mu)} = 54.7(2.5), \tag{37}$$

plotted as the shaded blue band in Figure 19. The error is dominated, not surprisingly, by the error from the unknown α_s^2 term.

We can compare this new result to a combination of our earlier results for m_b/m_c (4.51(4)) from [48] and m_c/m_s (11.85(16)) from [49]. These results were obtained entirely nonperturbatively by using the HISQ action for all the quarks. Then the ratio of lattice bare quark masses in the continuum limit is the ratio of $\overline{MS}$ masses at a given scale - the renormalisation factor cancels completely. From the numbers above we have $m_b/m_s = 53.4(9)$ which is plotted as the black point at $a = 0$ on Figure 19. Our new, completely independent, result agrees well with this earlier value although it is much less accurate.

VII. CONCLUSIONS

In this paper we have determined the Υ spectrum using the NRQCD formalism for the b quarks in lattice QCD. We include several improvements over our earlier work. The key improvements are:

- we use gluon field configurations with a fully $\mathcal{O}(\alpha_s a^2)$ improved gluon action and HISQ quarks in the sea, provided by the MILC collaboration;
- c quarks are now included in the sea;
- we take the NRQCD action to a new level of accuracy by including radiative corrections to the terms at next-to-leading relativistic order (v^4);
- we improve the method for tuning the b quark mass so that systematic errors are reduced to 0.5%.

With significantly improved systematic errors from NRQCD we are then able to determine the lattice spacing to better than 1% from the $2S-1S$ splitting. Using this we obtain $M(h_b) - M(1\overline{S})$ to 1.4% and $M(\Upsilon'') - M(\Upsilon)$ to 2.4% which is a strong test of NRQCD. This gives $M(h_b) = 9905(7)$ MeV to be compared with the experimental result of 9898.3(1.5) MeV [38] and $M(\Upsilon'') = 10375(22)$ MeV to be compared to the experimental result of 10355.2(5) MeV [35].

We have examined the Υ and η_b dispersion relations in much more detail than before, so that we can quantify the effect of the radiative corrections to the v^4 kinetic terms in the action. We are also able to show how small are the deviations from continuum rotational invariance. This enables us to tune the b quark mass to 0.5%.

Our result for the hyperfine splitting between the Υ and η_b states is much more accurate than in our earlier work because we have included the critical renormalisation of c_4 (the coefficient of the $\sigma\cdot\mathbf{B}$ term) in our analysis. We obtain $M(\Upsilon) - M(\eta_b) = 70(9)$ MeV now with a 13% error. This gives $M(\eta_b)$ of 9390(9) MeV to be compared to the experimental result of 9390.9(2.8) MeV.

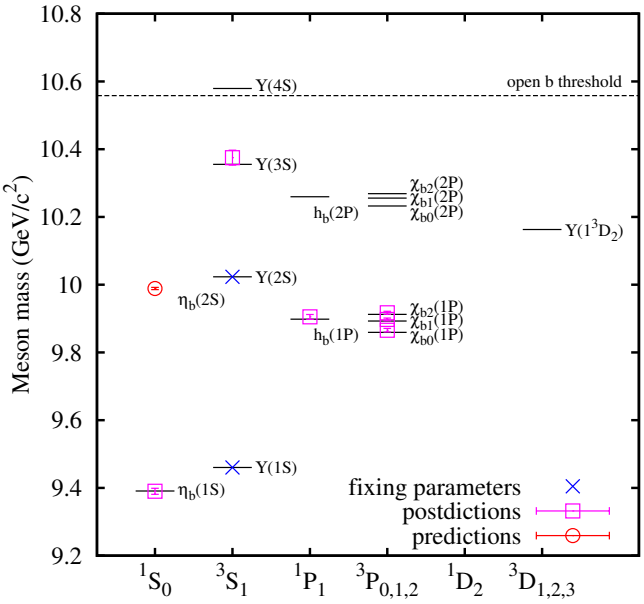

FIG. 20: The spectrum of bottomonium states from lattice NRQCD (colored symbols with error bars) compared to experiment (black lines). Blue crosses denote results used to tune parameters, pink open squares results to be compared to experiment and red circles predictions ahead of experiment [a]

[a]For simplicity we mark the Υ with a blue cross although in fact we use the spin-average of Υ and η_b to tune the b quark mass.

Our result for $M(\Upsilon') - M(\eta_b')$ is also much more accurate largely because of a huge improvement in the statistical error. We find a $2S$ hyperfine splitting that is half as big as the $1S$ hyperfine splitting at 35(3) MeV, predicting $M(\eta_b') = 9988(3)$ MeV.

These new results are collected together in a plot of the Υ spectrum from improved lattice NRQCD in Figure 20. We mark with different symbols those results used to tune parameters, those which correspond to masses already known from experiment, and those (the η_b') which are predictions. We include the P-wave fine structure from our results for $c_4 = 1.15$ on the fine lattices, set 5, since this c_4 is close to the perturbative value on those lattices. We include an additional 10% error for missing v^6 terms in our NRQCD action. D-wave Υ masses from our calculation will be reported elsewhere.

Light meson (π, K and η_s) masses and decay constants are also given here that enable us to determine the properties of the η_s meson and give a complementary determination of the lattice spacing to better than 1%. The calculation shows significantly improved discretisation errors over our earlier results on ensembles including 2+1 flavors of asqtad quarks [21]. The results on the properties of the η_s are in agreement with our earlier work.

However, our earlier result was not able to distinguish the mass and decay constant of the η_s from that that would be obtained in leading order chiral perturbation theory. We now obtain $M(\eta_s) = 0.6893(12)$ GeV and f_{η_s}=0.1819(5) GeV. In both cases these values disagree significantly, but by less than 1%, from the leading order expectation. The η_s particle is relatively insensitive to sea u/d quark masses and so it is very useful to have accurate results for its properties for tuning the s quark mass and determining the lattice spacing on other lattice ensembles.

The Υ $2S-1S$ and η_s determinations of the lattice spacing can be compared through a third parameter, r_1, from the heavy quark potential. We show that both determinations agree in the continuum and chiral limits and give a physical value for r_1 of 0.3209(26) fm. This can also be used to determine the lattice spacing on other lattice ensembles.

We also combine Υ and η_s calculations through a determination of the ratio of $\overline{MS}$ b quark to s quark masses of $m_b/m_s = 54.7(2.5)$, in agreement with our earlier result from HISQ quarks alone of 53.4(9) [48, 49].

Finally we comment on the effect of including c quarks in the sea. We have seen no significant effect on any of the observables that we have calculated compared to results obtained with 2+1 flavors of sea quarks. The results cannot be compared lattice spacing by lattice spacing because of changes to the lattice QCD action that reduce the size of discretisation errors in our new results. Final physical results can be compared, however, with and without sea c quarks to see if there is a difference. In our earlier 2+1 flavor calculations [14] we estimated that the presence of sea c quarks would shift the Υ and η_b masses downwards by 5 MeV through an induced additional local potential which was proportional to $\alpha_s^2\delta^3(r)/m_c^2$. This would have a smaller effect on radial excitations of the Υ than on the ground state masses and very little effect on P-wave states. We then estimate the effect on, for example the Υ $1P-1S$ splitting to be $\mathcal{O}(1\%)$. This would barely be visible above the errors in our current calculation and the errors in the earlier calculation were somewhat larger, so any comparison certainly has an error of greater than 1%. However, it is clear from our results that no unexpectedly large effect has appeared. For light hadrons we expect even smaller effects and there we can limit any differences in M_{η_s} and f_{η_s} to smaller than 1%, with the main error coming from our earlier calculation [21].

We are now combining b quark propagators from our improved NRQCD action with l, s and c propagators on these ensembles to study B, B_s and B_c meson masses and matrix elements. Significantly improved systematic errors should be possible both from the NRQCD action and because we are working much closer to physical light sea quark masses than before with an improved gluon and sea quark action.

Acknowledgments

We are grateful to the MILC collaboration for the use of their gauge configurations and particularly to Doug Toussaint for help in reading them and in providing values for r_1/a. The results described here were obtained using the Darwin Supercomputer of the University of Cambridge High Performance Computing Service as part of the DiRAC facility jointly funded by STFC, the Large Facilities Capital Fund of BIS and the Universities of Cambridge and Glasgow. This work was funded by STFC, MICINN, DGIID-DGA and NSF with support from the Scottish Universities Physics Alliance and the EU under ITN-STRONGnet.

Appendix A: Gauge Action

For clarity, the gauge action S_G used in the generation of the MILC ensembles will be summarised in this section. See [19]. The action is a tadpole and one-loop improved Lüscher-Weisz action,

$$\begin{aligned} S_G &= \beta\left[c_P\sum_P\left(1-\frac{1}{3}\mathrm{ReTr}(P)\right)\right. \\ &\quad +c_R\sum_R\left(1-\frac{1}{3}\mathrm{ReTr}(R)\right) \\ &\quad \left.+\,c_T\sum_T\left(1-\frac{1}{3}\mathrm{ReTr}(T)\right)\right] \end{aligned} \tag{A1}$$

where the sums are over plaquettes P, rectangles R and twisted loops (or parallelograms) T. The coefficients are calculated perturbatively through $\mathcal{O}(\alpha_s)$ including both gluonic loops [52] and contributions from HISQ sea quarks [20]. The tadpole improvement parameter was chosen to be the fourth root of the plaquette $u_{0P} = (\frac{1}{3}\mathrm{Re\ Tr}\langle P\rangle)^{1/4}$ and, via a perturbative calculation of the plaquette, gives an expression for the strong coupling constant $\alpha_s = -1.303615\log u_{0P}$. u_{0P} also appears in the gauge coupling as $\beta = 10/(g^2u_{0P}^4)$. The coefficients used are

$$\begin{aligned} C_P &= 1.0 \\ C_R &= \frac{-1}{20u_{0P}^2}(1-(0.6264-1.1746N_f)\log(u_{0P}^2)) \\ C_T &= \frac{1}{u_{0P}^2}(0.0433-0.0156N_f)\log(u_{0P}^2) \end{aligned} \tag{A2}$$

The inclusion of these terms mean that the gauge action is improved completely through order $\mathcal{O}(\alpha_s a^2)$. As mentioned in the text, sea quarks are included using the HISQ action [16] with a $U(3)$ projection (only) for the intermediate re-unitarization step.

Appendix B: Perturbative determination of radiative corrections to c_i coefficients in the NRQCD action and the mass renormalization

Spin-independent coefficients. The c_i coefficients appearing in the NRQCD action, equation 2, have expansion $1 + c_i^{(1)}\alpha_s + \mathcal{O}(\alpha_s^2)$. The $c_i^{(1)}$ for the kinetic terms, $i = 1, 5, 6$, are determined following the method of [26, 53]. The NRQCD quark self-energy is calculated through $\mathcal{O}(\alpha_s)$ and the $c_i^{(1)}$ are given by the requirement that the correct energy-momentum relationship be obtained through $\mathcal{O}(\alpha_s v^4)$. The terms proportional to $(\Delta^{(2)})^2$ in equation 2 can be merged together so that this term in δH appears as:

$$\tilde{c}_1(1 + \frac{am_b}{2n})\frac{(\Delta^{(2)})^2}{8(am_b)^3}. \tag{B1}$$

Thus only two radiative corrections need to be calculated for the complete set of kinetic terms at $\mathcal{O}(v^4)$, i.e. for $\tilde{c}_1$ and c_5. The radiative correction for $\tilde{c}_1$ then applies equally to c_1 and c_6.

The full inverse NRQCD quark propagator at $\mathcal{O}(\alpha_s)$ is

$$aG^{-1}(p) = Q^{-1}(p) - \alpha_s a\Sigma(p) \tag{B2}$$

where $ap = (a\mathbf{p}, ap_4)$ is a 4-vector in lattice Euclidean space. The pole in the propagator is identified as $a\omega(\mathbf{p}) = ip_4 a$. The expansion of $\omega(\mathbf{p})$ in powers of the spatial momentum can be used to identify the quark mass renormalisation factor Z_m and wavefunction renormalisation factor Z_2 but also to tune $\tilde{c}_1^{(1)}$ and $c_5^{(1)}$ to appropriate values. $Q^{-1}(p)$ is the quark propagator obtained at tree level from the NRQCD action, including the (as yet unknown) radiative corrections to $\tilde{c}_1$ and c_5. Its pole is then given by:

$$\begin{aligned} a\omega_0(\mathbf{p}) &= \frac{a^2\mathbf{p}^2}{2am_b} - \frac{(a^2\mathbf{p}^2)^2}{8(am_b)^3} + \alpha_s\left\{c_5^{(1)}\frac{a^4\mathbf{p}^4}{24am_b}\right. \\ &- \left.\tilde{c_1}^{(1)}\left(\frac{1}{2n} + \frac{1}{am_b}\right)\frac{(a^2\mathbf{p}^2)^2}{8(am_b)^3}\right\} \end{aligned} \tag{B3}$$

$\Sigma(p)$ is the one-loop self-energy and consists, as shown in Figure 21, of rainbow and tadpole diagrams as well as diagrams containing insertions of the one-loop piece of the tadpole-improvement factor, u_0. Writing $u_0 = 1 + \alpha_s u_0^{(1)}$, we have $u_0^{(1)} = 0.750$ for the Landau link tadpole parameter, u_{0L} [54]. We have

$$\omega(\mathbf{p}) = \omega_0(\mathbf{p}) - \alpha_s\Sigma(\omega_0(\mathbf{p}), \mathbf{p}) \tag{B4}$$

and can expand Σ to v^4 as:

$$\begin{aligned} a\Sigma(p) &= \Sigma_0(\omega) + \Sigma_1(\omega)\frac{a^2\mathbf{p}^2}{2am_b} \\ &+ \Sigma_2(\omega)\frac{(a^2\mathbf{p}^2)^2}{8(am_b)^3} + \Sigma_3(\omega)a^4\mathbf{p}^4. \end{aligned} \tag{B5}$$

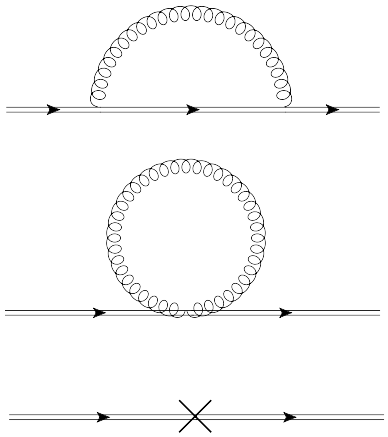

FIG. 21: The Feynman diagrams needed for the calculation of $\mathcal{O}(\alpha_s)$ corrections to the heavy quark self energy. From top to bottom, rainbow, tadpole and u_0 counterterm diagrams.

The Σ_i are extracted from suitable combinations of partial derivatives of Σ:

$$\begin{aligned} \Sigma_0 &= a\Sigma(\mathbf{p} = 0) \\ \Sigma_1 &= am_b\frac{\partial^2 a\Sigma}{\partial a^2 p_z^2}\bigg|_{\mathbf{p}=0} \\ \Sigma_2 &= (am_b)^3\frac{\partial^4 a\Sigma}{\partial a^2 p_z^2 \partial a^2 p_y^2}\bigg|_{\mathbf{p}=0} \\ \Sigma_3 &= \frac{1}{24}\left(\frac{\partial^4 a\Sigma}{\partial a^4 p_z^4} - 3\frac{\partial^4\Sigma}{\partial a^2 p_y^2 \partial a^2 p_z^2}\right)_{\mathbf{p}=\mathbf{0}}. \end{aligned} \tag{B6}$$

Each of the Σ_i also has an expansion in powers of ω as $\Sigma_i = \Sigma_{l=0}^{\infty}\Sigma_i^{(l)}\omega^l$. Then

$$a\omega(\mathbf{p}) = \frac{a^2\mathbf{p}^2}{2am_{b,r}} - \frac{(a^2\mathbf{p}^2)^2}{8(am_{b,r})^3} - \alpha_s a\delta\omega(\mathbf{p}) \tag{B7}$$

where $m_{b,r} = Z_m m_b$ and

$$Z_m = 1 + \alpha_s Z_m^{(1)} = 1 + \alpha_s(\Sigma_0^{(1)} + \Sigma_1^{(0)}) \tag{B8}$$

to this order. The correction term $\delta\omega$ is given by:

$$\begin{aligned} a\delta\omega &= W_0 + \\ &+ \left(W_1 + \tilde{c}_1^{(1)}\left(\frac{1}{2n} + \frac{1}{am_b}\right)\right)\frac{(a^2\mathbf{p}^2)^2}{8(am_b)^3} \\ &+ \left(W_2 - \frac{c_5^{(1)}}{24am_b}\right)a^4\mathbf{p}^4 \end{aligned} \tag{B9}$$

with

$$\begin{aligned} W_0 &= \Sigma_0^{(0)} \\ W_1 &= \frac{2\Sigma_0^{(1)}}{am_b} + 2\Sigma_0^{(2)} + \frac{3\Sigma_1^{(0)}}{am_b} + 2\Sigma_1^{(1)} + \Sigma_2^{(0)} \\ W_2 &= \Sigma_3^{(0)}. \end{aligned} \tag{B10}$$

The requirement that lattice NRQCD reproduce the low-energy physics of full QCD means that $\delta\omega$ can only be a pure energy shift independent of spatial momentum, i.e. the coefficients of $(\mathbf{p}^2)^2$ and $\mathbf{p}^4$ in equation B10 must be zero. Thus

$$\begin{aligned} \tilde{c}_1^{(1)} &= -\left(\frac{1}{2n}+\frac{1}{am_b}\right)^{-1} W_1 \\ c_5^{(1)} &= 24am_bW_2 \end{aligned} \tag{B11}$$

The Feynman rules were generated automatically using the HiPPy package and the Feynman lattice integrals for Σ and its derivatives were constructed and evaluated numerically using the HPsrc package and VEGAS contained therein [55, 56]. We use analytic differentiation using the TaylUR package in the HPsrc Fortran code together with numerical differentiation which, for sufficiently smooth functions, can be up to an order of magnitude faster than analytic differentiation.

Because the kinetic $(a^2\mathbf{p}^2)^2$ term is included at tree level both W_1 and W_2 are Infra-Red (IR) finite and so no IR regulation is needed although a gluon mass was used to regularize intermediate divergences. However, the integrals arising from the rainbow diagram still have large peaks in the IR region. These peaks arise because the differentiation generates extra powers of the heavy quark NRQCD propagator in the integrand. In this case to use numerical differentiation alone proves to be unstable and it is imperative to use a mixture of analytic and numerical approaches and also to introduce a suitable subtraction function to remove the most severe behaviour of the integrand. In contrast, the integrals arising from the tadpole diagram are well behaved because they contain no quark propagators but they are expensive to evaluate since the two-gluon vertex contains a large number of terms. In this case, numerical differentiation proved to be the most efficient for the higher order mixed derivatives without compromising accuracy. In all cases the temporal derivatives were done using the analytic method.

We checked that the results agree well with those of Morningstar [26, 53] for his gluon and NRQCD actions. For the simplest gluon and NRQCD actions the results agree with the analytic calculation of Monahan [57].

The contribution to the $c_i^{(1)}$ from the $u_0^{(1)}$ insertions of Figure 21 can be calculated analytically. This gives:

$$\begin{aligned} \frac{\tilde{c}_1^{(1)}}{u_0^{(1)}} &= -\frac{1}{8}\left(1+\frac{am_b}{2n}\right)^{-1}\left[\frac{12}{n^2}-\frac{1}{n}+\frac{1}{2am_b}\left(\frac{3}{n^2}-4\right)\right. \\ &+ \left.\frac{6}{(am_b)^2}\left(\frac{1}{n}-12\right)+\frac{6}{(am_b)^3}\right] \end{aligned} \tag{B12}$$

$$\frac{c_5^{(1)}}{u_0^{(1)}} = -\frac{4}{3}+\frac{1}{4am_b}+\frac{3}{(am_b)^2}-\frac{3}{8n(am_b)^2}-\frac{3}{4(am_b)^3}.$$

These contributions are sizeable and act to cancel contributions coming from the other diagrams, as part of the 'tadpole-improvement' mechanism [5, 26]. This is particularly true for $c_5^{(1)}$; less so for $\tilde{c}_1^{(1)}$, as in [26]. The $c_i^{(1)}$ values will then change depending on the tadpole-improvement parameter chosen, for example u_{0P} or u_{0L}, because the c_i must compensate perturbatively for changes in u_0. Here we use u_{0L} in the NRQCD action and this is the only u_0 that affects the c_i to $\mathcal{O}(\alpha_s)$. u_{0P} is used in the gluon action and counterterms from this will appear in the c_i at higher order.

TABLE XXI: Coefficients $\tilde{c}_1^{(1)}$ and $c_5^{(1)}$ that multiply α_s in the one-loop correction to the kinetic terms in the NRQCD action used here in conjunction with the improved gluon action described in Appendix A.

am_b	n	$\tilde{c}_1^{(1)}$	$c_5^{(1)}$
1.95	4	0.774(21)	0.392(17)
2.8	4	0.951(26)	0.406(11)
3.4	4	0.952(30)	0.445(10)

TABLE XXII: Values for α_V used in calculating the $\mathcal{O}(\alpha_s)$-corrected coefficients c_1, c_5, c_6 and c_4.

Sets	$1/a$ GeV	$\alpha_V^{(4)}(1.4/a)$	$\alpha_V^{(4)}(1.8/a)$	$\alpha_V^{(4)}(\pi/a)$
fine	2.2	0.32	0.28	0.225
coarse	1.6	0.39	0.33	0.255
very coarse	1.3	0.46	0.38	0.275

Table XXI gives the results for $\tilde{c}_1^{(1)}$ and $c_5^{(1)}$ for 3 different values of am_b and stability parameter $n = 4$. The mass values are not exactly the am_b values used for the numerical work in this paper but the $c_i^{(1)}$ show very mild dependence on am_b, so we can simply interpolate to the am_b values we are using. The results are different from those of [26] because both the gluon action and the NRQCD action have changed. However, qualitative features are the same in that the values are not large and only mild dependence on am_b is seen for am_b larger than 1. We note that the $c_i^{(1)}$ coefficients will change if higher order terms are added to the NRQCD action. For example [27] tests were done with an NRQCD action which included a term in δH of $-\Delta^{(6)}/(180am_b)$, removing $\mathcal{O}(a^6)$ discretisation errors from H_0. This changes $c_5^{(1)}$ to 0.017(4) for $am_b = 1.95$ and $n = 4$ to be compared with the result of 0.392(17) in Table XXI.

The coefficients in Table XXI need to be combined with a value for α_s to give final results for c_1, c_5 and c_6. The scale, q^*, used for α_s was taken as that calculated for the Brodsky-Lepage-Mackenzie scheme in Figure 10 of [26], assuming that this does not change significantly with the changes in the action used. This gives $q^* \approx 1.4/a$ for c_5 and $q^* \approx 1.8/a$ for $\tilde{c_1}$. We take α_s from [48], specifically the value $\alpha_{\overline{MS}}(M_z, n_f = 5) = 0.1183$. We convert this to α_V [58] and run perturbatively to values using $n_f = 4$ and appropriate scales q^*. The q^* values are calculated for the very coarse, coarse and fine ensembles using $a^{-1} \approx$ 1.3, 1.6 and 2.2 GeV respectively from Table X. The α_V values obtained are listed in Table XXII. These are

TABLE XXIII: Coefficients $Z_m^{(1)}$ and $c_4^{(1)}$ that multiply α_s in the one-loop correction to the mass renormalization and the $\sigma \cdot \mathbf{B}$ term in the NRQCD action respectively. These are calculated with the NRQCD action used here and the improved gluon action described in Appendix A. $A^{\rm NRQCD}$ in column 4 is $Z_m^{(1)} + 2\ln(am_b)/\pi$, as described in the text.

am_b	n	$Z_m^{(1)}$	$A^{\rm NRQCD}$	$c_4^{(1)}$
1.9	4	0.439(3)	0.848(3)	0.691(7)
2.65	4	0.263(5)	0.883(5)	0.775(8)
3.4	4	0.150(3)	0.929(3)	0.818(4)

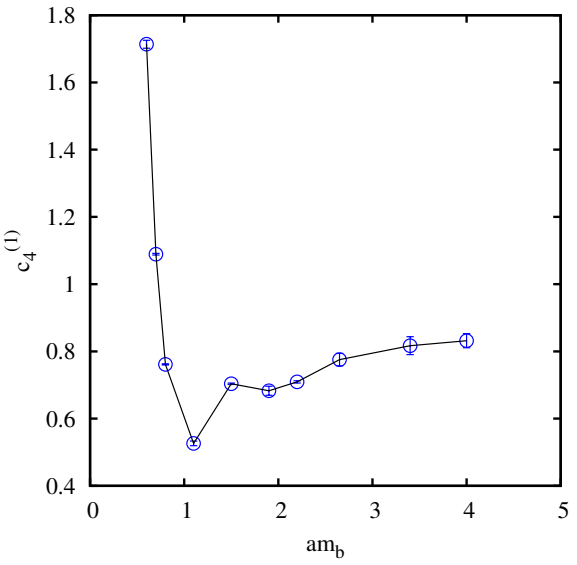

FIG. 22: The $\mathcal{O}(\alpha_s)$ coefficient in the perturbative expansion of c_4, coefficient of the $\sigma \cdot \mathbf{B}$ term, plotted against the bare b quark mass.

combined with the coefficients in Table XXI to give the values used in Table II. The coefficient $\tilde{c}_1^{(1)}$ was reduced slightly on the fine lattices (to 0.766) to account for the fact that the value of am_b used was slightly smaller than that for which the coefficient was calculated.

The remaining errors in the kinetic c_i coefficients after this one-loop correction has been made will be $\mathcal{O}(\alpha_s^2)$. From Table XXII we can see that $0.5\alpha_V^2$ ranges from 0.1 on the very coarse ensembles to 0.05 on fine. The impact of these errors can then be estimated from the size of the effect that we see on physical observables from the $\mathcal{O}(\alpha_s)$ corrections.

We have not corrected the coefficient of the Darwin term, c_2, in our NRQCD Hamiltonian. We have however assessed the effect of taking c_2 to be as large as 1.25 on the meson kinetic mass and on the hyperfine splitting and we find the effects to be small.

Mass renormalization. In Table XXIII we give values for $Z_m^{(1)}$, the coefficient of α_s in the mass renormalization of equation B8. Z_m was calculated previously for different parameter values in [59]. We also show the result of adding $2\ln(am_b)/\pi$ to $Z_m^{(1)}$ as $A^{\rm NRQCD}$. $A^{\rm NRQCD}$ will be used in section VI to derive the ratio m_b/m_s in the $\overline{MS}$ scheme. Only mild dependence on am_b is seen in $A^{\rm NRQCD}$.

TABLE XXIV: Coefficients d_1 and d_2 of spin-dependent 4-quark operators that give rise to a correction to the hyperfine splitting. These are calculated with the NRQCD action used here with the parameters given in columns 1 and 2 and the improved gluon action described in Appendix A.

am_b	n	d_1	d_2
1.9	4	$-\ln(1.9)$ + 0.796(4)	ln(1.9)/3 -0.311(1)
2.65	4	$-\ln(2.65)$ + 0.448(6)	ln(2.65)/3 -0.195(2)
3.4	4	$-\ln(3.4)$ + 0.038(8)	ln(3.4)/3 -0.058(2)

Spin-dependent terms. The perturbative renormalisation of field-dependent terms has to be done in a different way and this includes all the spin-dependent terms. Recently the radiative corrections to c_4 have become available [28]. They were calculated by matching the effective action in NRQCD to continuum QCD using the background field method. We give values for $c_4^{(1)}$ in Table XXIII appropriate to the am_b and n values we are using here.

A number of pieces go in to the calculation of $c_4^{(1)}$. These include renormalisation of the chromomagnetic moment, renormalisation of the wavefunction and, because c_4 multiplies a term in the bare lattice NRQCD Hamiltonian which includes the bare lattice quark mass, the mass renormalisation. $c_4^{(1)}$ is the sum of two pieces, one of which has polynomial dependence on the bare quark mass am_b and the other is proportional to $\log(am_b)$. The logarithmic term has coefficient $-3/(2\pi)$ [28]. Both terms are included in the total result given in Table XXIII - the logarithmic term is of similar size to the polynomial term over the range of am_b that we are using. The $c_4^{(1)}$ values are combined with values for $\alpha_V^{(4)}(\pi/a)$ (given in Table XXII) to give the results for the 1-loop corrected c_4 coefficients given in Table XIII.

Figure 22 gives a more complete picture of $c_4^{(1)}$ by plotting values as a function of am_b. We see relatively little am_b dependence until am_b becomes smaller than 1 when $c_4^{(1)}$ starts to diverge. This is typical of the behaviour of radiative corrections to coefficients in the NRQCD action.

Finally we give results for the coefficients of the spin-dependent 4-quark operators that contribute to the hyperfine splitting. These terms have coefficients d_1 and d_2 that multiply terms that would appear in the NRQCD action at order $\mathcal{O}(\alpha_s^2 v^3)$:

$$S_{4q} = d_1 \frac{\alpha_s^2}{(am_b)^2}(\psi^\dagger \chi^*)(\chi^T \psi) + d_2 \frac{\alpha_s^2}{(am_b)^2}(\psi^\dagger \sigma \chi^*)\cdot(\chi^T \sigma \psi). \quad \text{(B13)}$$

These terms are subleading compared to treelevel v^4 operators but contribute to the hyperfine splitting at the same order as α_s corrections to c_4 [28]. We do not include these 4-quark terms in our NRQCD action but we can estimate their effect because they give rise a shift in the relative energies of the Υ and η_b which is proportional to the 'wavefunction-at-the-origin', and given by:

$$\Delta E_{hyp} = \frac{6\alpha_s^2(d_2 - d_1)}{m_b^2}|\psi(0)|^2. \qquad \text{(B14)}$$

The relevant coefficients, d_1 and d_2 are given in Table XXIV. They were calculated previously for a slightly different NRQCD action in [28]. The coefficients are related by:

$$d_1 = -3d_2 - \frac{4}{9}(1 - \ln(2)) \qquad \text{(B15)}$$

where the term proportional to $(\ln 2 - 1)$ is from η_b annihilation to 2 gluons. This term increases the hyperfine splitting from equation B14 since it pushes the η_b mass down. When equation B14 is applied for just this piece we obtain an estimate of its size of about 1 MeV. This is smaller, but in agreement with, the earlier estimate of 2.4(2.4) MeV applied in section III C in deriving an appropriate spin-averaged $1S$ meson mass to tune the b quark mass against. For that purpose the shift is completely negligible, representing a tiny fraction of the η_b mass. For the hyperfine splitting it is a more important issue. For this we take the results from equation B14 because that provides a consistent treatment of all the 4-quark operator effects.

d_1 and d_2 are separated into logarithmic and nonlogarithmic pieces in Table XXIV. The nonlogarithmic piece has significant mass dependence here, becoming small at large ma. The logarithmic and nonlogarithmic terms in fact cancel for ma around 1.9. In assessing the error in the hyperfine splitting from missing higher order terms multiplying the 4-quark operators we are careful not to assume that this is generic behaviour.

We combine the d_1 and d_2 coefficients with $\alpha_V(\pi/a)$ values from Table XXII and values for $|\psi(0)|^2$ from our fits to obtain corrections to the hyperfine splitting that are applied in section III E 3.

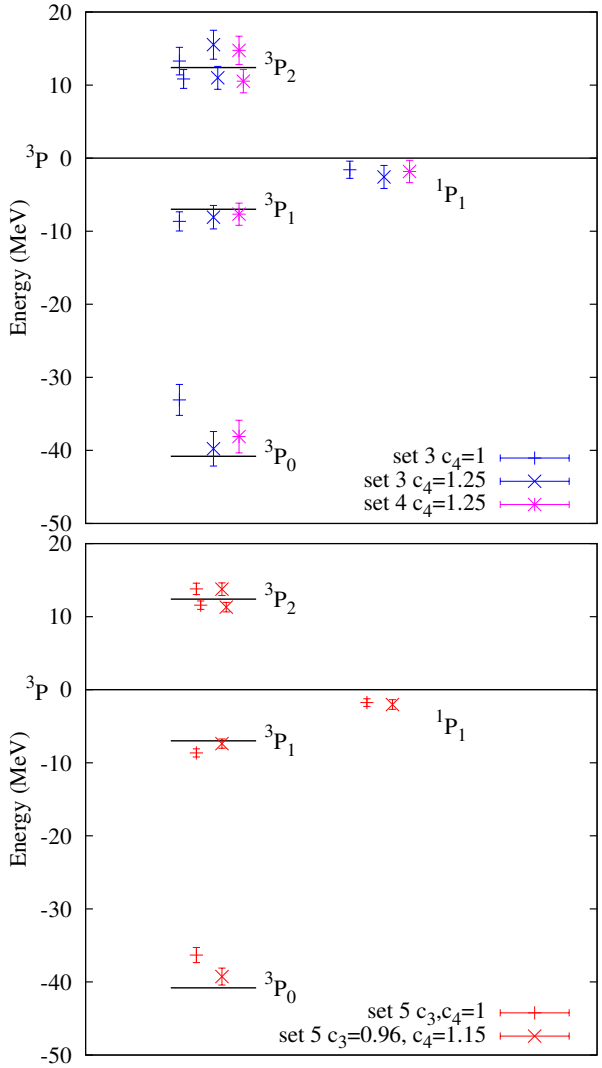

FIG. 23: The masses of the lowest-lying P-wave states in the Υ spectrum plotted relative to the spin-average of the ^3P states for the coarse lattices, sets 3 and 4 (top plot) and the fine lattices, set 5 (lower plot). In each plot we compare mass splittings for $c_4 = 1$ with a nonperturbatively tuned value for c_4 chosen to match a combination of mass splittings to experiment (see text). $c_3 = 1$ in all cases. For the $^3P_2$ states the ^3P_E is plotted to the left of the $^3P_{T_2}$.

Appendix C: Nonperturbative determination of radiative corrections to c_3 and c_4 coefficients in the NRQCD action

An alternative approach to tuning the spin-dependent coefficients c_3 and c_4 is from matching fine structure in the spectrum to experiment. Here we use the P-wave fine structure in the Υ spectrum to do this [2, 12]. The P-wave masses are shifted from the spin-average by amounts that depend on spin-spin coupling terms proportional to $\mathbf{S}\cdot\mathbf{S}$ or S_{ij} and spin-orbit terms proportional to $\mathbf{L}\cdot\mathbf{S}$. The spin-spin terms are proportional to c_4^2 and the spin-orbit terms to c_3. We can make a combinations of the ^3P state masses in which the eigenvalues of S_{ij} and $\mathbf{S}\cdot\mathbf{S}$ cancel, and a separate combination in which the eigenvalues of $\mathbf{S}\cdot\mathbf{S}$ and $\mathbf{L}\cdot\mathbf{S}$ cancel. Thus each of these combinations gives a result which should depend on only one of the spin-dependent couplings in our current NRQCD action. Comparing these combinations to experiment allows us to tune c_3 and c_4. Note that 4-quark operators, discussed in Appendix B with reference to their effect on S-wave hyperfine splittings, have negligible effect on P-wave states, and they therefore give a very clean determination of c_3 and c_4.

The eigenvalues for $\mathbf{L}\cdot\mathbf{S}$, S_{ij} and $\mathbf{S}\cdot\mathbf{S}$ for $^{2S+1}L_J$ states

	Set 3	Set 3	Set 4	Set 5	Set 5
	$am_b = 2.66$	$am_b = 2.66$	$am_b = 2.62$	$am_b = 1.91$	$am_b = 1.91$
	$c_4 = 1.0$	$c_4 = 1.25$	$c_4 = 1.25$	$c_4 = 1.0$	$c_4 = 1.15$
	$c_3 = 1.0$	$c_3 = 1.0$	$c_3 = 1.0$	$c_3 = 1.0$	$c_3 = 0.96$
$aE(1^1P_1)$	0.5655(23)	0.5247(22)	0.5253(20)	0.4833(10)	0.4478(11)
$aE(1^3P_0)$	0.5460(20)	0.5017(20)	0.5034(18)	0.4678(9)	0.4312(9)
$aE(1^3P_1)$	0.5611(24)	0.5213(26)	0.5218(24)	0.4802(10)	0.4454(11)
$aE(1^3P_E)$	0.5747(30)	0.5359(28)	0.5354(25)	0.4903(11)	0.4549(12)
$aE(1^3P_{T_2})$	0.5732(28)	0.5331(28)	0.5328(27)	0.4893(11)	0.4538(12)
$aE(1^1P_1) - aE(^3\overline{P})$	-0.0010(7)	-0.0016(10)	-0.0011(9)	-0.0008(2)	-0.0009(2)
$aE(1^3P_0) - aE(^3\overline{P})$	-0.0204(13)	-0.0246(14)	-0.0231(13)	-0.0163(4)	-0.0176(5)
$aE(1^3P_1) - aE(^3\overline{P})$	-0.0053(8)	-0.0050(10)	-0.0046(9)	-0.0039(2)	-0.0033(3)
$aE(1^3P_E) - aE(^3\overline{P})$	0.0082(12)	0.0096(12)	0.0089(11)	0.0062(3)	0.0062(4)
$aE(1^3P_{T_2}) - aE(^3\overline{P})$	0.0067(8)	0.0068(10)	0.0064(10)	0.0052(3)	0.0051(3)
$2aE(1^3P_2E) + 3aE(1^3P_2T_2)$	0.093(8)	0.104(9)	0.097(8)	0.072(3)	0.073(3)
$-3aE(1^3P_1) - 2aE(1^3P_0)$					
$0.4aE(1^3P_2E) + 0.6aE(1^3P_2T_2)$	-0.018(2)	-0.026(4)	-0.025(3)	-0.0153(7)	-0.0198(9)
$-3aE(1^3P_1) + 2aE(1^3P_0)$					

TABLE XXV: Fitted energies for P-wave states on sets 3, 4 and 5 for the NRQCD parameters given. The last two rows give the combination of energies used to determine c_3 and c_4. Errors are from statistics/fitting only.

	3	3	4	5	5
	$c_4 = 1$	$c_4 = 1.25$	$c_4 = 1.25$	$c_4 = 1$	$c_4 = 1.15$
	$c_3 = 1.0$	$c_3 = 1.0$	$c_3 = 1.0$	$c_3 = 1.0$	$c_3 = 0.96$
$5E(1^3P_2) - 3E(1^3P_1) - 2E(1^3P_0)$	0.151(13)	0.168(14)	0.160(13)	0.161(6)	0.162(7)
$E(1^3P_2) - 3E(1^3P_1) + 2E(1^3P_0)$	-0.028(4)	-0.042(6)	-0.041(5)	-0.0342(16)	-0.0442(20)

TABLE XXVI: Combinations of P-wave energies needed to fix c_3 and c_4 in GeV. Lattice spacing values are taken from Table X. Errors are statistical/fitting only.

$\{^3P_0, ^3P_1, ^3P_2, ^1P_1\}$ (i.e. $\{\chi_{b0}, \chi_{b1}, \chi_{b2}, h_b\}$) are:

$$\begin{aligned} \mathbf{L}\cdot\mathbf{S} &: \{-2,-1,1,0\}; \\ S_{ij} &: \{-4,2,-2/5,0\}; \\ \mathbf{S}\cdot\mathbf{S} &: \{1/4,1/4,1/4,-3/4\}. \end{aligned} \tag{C1}$$

We see that the $\mathbf{S}\cdot\mathbf{S}$ terms affect the splitting between the $^1P_1$ and the spin-average of the ^3P states. We expect this splitting to be small because, in a potential model approach, the accompanying spin-dependent potential would be a delta function at the origin with very little overlap for P-wave states. Both S_{ij} and $\mathbf{L}\cdot\mathbf{S}$ terms affect the splittings within the ^3P sector but not the splitting between $^1P_1$ and $^3\overline{P}$. The $\mathbf{L}\cdot\mathbf{S}$ terms give the conventional ordering of $^3P_0$, $^3P_1$ and $^3P_2$, but with the $^3P_2$ splitting from the $^3P_1$ larger than that between the $^3P_1$ and $^3P_0$. The S_{ij} terms will push down the $^3P_2$ relative to the others. Thus the final splittings depend on the relative strength of the accompanying potentials for these terms and, in NRQCD language, the coefficients c_3 and c_4.

The combination of spin-splittings that depends on c_4^2 (through S_{ij}) and is independent of c_3 is [2]

$$M(\chi_{b2}) - 3M(\chi_{b1}) + 2M(\chi_{b0}) \tag{C2}$$

with experimental value: -47.4(1.3) MeV [35], determining the errors on mass differences by adding the errors on the masses in quadrature. Likewise the combination that depends on c_3 only

$$5M(\chi_{b2}) - 3M(\chi_{b1}) - 2M(\chi_{b0}) \tag{C3}$$

with experimental value: 163.8(3.2) MeV [35]. Comparison of our results with experiment for these combinations then allows us to fix c_3 and c_4.

Table XXV gives the results for the energies in lattice units of the lowest-lying P-wave states for the am_b values given in Table III on the coarse (sets 3 and 4) and fine (set 5) lattices. The results were obtained from 5 exponential fits of the form given in equation 7 to the 2×2 matrix of correlators for each P-wave meson done as a single simultaneous fit. This enables us to extract mass differences more precisely from the fit than the individual masses and the splitting between each state and the spin-average of all the ^3P states is also given. Note that we give separate values for ^3P_2E and $^3P_2T_2$ lattice representations of the $J = 2$ state. Differences between the values obtained for T_2 and E would be a sign of discretisation errors. We do not have a significant signal for this but the E state is higher than the T_2 in all of our fits. The difference is about 3(2) MeV on the coarse lattices and 2(1) MeV on the fine lattices.

Results are given for the case $c_4 = 1$ and a nonzero value of c_4 chosen to give reasonable agreement with the experimental value of the combination in equation C2.

Results in GeV for the two combinations tested are given in Table XXVI using values of the lattice spacing from the $(2S-1S)$ splitting in Table X, and combining the E and T_2 representations for the $^3P_2$ state with the appropriate number of spin states. We see that $c_3 = 1$ within our errors, but c_4 needs to be larger than 1, more so on the coarse lattices than the fine. We take the same value of c_4 on both coarse sets since the tuning should not depend on the sea quark masses and indeed our results demonstrate that it does not.

Figure 23 shows the spectrum of P-wave states relative to the ^3P spin-average $(5M(\chi_{b2}) + 3M(\chi_{b1}) + M(\chi_{b0}))$. The results with $c_4 > 1$ clearly agree better with experiment than for $c_4 = 1$. The main effect of increasing c_4 is to push the χ_{b0} state down relative to the spin-average. Very little else changes. In particular we see that the splitting between the $^1P_1$ and the ^3P spin-average is very small and negative in all cases. It increases with increasing c_4 but, because the splitting itself is so small, this is not significant. We obtain a P-wave hyperfine splitting of 2(2) MeV on both coarse and fine lattices, where the experimental result is 1.6 ± 1.5 MeV [38].

On the fine lattices we took $c_4 = 1.15$, based on initial calculations. From Table XXVI and Figure 23 this appears to be an underestimate and an improved value would be 1.18. We also used $c_3 = 0.96$ but that value is indistinguishable within our errors from $c_3 = 1.0$. On the coarse lattices, $c_4 = 1.25$ is also a slight underestimate, although it agrees within statistical errors with the correct answer.

The final nonperturbatively tuned values for c_3 and c_4 that we obtain are then: $c_3 = 1.00(9)(2)(10)$ on coarse lattices and 1.00(4)(2)(10) on fine lattices. Our best estimates for c_4 are:

$$\begin{aligned} c_4(\text{coarse}) &= 1.28(7)(1)(5) \\ c_4(\text{fine}) &= 1.18(2)(1)(5). \end{aligned} \tag{C4}$$

The first error is from the statistical/fitting error on the P-wave masses along with the lattice spacing error. The second error is from experiment. The third error is a systematic error from v^6 terms in NRQCD that are missing from our calculation but that have effectively been absorbed into the value of c_3/c_4 from matching to experiment. The spin splittings could change by $\mathcal{O}(10\%)$ from v^6 terms. Note that c_4 gets closer to 1 as the lattice gets finer as we expect. Note also that the relationship between c_3 and c_4 that holds in potential models or NRQCD in the continuum because of Lorentz covariance [36] is not applicable to lattice NRQCD in this formulation.

The agreement between the c_4 coefficients obtained nonperturbatively and the c_4 coefficients obtained at $\mathcal{O}(\alpha_s)$ in Appendix B is good, and certainly within possible α_s^2 variation of the perturbative coefficients (see Table XIII).

Our nonperturbative results for c_4 and c_3 agree well with those derived for the same NRQCD action on different gluon configurations at similar lattice spacing in [12]. There spin-dependent terms at v_b^6 are also included in a separate calculation and then the values derived for the v^4 coefficients c_3 and c_4 change (both increasing). Note that in that paper the calculations were done with tree-level coefficients for all c_i and the results rescaled for the derived values of c_4.

Appendix D: Results for the Kinetic mass

We give here the tables of results for the ground-state energies and kinetic masses (as defined in equation 10) of the Υ and η_b mesons for different lattice meson momenta in units of $2\pi a/L$. We also give the spin-averaged $1S$ kinetic mass. Results are taken from simultaneous fits to local correlators with the given momentum and with momentum zero using the fit form in equation 7. The energies for each momentum and the energy difference which yields the kinetic mass are given directly by the fit. Correlations between the correlators mean that the error on the energy difference is typically smaller than the combined errors from the separate energies. This is particularly true of the 'on-axis' momenta which have only one non-zero component. So, for example, the kinetic mass for momentum (2,0,0) is more precise than that for (1,1,1).

The results are given for coarse ensemble set 3 and fine ensemble set 5 with separate results for the case where $c_{1,5,6}$ are taken to be 1 and the case where $c_{1,5,6}$ are α_s-improved. We take 9 exponential fits on set 3 and 7 exponential fits on set 5.

[1] C. T. H. Davies et al. (HPQCD, MILC and Fermilab Lattice), Phys. Rev. Lett. **92**, 022001 (2004), hep-lat/0304004.

[2] A. Gray, I. Allison, C. Davies, E. Dalgic, G. Lepage, et al. (HPQCD), Phys.Rev. **D72**, 094507 (2005), hep-lat/0507013.

[3] A. Gray, PhD thesis (University of Glasgow, 2004).

[4] G. Lepage, L. Magnea, C. Nakhleh, U. Magnea, and K. Hornbostel, Phys.Rev. **D46**, 4052 (1992), hep-lat/9205007.

[5] G. Lepage and P. B. Mackenzie, Phys.Rev. **D48**, 2250 (1993), phys. Lett. B., hep-lat/9209022.

[6] A. Bazavov et al., Rev. Mod. Phys. **82**, 1349 (2010), 0903.3598.

[7] Z. Hao, G. M. von Hippel, R. R. Horgan, Q. J. Mason, and H. D. Trottier, Phys. Rev. **D76**, 034507 (2007), 0705.4660.

[8] K. Orginos and D. Toussaint (MILC), Phys. Rev. **D59**, 014501 (1999), hep-lat/9805009.

[9] K. Orginos, D. Toussaint, and R. L. Sugar (MILC), Phys.

Rev. **D60**, 054503 (1999), hep-lat/9903032.
[10] G. P. Lepage, Phys. Rev. **D59**, 074502 (1999), hep-lat/9809157.
[11] S. Meinel, Phys. Rev. **D79**, 094501 (2009), 0903.3224.
[12] S. Meinel, Phys.Rev. **D82**, 114502 (2010), 1007.3966.
[13] C. T. H. Davies et al. (HPQCD), Phys. Rev. D in press (2010), 1008.4018.
[14] E. B. Gregory et al. (HPQCD), Phys. Rev. **D83**, 014506 (2011), 1010.3848.
[15] E. B. Gregory et al. (HPQCD), Phys. Rev. Lett. **104**, 022001 (2010), 0909.4462.
[16] E. Follana et al. (HPQCD), Phys.Rev. **D75**, 054502 (2007), hep-lat/0610092.
[17] E. Follana, C. T. H. Davies, G. P. Lepage, and J. Shigemitsu (HPQCD), Phys. Rev. Lett. **100**, 062002 (2008), 0706.1726.
[18] C. McNeile, C. T. H. Davies, E. Follana, K. Hornbostel, and G. P. Lepage (HPQCD) (2011), 1110.4510.
[19] A. Bazavov et al. (MILC), Phys.Rev. **D82**, 074501 (2010), 1004.0342.
[20] A. Hart, G. M. von Hippel, and R. R. Horgan (HPQCD), Phys. Rev. **D79**, 074008 (2009), 0812.0503.
[21] C. Davies, E. Follana, I. Kendall, G. Lepage, and C. McNeile (HPQCD), Phys.Rev. **D81**, 034506 (2010), 0910.1229.
[22] C. Aubin et al. (MILC), Phys. Rev. **D70**, 094505 (2004), hep-lat/0402030.
[23] R. Sommer, Nucl. Phys. **B411**, 839 (1994), hep-lat/9310022.
[24] D. Toussaint (private communication).
[25] B. Thacker and G. Lepage, Phys.Rev. **D43**, 196 (1991).
[26] C. J. Morningstar, Phys. Rev. **D50**, 5902 (1994), hep-lat/9406002.
[27] E. Mueller, PhD thesis (University of Edinburgh, 2009).
[28] T. C. Hammant, A. G. Hart, G. M. von Hippel, R. R. Horgan, and C. J. Monahan, Phys. Rev. Lett. **107**, 112002 (2011), 1105.5309.
[29] C. T. H. Davies et al., Phys. Rev. **D37**, 1581 (1988).
[30] C. T. H. Davies et al., Phys. Rev. **D50**, 6963 (1994), hep-lat/9406017.
[31] I. D. Kendall, PhD thesis (University of Glasgow, 2010).
[32] C. Gattringer and C. B. Lang, Lect. Notes Phys. **788**, 1 (2010).
[33] G. P. Lepage et al., Nucl. Phys. Proc. Suppl. **106**, 12 (2002), hep-lat/0110175.
[34] C. Bernard et al. (Fermilab Lattice and MILC), Phys. Rev. **D83**, 034503 (2011), 1003.1937.
[35] K. Nakamura et al. (Particle Data Group), J. Phys. **G37**, 075021 (2010).
[36] G. S. Bali, K. Schilling, and A. Wachter, Phys. Rev. **D56**, 2566 (1997), hep-lat/9703019.
[37] T. Burch et al. (Fermilab Lattice and MILC), Phys. Rev. **D81**, 034508 (2010), 0912.2701.
[38] I. Adachi et al. (Belle) (2011), 1103.3419.
[39] B. Aubert et al. (BABAR), Phys. Rev. Lett. **101**, 071801 (2008), 0807.1086.
[40] B. Aubert et al. (BABAR), Phys. Rev. Lett. **103**, 161801 (2009), 0903.1124.
[41] G. Bonvicini et al. (CLEO), Phys. Rev. **D81**, 031104 (2010), 0909.5474.
[42] R. Mizuk (Belle), Quarkonium Working Group meeting (2011).
[43] B. A. Kniehl, A. A. Penin, A. Pineda, V. A. Smirnov, and M. Steinhauser, Phys. Rev. Lett. **92**, 242001 (2004), [Erratum-ibid.104:199901,2010], hep-ph/0312086.
[44] A. A. Penin (2009), 0905.4296.
[45] C. Aubin et al. (MILC), Phys. Rev. **D70**, 114501 (2004), hep-lat/0407028.
[46] S. R. Sharpe and N. Shoresh, Phys. Rev. **D62**, 094503 (2000), hep-lat/0006017.
[47] A. Bazavov et al. (MILC), PoS **LAT2009**, 079 (2009), 0910.3618.
[48] C. McNeile, C. T. H. Davies, E. Follana, K. Hornbostel, and G. P. Lepage (HPQCD), Phys. Rev. **D82**, 034512 (2010), 1004.4285.
[49] C. T. H. Davies et al. (HPQCD), Phys. Rev. Lett. **104**, 132003 (2010), 0910.3102.
[50] Q. Mason, H. D. Trottier, R. Horgan, C. T. H. Davies, and G. P. Lepage (HPQCD), Phys. Rev. **D73**, 114501 (2006), hep-ph/0511160.
[51] Q. Mason (private communication).
[52] M. G. Alford, W. Dimm, G. P. Lepage, G. Hockney, and P. B. Mackenzie, Phys. Lett. **B361**, 87 (1995), hep-lat/9507010.
[53] C. J. Morningstar, Phys. Rev. **D48**, 2265 (1993), hep-lat/9301005.
[54] M. A. Nobes, H. D. Trottier, G. P. Lepage, and Q. Mason, Nucl. Phys. Proc. Suppl. **106**, 838 (2002), hep-lat/0110051.
[55] A. Hart, G. M. von Hippel, R. R. Horgan, and L. C. Storoni, J.Comput.Phys. **209**, 340 (2005), hep-lat/0411026.
[56] A. Hart, G. M. von Hippel, R. R. Horgan, and E. H. Müller, Comput.Phys.Commun. **180**, 2698 (2009), 0904.0375.
[57] C. Monahan, PhD thesis (University of Cambridge, 2011).
[58] C. T. H. Davies et al. (HPQCD), Phys. Rev. **D78**, 114507 (2008), 0807.1687.
[59] E. Dalgic, J. Shigemitsu, and M. Wingate, Phys. Rev. **D69**, 074501 (2004), hep-lat/0312017.
[60] Note that in our previous work [14] we had to allow for a mass shift from missing c quarks in the sea. That is no longer necessary here.
[61] Note that there is a typographical error in [50] so that the lattice logarithm is given the wrong sign in equation 11.

	(0,0,0)	(1,0,0)	(1,1,1)	(2,0,0)	(2,2,1)	(3,0,0)
$aE(^1S_0,\mathbf{P})$	0.25529(4)	0.26119(4)	0.27309(4)	0.27890(4)	0.30830(8)	0.30814(6)
$aE(^3S_1,\mathbf{P})$	0.28626(6)	0.29220(7)	0.30426(7)	0.31007(9)	0.33977(17)	0.33957(14)
$aM_{\rm Kin}(\eta_b)$	-	5.773(10)	5.767(7)	5.788(2)	5.787(7)	5.805(3)
$aM_{\rm Kin}(\Upsilon)$	-	5.716(25)	5.703(17)	5.739(7)	5.732(15)	5.753(11)
$\overline{aM}_{\rm Kin}(1S)$	-	5.730(20)	5.719(14)	5.751(6)	5.746(12)	5.766(8)

TABLE XXVII: Υ and η_b energies and kinetic masses in lattice units for various lattice momenta on coarse set 3 for b quark mass $am_b = 2.66$ and $c_{1,5,6}$ set to 1.

	(0,0,0)	(1,0,0)	(1,1,0)	(1,1,1)	(2,0,0)	(2,1,1)	(2,2,1)	(3,0,0)
$aE(^1S_0,\mathbf{P})$	0.26096(4)	0.26684(4)	0.27273(4)	0.27860(4)	0.28438(4)	0.29610(4)	0.31348(6)	0.31335(6)
$aE(^3S_1,\mathbf{P})$	0.29243(6)	0.29838(6)	0.30434(6)	0.31030(7)	0.31611(8)	0.32799(8)	0.34555(14)	0.34536(14)
$aM_{\rm Kin}(\eta_b)$	-	5.818(7)	5.819(7)	5.817(7)	5.839(3)	5.834(4)	5.844(7)	5.859(4)
$aM_{\rm Kin}(\Upsilon)$	-	5.747(18)	5.748(17)	5.742(17)	5.778(7)	5.764(9)	5.778(13)	5.798(12)
$\overline{aM}_{\rm Kin}(1S)$	-	5.764(15)	5.766(14)	5.761(14)	5.793(5)	5.782(8)	5.795(11)	5.813(10)

TABLE XXVIII: Υ and η_b energies and kinetic masses in lattice units for various lattice momenta on coarse set 3 for b quark mass $am_b = 2.66$ and $c_{1,5,6}$ set to their $\mathcal{O}(\alpha_s)$ improved values. Slight differences with Table VIII for zero momentum energies arise because we fit a single zero momentum correlator rather than a 5×5 matrix.

	(0,0,0)	(1,0,0)	(1,1,1)	(2,0,0)	(2,2,1)	(3,0,0)
$aE(^1S_0,\mathbf{P})$	0.24652(3)	0.25107(3)	0.26010(3)	0.26461(3)	0.28713(4)	0.28712(4)
$aE(^3S_1,\mathbf{P})$	0.27153(5)	0.27610(4)	0.28518(5)	0.28974(5)	0.31244(6)	0.31246(7)
$aM_{\rm Kin}(\eta_b)$	-	4.244(6)	4.252(6)	4.2548(14)	4.2516(23)	4.251(3)
$aM_{\rm Kin}(\Upsilon)$	-	4.222(14)	4.230(13)	4.225(3)	4.223(4)	4.215(6)
$\overline{aM}_{\rm Kin}(1S)$	-	4.228(12)	4.236(11)	4.2327(24)	4.230(4)	4.224(5)

TABLE XXIX: Υ and η_b energies and kinetic masses in lattice units for various lattice momenta on fine set 5 for b quark mass $am_b = 1.91$ and $c_{1,5,6}$ set to 1

	(0,0,0)	(1,0,0)	(1,1,0)	(1,1,1)	(2,0,0)	(2,2,1)	(3,0,0)
$aE(^1S_0,\mathbf{P})$	0.25827(3)	0.26278(3)	0.26727(4)	0.27173(3)	0.27620(3)	0.29850(4)	0.29847(3)
$aE(^3S_1,\mathbf{P})$	0.28390(5)	0.28844(4)	0.29299(6)	0.29747(5)	0.30199(5)	0.32451(6)	0.32447(6)
$aM_{\rm Kin}(\eta_b)$	-	4.278(7)	4.286(9)	4.287(6)	4.2914(14)	4.2920(23)	4.2951(19)
$aM_{\rm Kin}(\Upsilon)$	-	4.245(15)	4.251(17)	4.256(14)	4.2515(29)	4.2523(44)	4.2538(41)
$\overline{aM}_{\rm Kin}(1S)$	-	4.253(12)	4.260(15)	4.264(11)	4.2615(24)	4.2622(37)	4.2641(35)

TABLE XXX: Υ and η_b energies and kinetic masses in lattice units for various lattice momenta on fine set 5 for b quark mass $am_b = 1.91$ and $c_{1,5,6}$ set to their $\mathcal{O}(\alpha_s)$ improved values. Slight differences in zero momentum energies are seen compared to Table VIII because we used u_{0L}=0.85246 rather than 0.8525 and are fitting to single correlators rather than a 5×5 matrix.